

University of New Hampshire

## University of New Hampshire Scholars' Repository

---

Master's Theses and Capstones

Student Scholarship

---

Fall 2006

### Post-yield nonlinear behavior of structural steel beam-column elements

Josif Bicja

*University of New Hampshire, Durham*

Follow this and additional works at: <https://scholars.unh.edu/thesis>

---

#### Recommended Citation

Bicja, Josif, "Post-yield nonlinear behavior of structural steel beam-column elements" (2006). *Master's Theses and Capstones*. 190.

<https://scholars.unh.edu/thesis/190>

This Thesis is brought to you for free and open access by the Student Scholarship at University of New Hampshire Scholars' Repository. It has been accepted for inclusion in Master's Theses and Capstones by an authorized administrator of University of New Hampshire Scholars' Repository. For more information, please contact [Scholarly.Communication@unh.edu](mailto:Scholarly.Communication@unh.edu).

POST-YIELD NONLINEAR BEHAVIOR OF STRUCTURAL STEEL BEAM-COLUMN  
ELEMENTS

BY

JOSIF BICJA  
BS, University of New Hampshire, 2003

THESIS

Submitted to the University of New Hampshire  
in Partial Fulfillment of  
the Requirements for the Degree of

Master of Science  
in  
Civil Engineering

September, 2006

UMI Number: 1437614

### INFORMATION TO USERS

The quality of this reproduction is dependent upon the quality of the copy submitted. Broken or indistinct print, colored or poor quality illustrations and photographs, print bleed-through, substandard margins, and improper alignment can adversely affect reproduction.

In the unlikely event that the author did not send a complete manuscript and there are missing pages, these will be noted. Also, if unauthorized copyright material had to be removed, a note will indicate the deletion.

**UMI**<sup>®</sup>

---

UMI Microform 1437614

Copyright 2006 by ProQuest Information and Learning Company.

All rights reserved. This microform edition is protected against unauthorized copying under Title 17, United States Code.


ProQuest Information and Learning Company  
300 North Zeeb Road  
P.O. Box 1346  
Ann Arbor, MI 48106-1346

This thesis has been examined and approved.



---

Thesis Director, Thomas L. Attard, Ph.D.  
Assistant Professor of Civil Engineering



---

Charles H. Goodspeed, Ph.D.  
Associate Professor of Civil Engineering



---

Sean T. James, P.E.  
Senior Structural Engineer

July 26, 2006

Date

## ACKNOWLEDGMENTS

I would like to express my undying gratitude to my thesis adviser, Dr. Thomas L. Attard for his constant aid and support throughout the life of this thesis. Without him, this thesis would not have been possible. I would like to thank him for his patience and encouragement that carried me on through difficult times, and for his insights and suggestions that helped to shape my research skills. His valuable feedback and expertise contributed greatly to this thesis. His energy and great vision has always and will inspire me. In addition, gratitude is extended to the remaining committee members, Dr. Charles H. Goodspeed, and Mr. Sean T. James for providing valuable input and for their support for the thesis.

## TABLE OF CONTENTS

CHAPTER	PAGE
ACKNOWLEDGMENTS .....	iii
LIST OF TABLES .....	vi
LIST OF FIGURES .....	vii
ABSTRACT.....	x
INTRODUCTION .....	1
1.1 Overview .....	1
1.2 Scope.....	3
1.3 Objectives .....	4
NONLINEAR BEHAVIORAL CHARACTERISTICS OF STEEL .....	6
2.1 Background .....	6
2.2 Description of Material Response Model.....	13
2.2.1 Assumptions .....	15
2.2.2 Introduction to Relevant Terms .....	15
2.2.3 Test Verification of Material Response Model.....	16
AXIAL STABILITY.....	18
3.1 Overview .....	18
3.2 Euler Elastic Buckling .....	19
3.3 Effective Length of Columns .....	21
3.3.1 Degradation at Connection Level and Along Length of Member .....	23
3.4 Strength Equations of Columns .....	46
COMBINED BENDING AND AXIAL LOAD .....	50
4.1 Overview .....	50
4.2 Incremental Stresses Analysis Approach .....	52
4.3 Results .....	55
VERIFICATION AND VALIDATION OF THE PROPOSED MODEL.....	65
5.1 Overview .....	65
5.2 Numerical Solution Procedures for Nonlinear Problems .....	65
5.3 FEA Simulations .....	68
STRUCTURAL RESPONSE TO DYNAMIC LOADING .....	70
6.1 Overview .....	70
6.2 P-delta Effects on a Shear Building.....	71

SUMMARY AND CONCLUSIONS.....98  
APPENDIX: FEA SIMULATIONS .....101  
REFERENCES.....108

LIST OF TABLES

TABLE		PAGE
Table 3-1	AISC LRFD (2001) K-values for Columns.....	22
Table 3-2	Deflections Along Length of Column for $1.5\epsilon_y$ End Strain.....	37
Table 3-3	Computed Effective Length Factor K for Discrete Strain Levels.....	44



## LIST OF FIGURES

FIGURE		PAGE
Figure 2-1	Idealized Stress-Strain Curves: (a) Elastic, Perfectly Plastic; (b) Rigid, Perfectly Plastic; (c) Elastic, Linear Strain Hardening; (d) Elastic, Nonlinear Strain Hardening. ....	10
Figure 2-2	Isotropic Hardening: Yield Surface Expands in all Directions – Same Shape, Different Size. ....	11
Figure 2-3	Kinematic Hardening: Yield Surface Translates - Bauschinger Effect. ....	12
Figure 2-4	Bauschinger Effect for Uniaxial Loading.....	13
Figure 3-1	Typical Range of Column Strength vs. Slenderness Ratio.....	20
Figure 3-2	One-story SDOF Shear Frame Structure.....	24
Figure 3-3	Distribution of Strain and Stress for Elastic Range.....	25
Figure 3-4	Distribution of Strain and Stress for Post-yield Range. ....	28
Figure 3-5	Moment Distribution at Column. ....	31
Figure 3-6	Material Degradation at Plastic Hinge.....	32
Figure 3-7	Post-Yield Curvature Along Length of Column. ....	33
Figure 3-8	Total Curvature Along Length of Column.....	34
Figure 3-9	Post-Yield Curvature Diagram Along Length of Column.....	35
Figure 3-10	Deflections Along Length of Column for $15\varepsilon_y$ End Strain. ....	38
Figure 3-11	Displaced Column Shape Diagram Prior to Yielding.....	41
Figure 3-12	Displaced Column Shape Diagram after Yield.....	42
Figure 3-13	Deflections Along Length of Column for all Discrete End Strains..	44
Figure 3-14	Optimal Distribution of Effective Length Factors.....	45
Figure 3-15	Critical Stress as a Function of $\lambda_c$ (Englekirk, 1994).....	48

Figure 3-16	Modified Critical Axial Stress as a Function of $\lambda_c$ .....	49
Figure 4-1	Primary and Secondary Moments of Beam-Column Element.....	51
Figure 4-2	Combined Post-Yield Stress-Strain Relationship.....	56
Figure 4-3	Post-Yield Moment Curvature Diagram .....	58
Figure 4-4	Normalized Post-Yield Moment Curvature Relationship .....	59
Figure 4-5	Total Post-Yield Curvature Along Length of Column.....	60
Figure 4-6	Lateral Force-Displacement Curve.....	61
Figure 4-7	Stiffness versus Total Deflection.....	63
Figure 5-1	Full Newton-Raphson Method. ....	66
Figure 5-2	Modified Newton-Raphson Method.....	68
Figure 6-1	Artificial Earthquake Record (6.0g) for SDOF Shear Frame Structure.....	72
Figure 6-2	Hysteresis of a SDOF Shear Frame Structure (Artificial Excitation of 6.0g).....	73
Figure 6-3	Time History Response of a SDOF Shear Frame Structure (Artificial Excitation of 6.0g).....	74
Figure 6-4	Artificial Earthquake Record (1.0g) for SDOF Shear Frame Structure.....	75
Figure 6-5	Hysteresis of a SDOF Shear Frame Structure (Artificial Excitation of 1.0g).....	76
Figure 6-6	Time History Response of a SDOF Shear Frame Structure (Artificial Excitation of 1.0g).....	77
Figure 6-7	Four-story MDOF Shear Frame Structure.....	78
Figure 6-8	Artificial Earthquake Record (2.5g) for MDOF Shear Frame Structure.....	79
Figure 6-9	Hysteresis of 4 <sup>th</sup> Floor of a MDOF Shear Frame Structure (Artificial Excitation of 2.5g).....	80
Figure 6-10	Hysteresis of 3 <sup>rd</sup> Floor of a MDOF Shear Frame Structure (Artificial Excitation of 2.5g).....	81

Figure 6-11	Hysteresis of 2 <sup>nd</sup> Floor of a MDOF Shear Frame Structure (Artificial Excitation of 2.5g).....	82
Figure 6-12	Hysteresis of 1 <sup>st</sup> Floor of a MDOF Shear Frame Structure (Artificial Excitation of 2.5g).....	83
Figure 6-13	Time History Response of 4 <sup>th</sup> Floor of a MDOF Shear Frame Structure (Artificial Excitation of 2.5g).....	84
Figure 6-14	Time History Response of 3 <sup>rd</sup> Floor of a MDOF Shear Frame Structure (Artificial Excitation of 2.5g).....	85
Figure 6-15	Time History Response of 2 <sup>nd</sup> Floor of a MDOF Shear Frame Structure (Artificial Excitation of 2.5g).....	86
Figure 6-16	Time History Response of 1 <sup>st</sup> Floor of a MDOF Shear Frame Structure (Artificial Excitation of 2.5g).....	87
Figure 6-17	San Fernando Earthquake Record for MDOF Shear Frame Structure.....	88
Figure 6-18	Hysteresis of 4 <sup>th</sup> Floor of a MDOF Shear Frame Structure (San Fernando 5x).....	89
Figure 6-19	Hysteresis of 3 <sup>rd</sup> Floor of a MDOF Shear Frame Structure (San Fernando 5x).....	90
Figure 6-20	Hysteresis of 2 <sup>nd</sup> Floor of a MDOF Shear Frame Structure (San Fernando 5x).....	91
Figure 6-21	Hysteresis of 1 <sup>st</sup> Floor of a MDOF Shear Frame Structure (San Fernando 5x).....	92
Figure 6-22	Time History Response of 4 <sup>th</sup> Floor of a MDOF Shear Frame Structure (San Fernando 5x).....	93
Figure 6-23	Time History Response of 3 <sup>rd</sup> Floor of a MDOF Shear Frame Structure (San Fernando 5x).....	94
Figure 6-24	Time History Response of 2 <sup>nd</sup> Floor of a MDOF Shear Frame Structure (San Fernando 5x).....	95
Figure 6-25	Time History Response of 1 <sup>st</sup> Floor of a MDOF Shear Frame Structure (San Fernando 5x).....	96

## ABSTRACT

### POST-YIELD NONLINEAR BEHAVIOR OF STRUCTURAL STEEL BEAM-COLUMN ELEMENTS

By

Josif Bicja

University of New Hampshire, September, 2006

One of the most effective mechanisms available for the dissipation of the energy input to a structure during an earthquake is through inelastic deformation. It is imperative to accurately model and predict these behaviors because of the safety that can ultimately be added to the integrity of a structure under such severe loading events. The presented method of analysis has the unique feature in its exact inclusion of the coupling between axial force, primary and secondary moments and their conjugate axial and bending strains, and, most importantly, the incorporation of the effect of curvature along the length of the member.

Degradation of the material, once yielding has occurred at certain locations that can experience such higher-order degradation levels is accurately modeled, and the structural behavior for in-plane lateral dynamic loading of 2D shear frame beam-columns is predicted with particular reference to material nonlinearity and taking into consideration any geometrically nonlinear effects such as *P-delta* phenomena. The structural performance prediction is complex due to nonlinear material properties, uncertainties in earthquake loading, and many other factors. However, the structural response of simple sections is

predicted herein through the proposed constitutive nonlinear strain hardening model that assesses the material degradation through the spread of plasticity.

Using detailed incremental procedures, the stress-strain relationship is derived for beam-column element. The proposed methodology ultimately provides accurate force-lateral deflection curves. The validity of the proposed model is examined by comparing it with results of the Finite Element Analysis (FEA). The results of the proposed rigorous model compare favorably to the results of the FEA, and indicate that the proposed incremental approach is very reasonable, due to the small discrepancy when compared to the FEA.

## CHAPTER 1

### INTRODUCTION

#### **1.1 Overview**

Civil structures, such as buildings, parking garages and bridges, are designed to resist two types of forces: (1) vertical (gravitational) forces produced from the self dead weight, and occupancy loads; and (2) lateral forces caused by earthquakes or wind loading. These types of forces induce at each column, of each story of the building, axial forces, lateral shear forces and overturning moments. The overturning moments have two components: (1) the primary moments resulting from the lateral loads; and (2) the secondary moments resulting from the vertical loads acting over the incremental moment arms that are originated by the lateral deflections. Civil structures are designed to remain elastic and exhibit little or no damage as a result of normal service conditions. For extreme loadings, i.e., infrequent earthquakes, however, it is not economical to design structures that can remain entirely elastic. They must be designed on the basis of minimum weight, which invariably means designing into the plastic range to obtain optimal load-to-weight ratios. The term plastic, derived from the Greek word "plasticos" meaning "to form" refers to a property of a material to undergo a non-reversible change of shape in response to stress. By design, structures are expected to suffer minor damage without compromising public safety and welfare, when subjected to large infrequent earthquakes.

Steel has traditionally been perceived to be an elastic material (Englekirk, 1994). A purely elastic theory and analysis has been widely used by engineers during the past decades. In analysis of statically indeterminate structures, internal forces are distributed based on the relative stiffness of the individual structural elements (i.e., beams and columns). Relative element stiffnesses within a structure change continuously under dynamic loading and can be significantly different from their assumed elastic values (Karabinis and Kiousis, 2001). Due to complexity of nonlinear analysis, no attempts have been made to take into account the nonlinear strain hardening properties of steel when such structures are analyzed. Present-day design codes are based on a limit-state design philosophy. Strength limit state concepts were first introduced into design in 1961 by the American Institute of Steel Construction (AISC) (Englekirk, 1994). Deformations and stability of such design philosophies rely heavily on the elastic-based theory. Such limit state design has incorporated elastic-based strength design criterion. The day-to-day design methodology in structural steel has not attempted to develop an inelastic based criterion wherein a simplified perfectly plastic stress distribution is assumed when calculating the strength limit state of a structural system.

Steel structures will often incur nonlinear "plastic" behavior, in which steel beams and columns undergo permanent displacements and deformations during large earthquake-induced ground motions. A key requirement for modeling the mechanical response of a structure is knowledge of realistic estimates of how the ground beneath the structure will move during an earthquake. It is also imperative to locate the damage of a structural system,

when subjected to a hypothetical earthquake loading, in order to redesign and prevent structural failure.

## **1.2 Scope**

The purpose of this research was to investigate the detailed post-yield behavior of 2D shear frame steel beam-columns subjected to combined earthquake and gravity loadings under extreme conditions. A shear frame building is defined as a structure that can be idealized to have inextensible columns and rigid floors so that no joint rotation occurs at the horizontal section at the level of the floors when the system is subjected to dynamic loadings. In this perspective, the deflected building will have many characteristics of a cantilever beam that is deflecting by shear forces, hence the name shear structure. That is not to say that axial forces have been neglected for such type of structures. The vertical loads in conjunction with lateral deflections of columns produce additional moments that are so-called *P-delta* effects. Such phenomena are discussed in a much greater detail in the following chapters. To satisfy the definition of a shear frame structure it is assumed that: (1) the total mass of the building is concentrated at each level of the floors; (2) the beams on each floor are infinitely rigid as compared to the columns; and (3) the lateral displacement of the structure is dependent of the *P-delta* effects. These assumptions transform the problem from a structure with an infinite number of degrees of freedom (DOF), due to the distributed mass, to a structure that has as many degrees as it has lumped masses at the floor levels (Paz, 1997).



Structural performance prediction is complicated by uncertainties in structural material properties, earthquake modeling including the stationary or non-stationary nature of the motion, initial conditions, which would input energy into the system that would need to be dissipated during the response analysis, and many other factors. From a material mechanics point of view, the real behavior of steel framed structures is, in general, nonlinear and of a rather complex nature. If the yield strength is exceeded in the cross-section of a member, then Hooke's law ceases to be valid. A previously established nonlinear mechanism model developed for these cases is used to incrementally separate stresses generated by the primary moments, axial effects and secondary *P-delta* effects and ultimately to effectively evaluate and predict the structural response of steel beam-columns. The proposed advanced method of incremental analysis – adopted throughout this research – towards the assessment of structural response, models the structural behavior due to earthquake motions through the post-yield behavior of the ductile steel components of the frame. Various material nonlinearities such as secondary moment and spread of plasticity of steel beam-column elements are modeled and determined in computational detail.

### **1.3 Objectives**

The primary objective of this research was to compute the inelastic deformations of steel beam-column elements through a nonlinear constitutive relationship under a cyclic and dynamic loading. This is accomplished within an iterative scope where the analysis of the bending stresses, axial stresses, and the

resulting *P-delta* effects are determined per strain increment over the range of all possible strains leading towards the failure of the system. Not only should the structural response be accurately evaluated in this light but also be reasonably predicted, so that design engineers know what to expect during an earthquake or other large-scale extreme events that might challenge the integrity of the structure. The calculations should be quick, simple, and accurate to facilitate the iterative structural design process and explore numerous combinations of structural systems in a reasonable amount of time.

As such, the proposed incremental approach enables the analysis of these phenomena to be made where all nonlinearities are evaluated along extremely small linear stress-strain segments. Ultimately, the results closely conform to those of a finite element analysis, which validates the incremental method of analysis and also indicates that the small differences in the monotonic responses are a result of the added accuracy and detail given to the *P-delta* analysis using the proposed approach. These small differences carry an important role in predicting the accurate cyclic responses of buildings under stationary dynamic loading since errors become amplified over the course of a hysteresis. The approach presented herein also opens the door to enable other phenomena pertaining to local failure responses to be included in an analysis, including web crippling, flange buckling, etc., which could be seamlessly analyzed within this incremental framework.

## CHAPTER 2

### NONLINEAR BEHAVIORAL CHARACTERISTICS OF STEEL

#### **2.1 Background**

The mechanical behavior of steel is fundamentally described by an appropriate stress-strain relationship. Determination of stresses from measured surface strains is a routine task in experimental stress analysis. Under a linear elastic setting, techniques for such tasks are simple and well established. Robert Hooke developed a basic stress-strain relationship in the seventeenth century (Englekirk, 1994).

$$\sigma = \varepsilon \times E \quad (2.1.1)$$

In equation (2.1.1),  $\sigma$  represents the material stress;  $\varepsilon$  represents the material strain, and  $E$  is the calculated Young's modulus of elasticity of the material. Elastic strain and stress are uniquely related regardless of the particular loading (i.e., monotonic or cyclic) that produces the actual stress. The elastic term implies that deformations disappear completely after the removal of applied forces and any change in shape can only be maintained under a continuous action of forces (Doltsinis, 2000). Under moderate additional forces, beyond the elastic limit, permanent deformations develop. Such deformations can be considered characteristics of plasticity. During plastic deformation, a stress state remains on the boundary of the elastic region, that is, in a plastic state as the material degrades nonlinearly. Thereby, loading from a plastic state leads to

another plastic state (Shames and Cozzarelli, 1997). The early flow or incremental theory of plasticity relates the increments of plastic strain to the stress, and was developed in an earlier work by Handelman and Prager (Handelman and Prager, 1948). This flow theory can be described incrementally according to the loading path (Needleman, 1985). It should be further noted that plastic deformation is independent of the time under load (Mendelson, 1999). The following chapters will discuss the effects of the strain rate phenomenon in more detail.

In many situations the theories of plasticity are often needed in the interpretation of experimental results (Sutton, Deng, et al. 1996). Constitutive equations or stress-strain laws, that represent mathematical models, are often developed to describe the macroscopic material behavior that results from the internal constitution of a material. To establish the constitutive relationship the plasticity formulation takes the most important part since the behavior of structural steel under earthquake-induced ground motions shows that most deformation occurs in the inelastic range. Using constitutive models, it is imperative to accurately and efficiently model the behavior of steel. These constitutive laws play a crucial role providing reliability to the results obtained from the numerical procedures.

While significant advances have been made during the past decades in the development of constitutive models towards assessments of the post-yield behavior of structural steel members, a difficulty remains in that many new models involve complex mathematical formulations and manipulations. Models have been developed extensively to include destabilizing the effects of both

material and geometric nonlinearities (Plastic, 1965; Porter and Powell, 1971; Orbison, 1982; King, et al. 1992; Attalla, et al. 1994). Pettersson and Popov (1977) have examined inelastic behavior using translating multi-surface yield models while Marcon, et al. (1999) investigated a formulation for the incremental determination of stresses in strain measured levels. Barsan and Chiorean (1999) offered a finite element prospective for gradual yielding of cross-sections using the inelastic force strain relationships. White (1985) has discretized members both along their length and through their cross section to track the gradual development of inelastic zones. Other investigators have introduced several hinges prior to reaching the inelastic limit point (Ziemian, et al. 1992a, b; Vogel, 1985). However, the hinge methods without consideration given to the spread of plasticity have been shown to overestimate the limit strength when structural behavior is dominated by the instability of a few members (McGuire, et al. 2000; King, et al. 1992; White, et al. 1993).

Therefore, the post-elastic stress distribution across a member's length is needed to accurately assess material degradation caused by the gradual spread of yielding (Attard, 2003). This enables a system's overall energy dissipation (Chen and Powell, 1982) to be determined and member responses to be predicted. Although design codes, such as Uniform Building Code (UBC, 1997) use factors that account for the ductility and inelastic behavior in structures, they do not detail the nature of the material degradation; this often results in overconservative seismic design (Attard, 2005). Liew (1997) has addressed the member deterioration using semirigid connections, although

gradual stiffness degradation is not accounted for and results in inaccurate lateral displacements (Gao and Haldar, 1995).

Because of the complex nature of the stress-strain curve, it has become customary to idealize this curve in various ways (Johnson and Mellor, 1962). Figure 2-1 shows idealized stress-strain curves that can be used to describe material behavior. This research concentrates and uses the specific nonlinear strain hardening model that is depicted in Figure 2-1.(d). The model is formulated using dislocation theory (Attard, 2005) and expresses the gradual degradation in the plastic modulus.

In Figure 2-1.(d) the stress-plastic strain relationship occurs once the material has started to yield. At a given stress level beyond yield, there is a certain material degradation factor that is incorporated. For cyclic loading, the same stress can be reached by unloading from any higher point of the hardening curve, and may therefore be associated with different values of plastic strain unless the preceding load history is specified. For this reason the relations between incremental variations of stress and plastic strain along a prescribed path is examined.

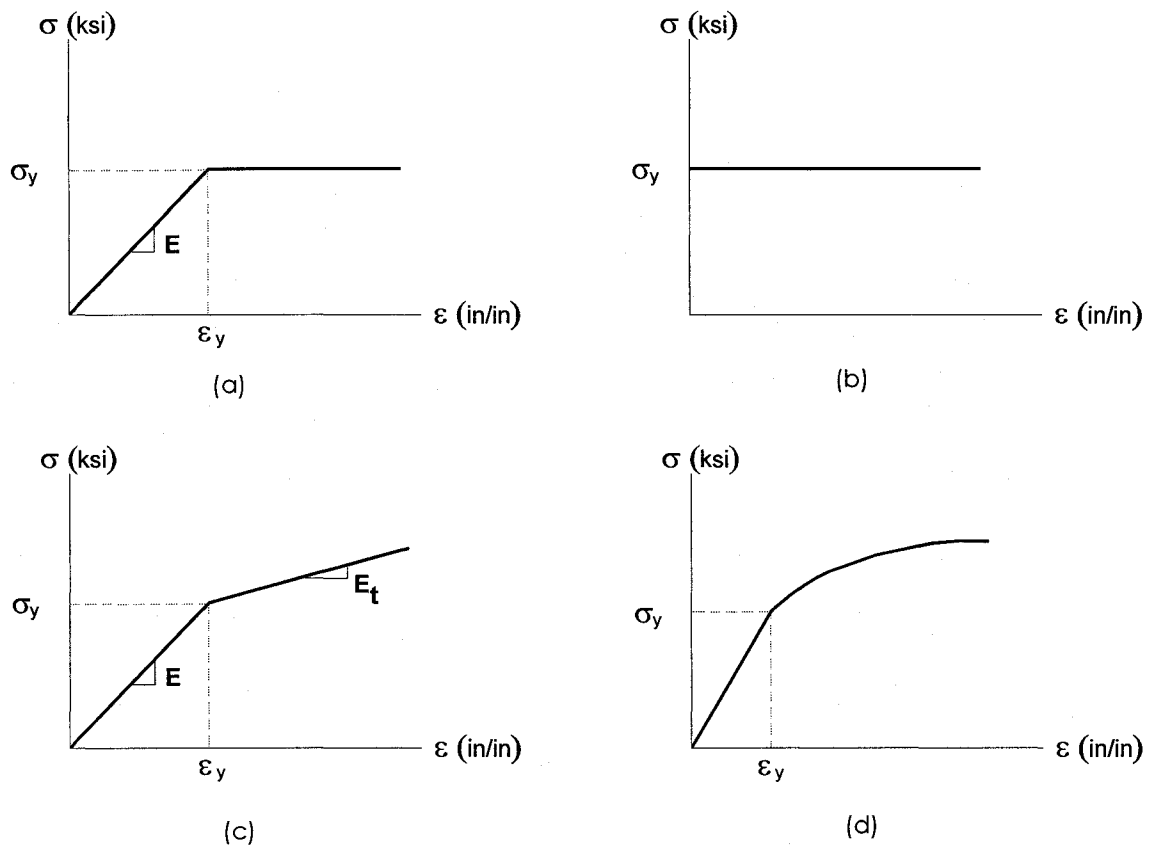


Figure 2-1 Idealized Stress-Strain Curves: (a) Elastic, Perfectly Plastic; (b) Rigid, Perfectly Plastic; (c) Elastic, Linear Strain Hardening; (d) Elastic, Nonlinear Strain Hardening.

For changes in plastic strain, the applied stress must be raised to a higher stress state that is ultimately attained in the past by the material. An incremental increase in stress produces an increment in plastic strain. Conversely, a reduction in stress will cause a decrease in strain, which follows a path parallel to the original path of the elastic curve. This behavior is described by either isotropic or kinematic hardening. Isotropic hardening assumes that the mechanism that produces hardening acts equally in tension and compression. Such behavior is shown in Figure 2-2 for bi-axially loaded systems in stress-space where  $\sigma_1$  and  $\sigma_2$  are the principal stresses in the material. In this case, the post-

yield material behavior is described by both a flow rule and a hardening rule (Dafalias and Popov, 1975).

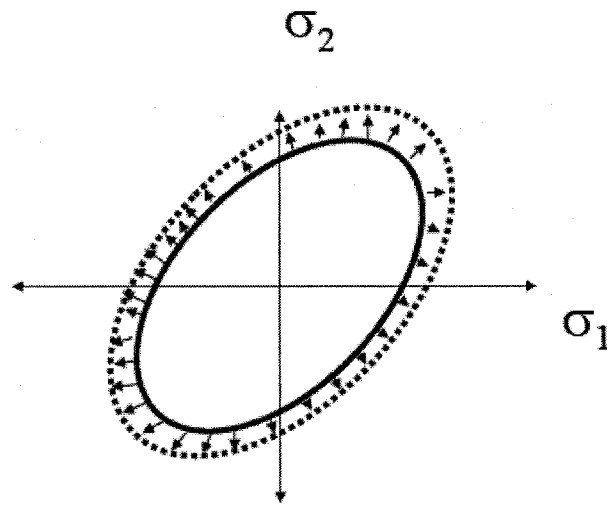


Figure 2-2 Isotropic Hardening: Yield Surface Expands in all Directions – Same Shape, Different Size.

Experimental evidence supports the hypothesis that the magnitude of the yield stress attains the same value under tension or compression. This statement applies to separate tests under tensile or compressive action, not to combined loading sequences (Doltsinis, 2000). If, however, the material is first permanently deformed by uniform tension and the load is removed and the material is reloaded in compression, the yield point obtained in compression will be considerably less than the initial yield in tension. This has been explained as a result of residual stresses left in the material due to the annihilation of atomic bonds once a material has yielded; this is an anisotropic effect in material behavior. For hot-rolled structural steel shapes, residual stresses result from several sources: (1) uneven cooling which occurs after hot rolling; (2) punching of holes and cutting operations during fabrication; and (3) welding. Materials



may also have initial anisotropy due to manufacturing processes. A better explanation is based on the anisotropy of the dislocation field produced by loading. This effect is called the Bauschinger effect, and is present whenever there is a reversal of the stress field (Mendelson, 1999). To account for the Bauschinger effect, Prager introduced the kinematic hardening model, in which the total elastic range is maintained constant by translating the initial yield surface without deforming it (Prager, 1955). In such a model, dislocation in the microscopic scale undergoes extensive rearrangement upon reversal of stress, and dislocation accumulation is only partly reversible due to the bond annihilation mentioned earlier. The kinematic hardening model is shown in Figure 2-3 once more under bi-axial loading conditions.

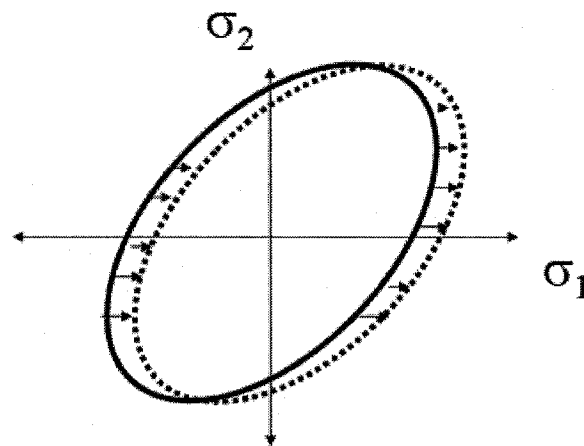


Figure 2-3 Kinematic Hardening: Yield Surface Translates - Bauschinger Effect.

For instance, if a specimen is loaded beyond the yield stress in uniaxial tension, then unloaded from the tensile zone and reloaded into the compression zone, it follows that the new yield stress point is going to be smaller in magnitude than

the initial yield point in tension. This phenomena known as Bauschinger effect, is shown in Figure 2-4.

Attempts have been made to improve the kinematic hardening model although the model itself is more mathematically complex. For small plastic strains the isotropic hardening model is sufficiently accurate with test results (Mendelson, 1999). However, in this research the ultimate plastic strain,  $\epsilon_{p,max}$ , is assumed to attain a strain of  $15\epsilon_y$  in the outermost fiber, thus the isotropic hardening model could yield erroneous results. This is elaborated in to a much greater detail in the following chapters.

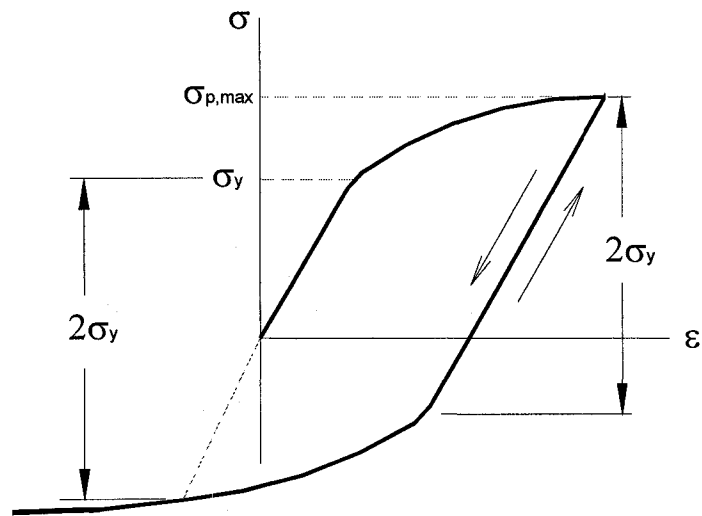


Figure 2-4 Bauschinger Effect for Uniaxial Loading.

## **2.2 Description of Material Response Model**

Accurate analysis of steel frame structures, when subjected to dynamic loads, requires an accurate model that describes the material response after yield and especially under cyclic loading conditions. This research uses a

constitutive model proposed by Attard (2005), which was intended to represent the effects of material behavior through a gradual stiffness degradation used in conjunction with a material flow rule for beam elements (i.e., no axial loading). The model is implemented and modified herein for the combined axial load and bending effects where an additional *P-delta* term is also included.

Attard (2003) proposed a detailed nonlinear strain hardened model that can be used to model the backstress evolution of the yield surfaces (see Figure 2-3 and under a bi-axial load environment) assuming a kinematically strain-hardened condition. The constitutive model itself can also be expressed in terms of the post-yield strain ( $\sigma = f(\epsilon)$ ) and used to model the uniaxial stress-strain behavior in in-plane elements. Thus, the model is developed starting at the material yield state where the gradual degradation of the stiffness is modeled, and the plastification process is defined through the cross-sectional depth and over some finite length of the structural member. The nonlinear constitutive model has been used under a cyclic loading environment where the force-deflection hysteresis has been verified (for conditions where the strain rate is negligible). As such, the model is predicated on two parameters – one of which is an evolutionary hardening index parameter that predicts the ultimate failure of ductile materials by capturing a more realistic nonlinear post-yield response of structural members. The model is rate independent, and is described by a smooth and integratable mathematical function (Attard, 2005).

### **2.2.1 Assumptions**

The nonlinear constitutive model has been applied by Attard (2003) for in-plane lateral dynamic loading of 2D shear frame members. It is assumed that an adequate bracing system and sufficient stiffeners are applied to compact sections to provide the necessary resistance to any beam and local buckling effects (LRFD, 2001). The residual stresses due to the manufacturing processes and shear stresses have been neglected. Furthermore, it is assumed that plane sections within the beam before bending remain plane after bending, and the neutral plane of a beam is a plane whose length is unchanged by the beam's deformation.

The material is assumed to be virgin, isotropic and homogenous. This research utilizes such a model but under the combined primary and the secondary effects due to dynamic lateral loads acting in conjunction with the applied gravity axial loads.

### **2.2.2 Introduction to Relevant Terms**

The post-elastic stress function,  $\sigma_x$ , is given by equation (2.2.2.1) as defined by Attard (2003) in non-incremental form and is a function of the cross-sectional depth  $y$  and the post-elastic stress state  $e$ .

$$\sigma_x = \sigma_y - \alpha \cdot \sigma_y \cdot \left(2 + \frac{1}{\Delta \varepsilon}\right) + \frac{2 \cdot \alpha \cdot \sigma_y \cdot y}{e} \cdot \left(1 + \frac{1}{\Delta \varepsilon}\right) - \frac{\alpha \cdot \sigma_y \cdot y^2}{\Delta \varepsilon \cdot e^2} \quad (2.2.2.1)$$

The depth of linear elastic behavior through the cross-section is given by  $e$ . The stress and strain at the yield state are given by  $\sigma_y$  and  $\varepsilon_y$ , respectively. The

second of the two parameters,  $\Delta_\varepsilon$ , is defined as the plastic strain coefficient and is given by equation (2.2.2.2) below.

$$\Delta_\varepsilon = \frac{(\varepsilon_u - \varepsilon_y)}{\varepsilon_y} \quad (2.2.2.2)$$

The hardening index parameter,  $\alpha$ , fits a postelastic nonlinear material response curve to a linearized guide by defining an average modulus between the yield and ultimate states. Using this hardening index,  $\alpha$ , a continuous parabolic function is determined for any post-elastic state. The index value of zero indicates a complete degradation of the modulus and represents the elastic-perfectly plastic state. The post-elastic stress distribution is defined using the stretch value,  $a$ , which remains constant throughout the loading history for homogeneous materials.

$$a = \frac{-\alpha\sigma_y}{\Delta_\varepsilon\varepsilon_y^2} \quad (2.2.2.3)$$

Because the stresses calculated from equation 2.2.2.1 above are history-dependent, the accuracy of the final stress state is naturally dictated by the step size of the strain increment. To minimize the errors associated with large strain increments, the value of the attainable ultimate plastic strain is subdivided in a total of  $N$  increments.

### **2.2.3 Test Verification of Material Response Model**

The detailed nonlinear strain hardening model that is proposed by Attard (2003) has been verified for beam elements using the published results of a cantilevered test specimen. The specimen was tested at the Earthquake Engineering Research Center located at the University of California at Berkeley in

the 1960s (Englekirk, 1994). The tested specimen was a W18x50 hot-rolled steel section and was subjected to a quasi-static loading. The results of the model correlated well with the test results of the cantilevered beam (Attard, 2003).

## CHAPTER 3

### AXIAL STABILITY

#### **3.1 Overview**

Structures are composed of several vertical and lateral resistant elements that are required to support various conceivable loads that the structure may experience during its lifetime. The most vital components of a structure are the columns. The behavior of columns in earthquakes is very important since single column failures may lead to additional failures and result in total building collapses. All the foreseeable loads are transferred to such structural members through the beam-column connections.

Beam-column connections are essential to the behavior of frame structures in their response to earthquake ground shaking. There are two fundamental functions that these connections must perform. The most basic of these is to provide a transfer of gravity loads from the beam to the column so that the beam remains attached to the structure. The second, and perhaps the more critical function, is to provide rigidity against lateral sidesway and to provide for transfer of sidesway related flexural stresses between the beams and columns. The beam-column connection must retain the ability to perform both of these functions for the realistic levels of loading likely to be induced by the combined effects of gravity and earthquake-induced loading. Beyond considerations of the ability of the connection to provide transfer of beam shears

resulting from gravity loading, the characteristics of connections that are important to assessment of the structure's overall behavior are those that affect how much lateral drift will be induced in the structure, when subjected to ground shaking.

Columns are rarely, if ever, actually carrying only axial compression. It is well known from basic strength and mechanics of materials that short columns will behave inelastically and will not buckle whereas intermediate and long columns could buckle as a result of instability prior to developing the full stress capacity in the material.

Column failure is the primary cause of structure collapse in an earthquake event. The most frequent observed cause of structural failure in the Mexico City Earthquake of 1985, Loma Prieta Earthquake of 1989, and Northridge California Earthquake of 1995 was linked to inadequate beam-to-column and slab-to-column connections (Kassawara, 1989). Failure occurred at the connection level where the columns were over stressed by the earthquake-induced ground motions. The majority of steel buildings exhibited fracture connection failures or other types of structural degradation at such locations during the time-history cyclic behaviors.

### **3.2 Euler Elastic Buckling**

Leonhard Euler introduced the elastic column buckling theory in 1744 (Salmon and Johnson, 1996). The fundamental buckling load for a column that is pinned at each end is given by equation (3.2.1).



$$P_{cr} = \frac{\pi^2 E}{(L/r)^2} A_g \quad (3.2.1)$$

$L$  is the length of the column,  $r$  is the radius of gyration and  $A_g$  is the gross-sectional area of the column. Equation (3.2.1) is derived from a second order ordinary differential equation of a deflected shape of an elastic column subjected to bending. Euler's derivation of the critical axial load was often ignored because it did not agree with experimental results. It was until 1946 when Shanley (1946, 1947) reasoned that it was actually possible for a column to bend and still have increasing axial compression, but that it begins to bend upon reaching what is commonly referred to as the buckling load. Test results for various slenderness ratios are shown in Figure 3-1 (Salmon and Johnson, 1996).

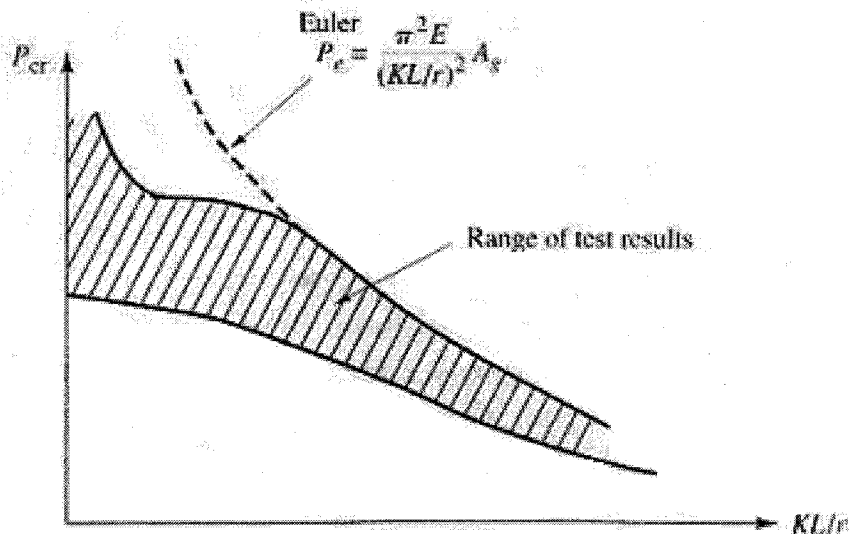


Figure 3-1 Typical Range of Column Strength vs. Slenderness Ratio.

### **3.3 Effective Length of Columns**

The concept of effective length is well established in the minds of most practicing engineers. The effective length factor  $K$ , is the equivalent pinned-end length of the  $i^{\text{th}}$  column ( $K_iL$ ) at which the end rotations are unrestrained. For 2D shear frame structures the effective length factor  $K$  is usually developed from a knowledge of the Euler buckling behavior of columns by stating that the effective length is equal to the distance between the points of contraflexure (Smyrell, 2001).

In most common situations it is difficult to evaluate the degree of moment restraint at the connection; as such, the effective length concept is one of the methods of estimating the interaction effects of the total frame on a compression element being considered. This concept uses  $K$  factors to equate the strength of a framed compression element of length  $L$  to an equivalent pin-ended member of length  $KL$  subjected to axial load only (LRFD, 2001). Unlike current procedures recommended by the design codes, such as AISC LRFD (2001), this research evaluates and computes the effective length factors for combined bending loads using the established nonlinear post-yield model in equation 2.2.2.1. In particular, the  $K$ -factors are established for various degrees of plastic states as the frame shown in Figure 3-2 gradually degrades at the top and bottom of each column going from a fix-fix condition to an idealistic pin-pin connection (mechanical hinge) under sidesway conditions.

The AISC LRFD (2001) specification presents a table to assist in the estimation of effective length for different end conditions. Theoretical and design values are recommended. The conservative design values are

recommended by the Structural Stability Research Council (SSRC) and are generally used in a design office setting unless the proposed end conditions truly match the theoretical conditions.

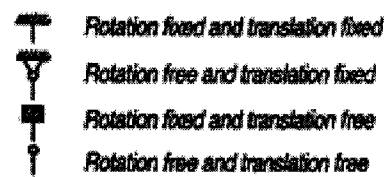
Table C-C2.1 K Values for Columns						
Buckled shape of column is shown by dashed line.	(a)	(b)	(c)	(d)	(e)	(f)
Theoretical K value	0.5	0.7	1.0	1.0	2.0	2.0
Recommended design value when ideal conditions are approximated	0.65	0.80	1.2	1.0	2.10	2.0
End condition code						

Table 3-1 AISC LRFD (2001) K-values for Columns.

It is assumed that foundations of the column base of 2D shear frame structures, considered in this research, restrain the rotations and the end condition is assumed to be fixed. It is further assumed that shear frames, by their definition, restrain the rotations at the tip of the column since the horizontal member is assumed to remain rigid and does not deflect.

### **3.3.1 Degradation at Connection Level and Along Length of Member**

The post-elastic distribution across the column length would need to be accurately assessed as the material is degrading by the gradual spread of yielding. Lumping the full plastification into a single point does not lead to a prediction of accurate lateral displacements. It is commonly agreed that a proper measure of spread and concentration is necessary to accurately measure the structure's lateral displacements induced by seismic loads (Bayrak and Sheikh, 2001). Lumping the full plastification into a single point does not provide a sound design for engineers (Englekirk, 1994). The accurate modeling of the spread of yielding is necessary to predict the degradation at the connection level by also incorporating the rotational effects. The degradation occurs once the material has started to yield.

The progression of the mechanical hinge occurs generally for shear frame structures, when there is an abrupt 75 percent decrease in floor-level stiffness (UBC, 1997). Prior to mechanical hinge development, there is a gradual decrease in stiffness before the full degradation has occurred. For ease of calculations and to prove the theory of the proposed model, a rectangular column cross section has been considered. The rectangular cross section is geometrically continuous and the continuous constitutive model shown by equation (2.2.2.1) can be implemented directly. For other frame sections, such as I-sections and tube sections, the geometric discontinuity requires an indirect approach in order to utilize the constitutive model. This is due to an ambiguity in the development of the post-yield curvature distribution across the member length, which is dependent on the instantaneous level of attained curvature for

a given cross sectional characteristic as shown by Attard (2003). Because of the nonlinear form of equation (2.2.2.1), two spread distances determined from two independent characteristics (i.e., see equation (2.2.2.1)) at the member end cannot be summed to produce the true spread length. For I-sections and tube sections, a second order mathematical model can be defined to correlate the moment between the actual section and the mathematical section over the entire length of post-yield spread (Attard, 2003).

For a given state of post-yield stress through the cross-section, deflections can be computed along the length of the column at various finite strains. As such, the degradation in the material is modeled particularly along the length of the column.

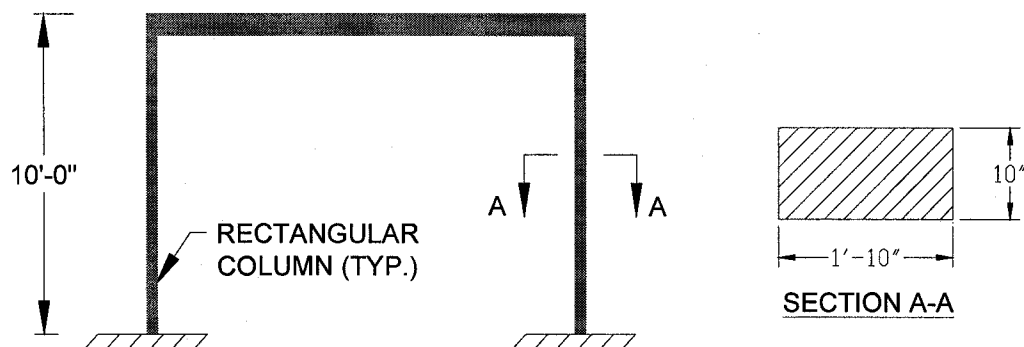


Figure 3-2 One-story SDOF Shear Frame Structure.

Figure 3-2 shows the shear frame structure referred to earlier that is taken into consideration to derive the effective length factors.

Curvature,  $\phi$ , and strain,  $\epsilon$ , are related by the following equation:  $\phi = \frac{-\epsilon}{y}$ ,

given that plane sections remain plane after bending and assuming that the

angle of rotation is small. For linear elastic behavior  $M = \frac{I\sigma}{y}$ , where  $y$  is the

distance of interest away from the neutral axis.

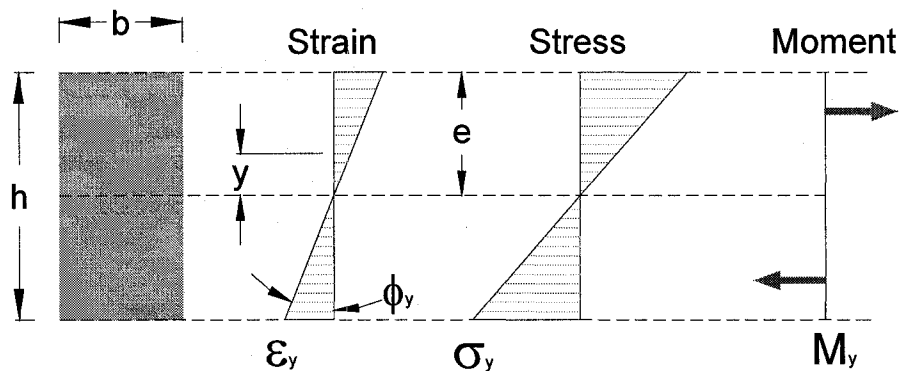


Figure 3-3 Distribution of Strain and Stress for Elastic Range.

Combining these two relationships, the curvature,  $\phi$ , can be stated as a function

of the moment ( $M$ ), flexural stiffness ( $I$ ) and the Modulus of Elasticity ( $E$ ):  $\phi = \frac{-M}{EI}$ .

Integrating the stress distribution along the cross section, as shown in Figure 3-3,

one can solve for the yield moment,  $M_y$ . Denoting by  $\sigma_x$  the normal stress at a

given point of cross section, it can be written that:  $\frac{\sigma_x}{\sigma_y} = \frac{y}{h/2} \Rightarrow \sigma_x = \frac{2y\sigma_y}{h}$ . The

yield moment ( $M_y$ ) can be expressed as:  $M_y = 2 \int_0^e [y(\sigma_x)b]dy$ , where  $e$  is defined

as the depth of linear elastic behavior. Substituting  $\sigma_x$  in the expression for  $M_y$

and integrating it, it follows that:

$$M_y = \frac{b\sigma_y e^2}{3} \quad (3.3.1.1)$$

Current design codes such as AISC LRFD and the American Association of State Highway and Transportation Officials LRFD Bridge Design Specifications (AASHTO) have implemented the elastic perfectly plastic stress-strain relationship. For this

model, the plastic moment ( $M_p$ ) can be expressed as:  $M_p = 2 \int_0^{h/2} [y(\sigma_x)b]dy$ .

Solving for  $M_p$  yields the following equation:

$$M_p = \frac{b\sigma_y h^2}{4} \quad (3.3.1.2)$$

As previously discussed, equation (2.2.2.1) describes the stress-strain distribution for the proposed nonlinear strain hardening model that is depicted in Figure 2-1.(d). When the outermost fiber reaches a stress equal to the yield stress, the moment associated with this stress state is described by equation (3.3.1.1).

As additional moments in excess of  $M_y$  are applied, the induced stress is increased by an incremental plastic stress,  $\Delta\sigma_p$ , until the ultimate state  $\sigma_{p,max}$  (ultimate plastic stress) is reached. At this ultimate state, the outermost fiber has a strain of  $\varepsilon_{p,max}$ , which can be expressed as:

$$\varepsilon_{p,max} = \varepsilon_e + \varepsilon_p \quad (3.3.1.3)$$

$$\varepsilon_p = 15\varepsilon_y - \varepsilon_y \quad (3.3.1.4)$$

The elastic strain,  $\varepsilon_e$ , is equal to  $\varepsilon_y$  in the post-yield stress state and is computed by equation (2.1.1).

Carbon steels and high strength, low-alloy steels possess a decided plastic plateau, after yielding has occurred, and this makes the experimental

identification of the yield stress fairly uncomplicated. At the end of the plastic plateau, an increase in applied load will be required to further strain the steel. The nonlinear strain hardening equation (2.2.2.1) describes such behavior. The ultimate plastic strain,  $\varepsilon_{p,max}$ , is assumed to attain a strain of  $15\varepsilon_y$  in the outermost fiber as suggested by Englekirk (1994) and verified by Attard (2003) for beam elements using the published results of a cantilevered test specimen.

Internal moments for a certain post-elastic stress state are calculated through integration (Englekirk, 1994). By accurately modeling the degradation of the material at the connection level, the distribution of curvatures along the member length where the spread of yielding has occurred can be used to predict the force vs. lateral displacement responses. Thus to begin, the strain increment used to determine the spread of yielding over the member length is defined as  $\Delta\varepsilon_p$  and is calculated as:

$$\Delta\varepsilon_p = \frac{\sigma_y}{100(E)} \quad (3.3.1.5)$$

The total post-yield strain at step  $i$ , is then defined as:

$$\varepsilon_{p_i} = \varepsilon_e + \Delta\varepsilon_p \quad (3.3.1.6)$$

and the total post-yield strain at step  $i+1$ , is defined as:

$$\varepsilon_{p_{i+1}} = \varepsilon_{p_i} + \Delta\varepsilon_p \quad (3.3.1.7)$$

To minimize the errors associated with large post-yield strain increments, the value of the ultimate plastic strain,  $\varepsilon_{p,max}$ , is subdivided in a total of  $N$  increments, where  $N$  is defined as:

$$N = \frac{\varepsilon_{p,max} - \varepsilon_e}{\Delta\varepsilon_p} \quad (3.3.1.8)$$



For ASTM A36 steel, after substituting equations (3.3.1.3) and (3.3.1.5) into equation (3.3.1.8), the total increments,  $N$ , are equal to 1,400.

The post-yield strain-curvature relationship is described incrementally and is shown in Figure 3-4.

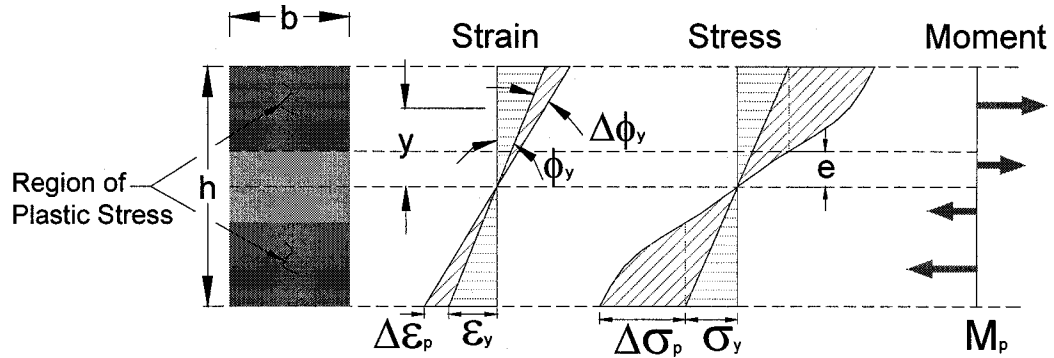


Figure 3-4 Distribution of Strain and Stress for Post-yield Range.

The incremental change in curvature,  $\Delta\phi_i$ , at step  $i$ , is written as:

$$\Delta\phi_i = \frac{\epsilon_{p\_i} - \epsilon_e}{h/2} = \frac{\Delta\epsilon_i}{h/2} \quad (3.3.1.9)$$

At step  $i+1$ , the incremental change in curvature,  $\Delta\phi_{i+1}$ , is written as:

$$\Delta\phi_{i+1} = \frac{\epsilon_{p\_i+1} - \epsilon_e}{h/2} = \frac{\Delta\epsilon_{i+1}}{h/2} \quad (3.3.1.10)$$

and at step  $i$ , the depth of linear elastic behavior  $e_i$ , is defined as:

$$\frac{\epsilon_{p\_i}}{h/2} = \frac{\epsilon_e}{e_i} \Rightarrow e_i = \frac{\epsilon_y}{\epsilon_{p\_i}} \left( \frac{h}{2} \right) \quad (3.3.1.11)$$

At step  $i+1$ , the depth of linear elastic behavior  $e_{i+1}$ , is defined as:

$$\frac{\epsilon_{p\_i+1}}{h/2} = \frac{\epsilon_e}{e_{i+1}} \Rightarrow e_{i+1} = \frac{\epsilon_y}{\epsilon_{p\_i+1}} \left( \frac{h}{2} \right) \quad (3.3.1.12)$$

The relationship between  $e$ , and strain at  $\frac{h}{2}$  is defined by equations (3.3.1.11) and (3.3.1.12) and is shown in Figure 3-4. When  $\varepsilon_{p,max}$  is equal to the ultimate strain of  $15\varepsilon_y$ , the depth of linear elastic behavior is equal to  $\frac{h}{30}$ . Each state of stress – once yielding has occurred – is characterized by the linear elastic depth  $e$ . The post-yield state  $e$  can not theoretically be exactly zero, and therefore, it is simply said to approach zero as the ultimate plastic strain  $\varepsilon_{p,max}$  is approached.

Using the nonlinear stress distribution in equation (2.2.2.1) and assuming an ultimate strain of  $15\varepsilon_y$  in the outermost fiber, equation (2.2.2.2) becomes equal to 14. The internal moments for a rectangular cross section of depth  $h$  and width  $b$ , can be determined by integrating the following equation:

$$M = 2 \left[ \int_0^e [y(\sigma_x)b]dy + \int_e^{h/2} [y(\sigma_x)b]dy \right] \quad (3.3.1.13)$$

Substituting equation (2.2.2.1) into equation (3.3.1.13) for the ultimate strain of  $15\varepsilon_y$ , and integrating, it follows that:

$$M = \sigma_y \left[ \frac{-29\alpha h^2}{56} + \frac{h^2}{4} + \frac{5\alpha h^3}{28e} - \frac{\alpha h^4}{448e^2} + \frac{19\alpha e^2}{28} - \frac{e^2}{3} \right] \quad (3.3.1.14)$$

The post-elastic moment,  $M$ , is valid for any state stress characterized by  $e$  (or the linear portion that remains elastic through the cross-section). Substituting  $e$  equal to  $\frac{h}{30}$  in equation (3.3.1.14) gives the following ultimate internal moment  $M_u$ :

$$M_u = \sigma_y b h^2 \left[ \frac{4459\alpha}{1575} + \frac{337}{1350} \right] \quad (3.3.1.15)$$

When  $\alpha$  is equal to 1, and the depth of linear elastic behavior is equal to  $\frac{h}{2}$  (yield just started to occur), equation (3.3.1.14) reduces to equation (3.3.1.1). When  $\alpha$  is equal to zero, then the response reduces to the perfectly plastic case as shown in Figure 2-1 (a), and equation (3.3.1.15) reduces to equation (3.3.1.2).

The hardening index parameter,  $\alpha$ , as described in chapter 2, is implemented to fit a post-elastic nonlinear material response curve using a linearized guide that is defined as an average modulus between the yield state and some post-yield state. The hardening index enables the constant parabolic distribution to describe the post-yield activity and is determined based on the specific type of material (Attard, 2003). To derive the effective length factors, a hardening index of 0.25 has been chosen, as it provides comparable results with a tested specimen as shown by Attard (2003). Predicting the hardening index could be based on the average degradation between yield and ultimate stress state. An index of 0.25 implies that the average post-yield modulus is reduced to 25 percent of the original modulus. Generally, for shear frame structures, the post-yield stiffness is assumed to be 25 percent of the original floor-level stiffness at the start of an idealized mechanical hinge (UBC, 1997). The nonlinearity is characterized while retaining some common ground with some level of intuition, experience and engineering judgment (Attard, 2003). As discussed above, when  $\alpha$  is chosen as zero, then the response reduces to the perfectly plastic case as shown in Figure 2-1 (a).

The nonlinear post-yield spread is determined over some distance  $q'$  from each end of the column as shown in Figure 3-5.

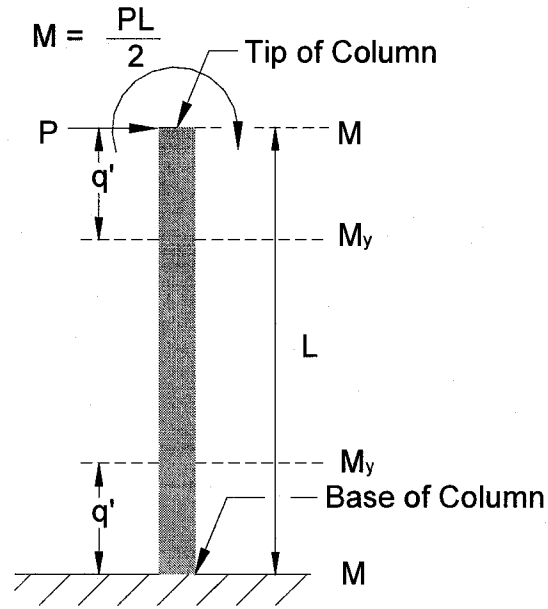


Figure 3-5 Moment Distribution at Column.

This spread distance is calculated through the finite member discretization. The distance from the end of column to the just-yielded strain is defined as  $q'$ . The end of the column can have any strain less than equal to the ultimate plastic strain,  $\epsilon_{p,max}$ . When full plastification occurs at the tip of the column (see Figure 3-5),  $q'$  is equal to the plastic hinge length,  $L_p$  as shown in Figure 3-6. The distance from the full plastified end to any strain greater than equal to the yield strain,  $\epsilon_y$  is defined as  $q$ . These two variables are not additive in finding  $L_p$ , because of the curvature nonlinearity. The spread length  $q'$  can be written as:

$$\frac{M}{L} = \frac{M_y}{L - 2q'} \Rightarrow q' = \frac{L}{2M} [M - M_y] \quad (3.3.1.16)$$

Combining equations (3.3.1.14) and (3.3.1.15), it can be written that:

$$q = \frac{L}{2} - \frac{4725L}{h^2(26754\alpha + 2359)} \left[ \frac{-29\alpha h^2}{56} + \frac{h^2}{4} + \frac{5\alpha h^3}{28e} - \frac{\alpha h^4}{448e^2} + \frac{19\alpha e^2}{28} - \frac{e^2}{3} \right] \quad (3.3.1.17)$$

The plastic hinge is found when ultimate plastic strain  $\epsilon_{p,max}$  is equal to equation (3.3.1.3). At this stress state, the depth of linear elastic behavior is equal to  $\frac{h}{30}$ . The distance from the hinge to various strain levels (less than  $\epsilon_{p,max}$ ) can be computed by equation (3.3.1.17).

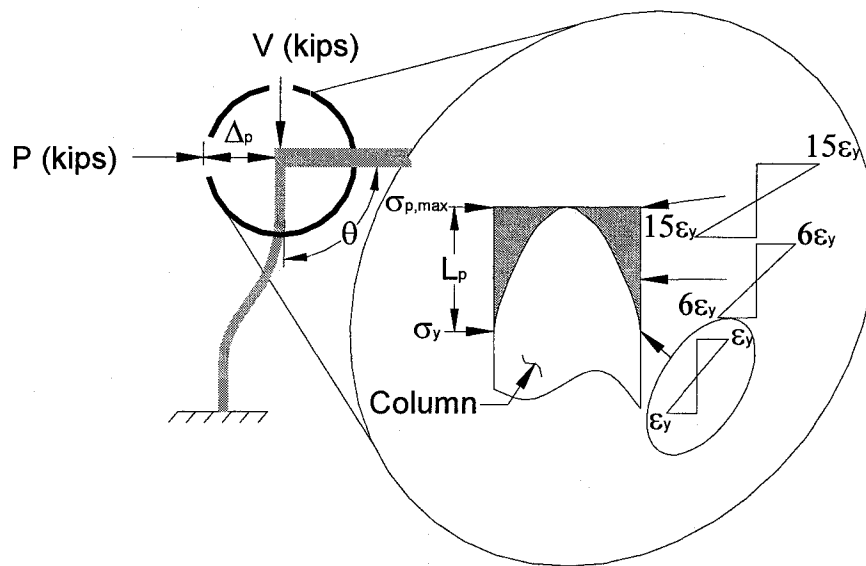


Figure 3-6 Material Degradation at Plastic Hinge.

Conversely, the distance from the end of the column for any strain level to the just-yielded strain is defined by  $q'$ . Substituting equation (3.3.1.1) to equation (3.3.1.14), and then into equation (3.3.1.16) yields the following equation for  $q'$ :

$$q' = \frac{L}{2} - \frac{Lh^2}{12 \left[ \frac{-29\alpha h^2}{56} + \frac{h^2}{4} + \frac{5\alpha h^3}{28e} - \frac{\alpha h^4}{448e^2} + \frac{19\alpha e^2}{28} - \frac{e^2}{3} \right]} \quad (3.3.1.18)$$

Figure 3-7 shows the distribution of  $q'$  for various strain levels at the end of the column. As the outermost strain level increases the post yield curvature moves away from the end of the column. The post-yield length (PYL) is equal to 49.55 inches when the ultimate plastic strain  $\epsilon_{p,max}$  is equal to  $15\epsilon_y$  for the shear frame structure shown in Figure 3-2. By developing the post-yield curvature, displacements are computed through finite elements at discrete strain levels along distance  $q$ .

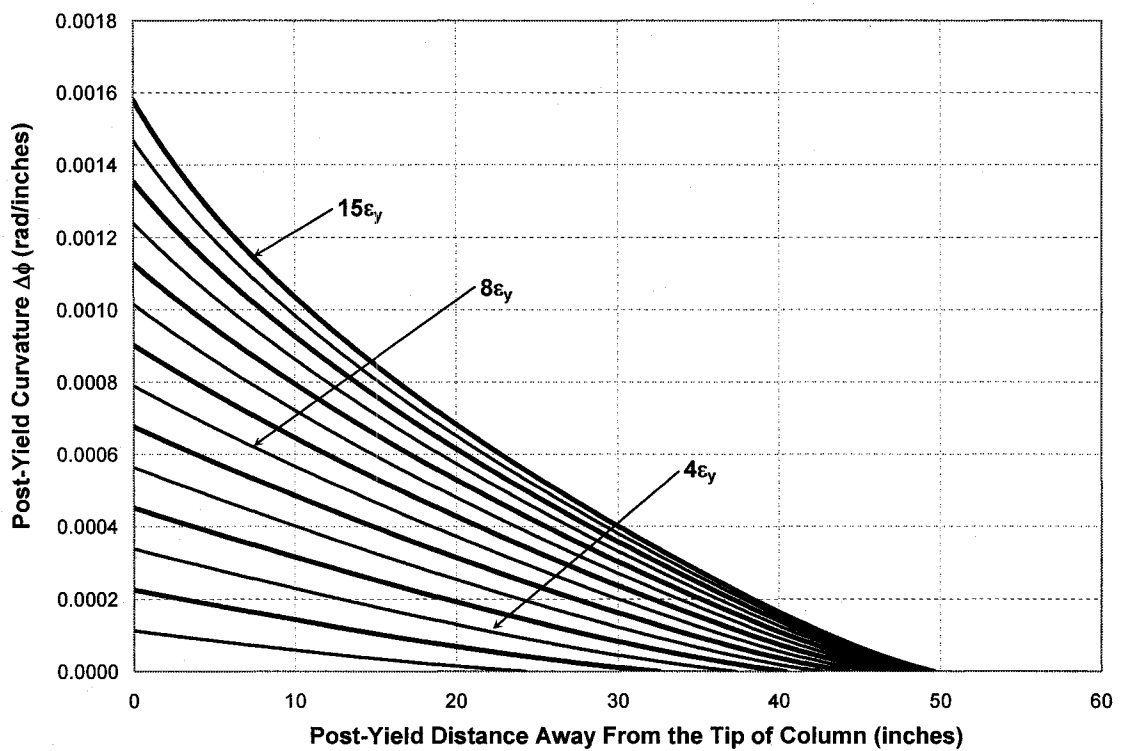


Figure 3-7 Post-Yield Curvature Along Length of Column.

Total curvature – for the ultimate state – along the length of the column is shown in Figure 3-8. The curvature has a nonlinear characteristic away from the distance along the length of the column where the material has just started to yield.

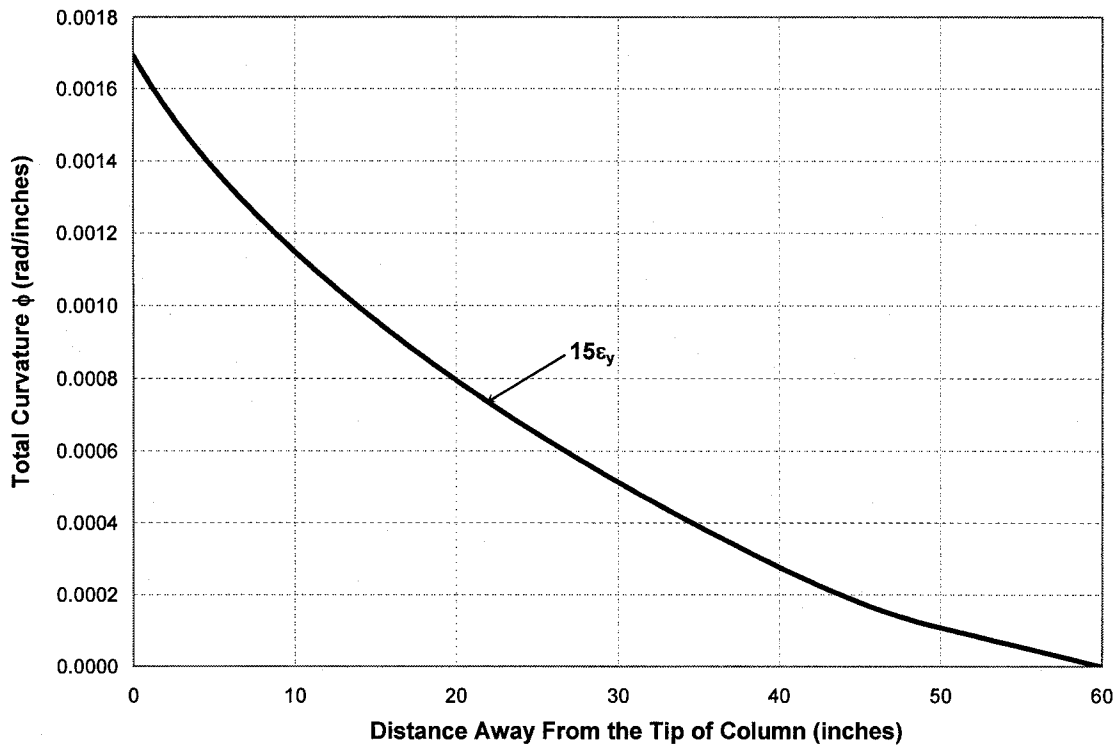


Figure 3-8 Total Curvature Along Length of Column.

Figure 3-9 shows the post-yield curvature along the length of the column. The shape of the post-yield curvature is symmetrical about the centerline of the member since the loading is symmetrical, i.e., each end of the shear frame column has a moment of  $\frac{PL}{2}$ . Lateral member tip deflections are computed via numerical integration techniques. The continuous post-yield curvature function is subdivided into a finite number of elements of thickness  $d(\Delta\phi)$  as shown on Figure 3-9. When the strain at the end of column is equal to  $15\epsilon_y$  the distance  $q$  to the just yielded strain would equal the plastic length  $L_p$ .

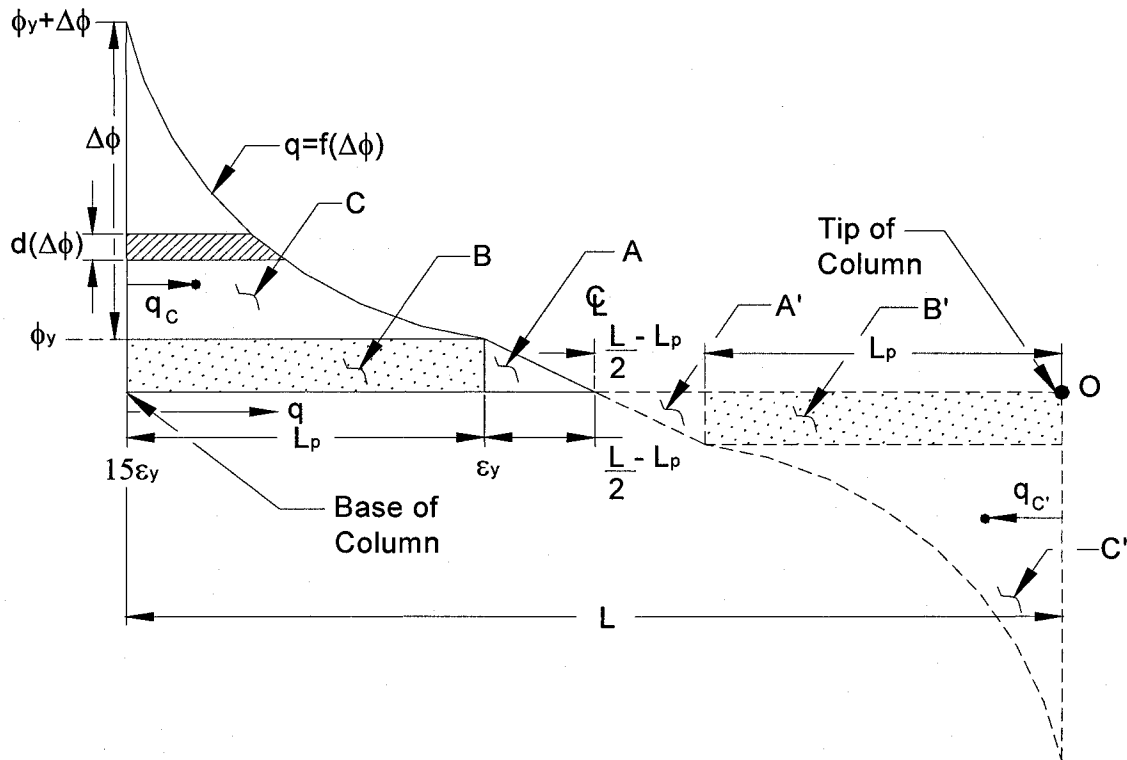


Figure 3-9 Post-Yield Curvature Diagram Along Length of Column.

At the plastic length  $L_p$ , the change in curvature is  $\Delta\phi = \frac{14\epsilon_y}{h/2}$  when solving

equation (3.3.1.10) for the total number of increments,  $N$ , as defined by equation (3.3.1.8). The conjugate-beam analysis, which relies on the principles of statics, whereby moments are summed about the inflection point at the center height of the column,  $L/2$ , is implemented to compute the tip deflections in conjugation with numerical integration techniques. The conjugate-beam method does not require the stress to be proportional to the strain; it simply requires a definition of curvature to predict deflections irrespective of the state of stress (Englekirk, 1994). When the plastic hinge length  $L_p$ , has developed, the deflections at the tip of the



column can be found by summing up the area under the curvature diagram about the point O, as shown in Figure 3-9.

$$\begin{aligned} \Delta u_{,15\varepsilon_y} = & \phi_y \left[ L_p \left( L - \frac{L_p}{2} \right) + \frac{1}{2} \phi_y \left[ \frac{L}{2} - L_p \right] \left( \frac{L}{2} + \frac{2}{3} \left( \frac{L}{2} - L_p \right) \right) + C \left( \frac{L}{2} + \left( \frac{L}{2} - q_c \right) \right) \right] - \\ & - \phi_y \left[ L_p \left( \frac{L_p}{2} \right) - \frac{1}{2} \phi_y \left[ \frac{L}{2} - L_p \right] \left( L_p + \frac{1}{3} \left( \frac{L}{2} - L_p \right) \right) \right] - C'(q_c) \end{aligned} \quad (3.3.1.18)$$

The nonlinear post-yield curvature is integrated and accurate deflections are computed as the material is degrading via the gradual spread of yielding. In a similar manner and using the same techniques, the deflections can be computed along the length of the member at each discrete strain level (i.e.,  $1\varepsilon_y$ ,  $2\varepsilon_y$ ,  $3\varepsilon_y$ ... $15\varepsilon_y$ ) by only knowing the curvature distribution and the boundary condition. Given these two knowns, the deformations and rotations along the length of the member can be computed, regardless of whether or not it is a determinate system. Table 3-2 gives the computed deflections along the length of the column when the maximum strain has reached the ultimate value of  $15\varepsilon_y$ . As an example using the shear frame in Figure 3-2, the column height is 120 inches and the cross section is assumed to be rectangular (10in. x 22in.) and composed from a grade A36 steel; this is chosen as an example where the model in equation (2.2.2.1) had also been successfully applied to a wide-flange section (Attard, 2005). The distance from the maximum strain of  $15\varepsilon_y$  to the location where the strain has just started to yield ( $\varepsilon_y$ ) was calculated as 49.55 inches. At this location, the deflection is computed as 1.946 inches by

numerically integrating the continuous post-yield curvature distributions in Figure 3-9. Similarly, the deflection from  $15\varepsilon_y$  to any other discrete strain level is given in Table 3-2 below.

<b>Strain Level (in/in)</b>	<b><math>\Delta</math> – Deflections (inches)</b>	<b>q (inches)</b>
$\varepsilon_y$	1.946	49.555
$2\varepsilon_y$	2.197	42.456
$3\varepsilon_y$	2.375	37.204
$4\varepsilon_y$	2.527	32.463
$5\varepsilon_y$	2.660	28.069
$6\varepsilon_y$	2.774	23.980
$7\varepsilon_y$	2.869	20.185
$8\varepsilon_y$	2.947	16.675
$9\varepsilon_y$	3.009	13.449
$10\varepsilon_y$	3.057	10.506
$11\varepsilon_y$	3.091	7.843
$12\varepsilon_y$	3.114	5.462
$13\varepsilon_y$	3.129	3.361
$14\varepsilon_y$	3.136	1.540
$15\varepsilon_y$	3.138	0.000

Table 3-2 Deflections Along Length of Column for  $15\varepsilon_y$  End Strain.

Figure 3-10 shows the graph of deflections along the column length. In other words, this can also be considered as the displaced shape of the column from the just yielded cross section to the cross section where the ultimate plastic strain  $\varepsilon_{p,max}$  of  $15\varepsilon_y$  has been reached. The displaced shape has a parabolic characteristic where an equation of the form  $y = ax^2 + bx + c$  best describes the deflected curve. The R-square correlation factor is equal to 0.999. This statistic R-square factor tells us how successful the fit is in explaining the variation of the data. The R-square factor is approximately equal to 1, indicating that a greater

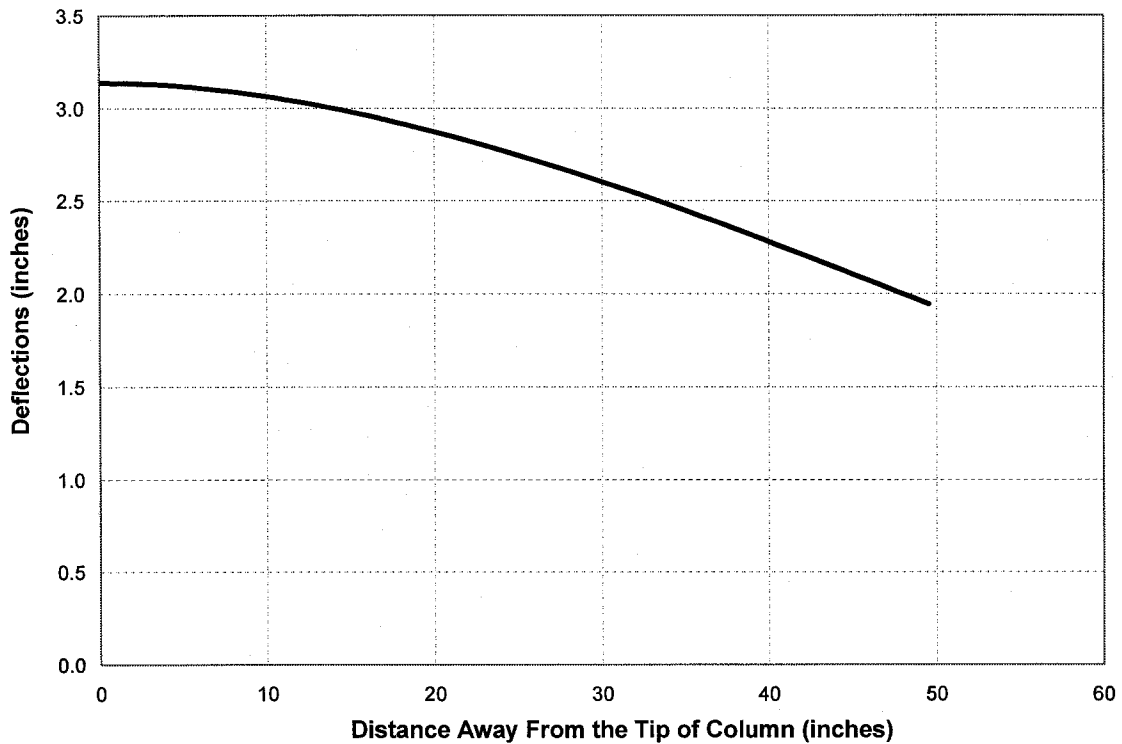


Figure 3-10 Deflections Along Length of Column for  $15\epsilon_y$  End Strain.

proportion of variance is accounted for by the model.

The equation of the deflected curve is differentiated to obtain the location where the slope is equal to zero. Intuitively, the deflected curve would have the zero slope at some distance away from the end of the column, where the maximum ultimate strain has been reached. Taking the first derivative of the obtained equation allows calculating the distance from the end of the column to where the deflected curve would have a slope of zero. The importance of calculating this distance is explained below.

It can be seen in Figure 3-11 that the right angle exists in the elastic analysis (i.e., yield has not yet occurred) of shear frame structures as defined in

chapter 1. Once the material has started to yield the angle of rotation  $\theta$  is no longer  $\frac{\pi}{2}$  radians. Angle  $\theta$ , shown in Figure 3-12, increases as the material starts to degrade by the gradual spread of yielding. Consequently, as described above the effective length factor would increase gradually as the ultimate state is approached. Unlike the current design code procedures, wherein a constant effective length factor has been used, this research assesses the axial stability of steel beam-column elements by gradually updating the  $K$  factor as the material starts to degrade. The optimal distribution of  $K$  factors at each post-yield strain is explained in the following section.

Various investigators have provided charts to determine the effective length factors for commonly encountered situations. Effective length factors  $K$  are given by Anderson and Woodward (1972) for stepped columns, Sandhu (1972) for columns having an intermediate axial load, Lu (1965) for gabled frames, Fraser (1989) for pin-based crane columns, Stoman (1989) for cross bracings, Rutenberg and Scarlat (1990) for columns in one-story buildings and Hassan (1968) for one-story, one-bay frames, having vertical loads applied to the columns at an intermediate point in addition to the load at the top (Salmon and Johnson, 1996).

Columns will buckle inelastically in region C of Figure 3-15 (i.e.,  $\lambda_c < 1.5$ ). When the column is behaving inelastically and the beam is elastic, an adjustment factor is introduced in the restraint factor  $G$  of alignment charts that were originally developed by O. J. Julian and L. S. Lawrence as presented by T. C. Kavanagh (1962). There is precedent for modifications of effective length

factors already in current AISC LRFD practice denoted by the *inelastic stiffness reduction factor* – typically represented by the notation *SRF* – used in column buckling solutions or the calculation of effective length factors. Furthermore, it is important to note that such stiffness reduction factors are not easily implemented and mistakes are often made as noted by Harichandran (1991).

For unbraced structures, an arbitrary selection of effective length factor  $K$  is not satisfactory for design (Salmon and Johnson, 1996). An arbitrary selection could be considered the effective length factor values that are given in Table 3-1. A simpler, more transparent and more accurate analysis-design approach is discussed below to accurately compute and determine the effective length factors.

The lateral stability of the shear frame structures depends upon the bending stiffness of rigidly connected beams and columns. For a shear frame structure, the beam is assumed to be rigid and it restrains the end of the column from rotating. To compute the effective length factor  $K$ , the column of the shear frame structure shown in Figure 3-2 is shown below in detail. It is emphasized that the angle  $\theta$ , is  $\frac{\pi}{2}$  radians prior to yielding.

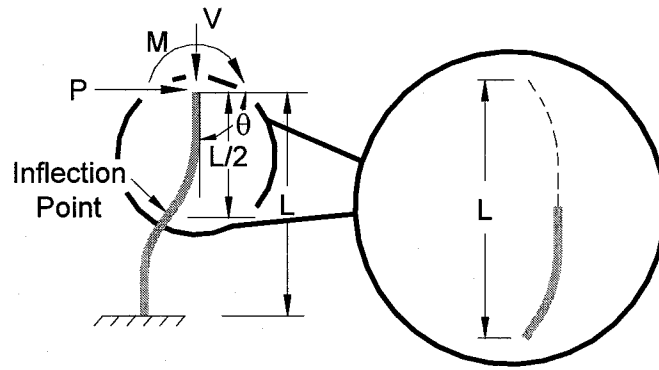


Figure 3-11 Displaced Column Shape Diagram Prior to Yielding.

The displaced shape would be as depicted in Figure 3-11. The inflection point is at mid-height ( $\frac{L}{2}$ ). Drawing an 'imaginary' line (represented by the dashed line) from the tip of the column, as shown in Figure 3-11, the effective length factor  $K$  can be derived. As it is seen from Figure 3-11, the effective length factor  $K$  will be equal to unity for elastic behavior. The degradation of the material at the connection level will create a soft-story structure. The end rotations are no longer restrained as the material starts to degrade by the gradual spread of yielding. Furthermore, the angle of rotation  $\theta$  is no longer  $\frac{\pi}{2}$  radians. Once the material has started to develop the PYL (post-yield length), the effective length factor shown above for the elastic behavior is no longer valid. By determining the distance from the end of the column to where the deflected curve of the column would have a slope of zero, as explained above, an accurate effective length factor can be predicted for any state of post-yield strain (or stress). This is necessary in calculating the potential contribution of the buckling stresses to the overall state of stress in the material via equation (3.2.1)

where  $K$  impacts the length  $L$ . Therefore, at each strain increment according to equation (3.3.1.5), the stress-strain diagram is potentially adjusted to account for any reduced capacity due to any buckling, where the buckling is projected onto the post-yield states using Figure 3-1 and knowing the compactness of the section. This is elaborated in to a greater detail extent later.

Figure 3-12 shows the displaced shape of the column after yielding has occurred. The 'imaginary' additional length that is computed above the shear frame in Figure 3-2, due to the PYL, will increase the effective length factor  $K$ . This 'imaginary' length is a result of the sidesway that the frame experiences and the degrading nature of the beam-column connection as shown in the figure. The 'imaginary' additional distance, when the ultimate plastic strain  $\epsilon_{p,max}$  of  $15\epsilon_y$  has been reached, is equal to 21.570 inches. This gives an effective length factor of 1.180.

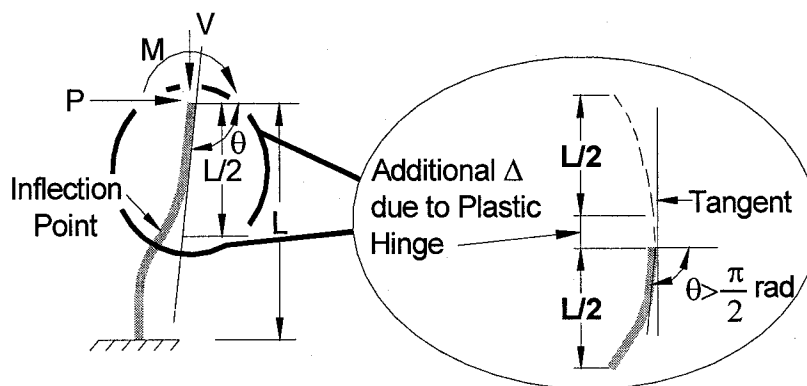


Figure 3-12 Displaced Column Shape Diagram after Yield.

Table 3-1 gives a theoretical effective length factor  $K$  equal to 1.0 for condition (c) (fixed end with other end restrained against rotations, i.e., a shear frame structure). It is important to note that this is for the elastic solution of the buckled shape of the column. In structural design philosophy, AISC LRFD (2001) recommends the effective length factor  $K$  to be equal to 1.2. The calculated  $K$  factor of 1.180 compares favorably with the recommended  $K$  factor for the ultimate plastic strain of  $1.5\varepsilon_y$ . It is important to note that this similarity validates the calculation approach for finding  $K$  for other states of degradation. While the  $K = 1.2$  factor is acceptably close to the calculated value herein ( $K = 1.18$ ), other  $K$  factors for other states of degradation (where the connection state lies somewhere between that of fixed and pinned) remain undetermined via the Code. It is for this reason that it was necessary to calculate all other  $K$  values for all other states since the stress-strain model in equation (2.2.2.1) will be discretized into 1,400 states – where 1,398 states lie somewhere in between yield and ultimate and are characterized by something between a fixed – end and a pinned-end. This ultimately enables the buckling effects to be adequately calculated at each post-yield strain state, by again, projecting the Euler buckling curve in Figure 3-1 onto the post-yield domain. As such, the deflections at each discrete strain state along length of the column are computed, as explained above, and are shown in Figure 3-13. For each discrete strain level, the effective length factors  $K$  are similarly calculated and are shown in Table 3-3 below.



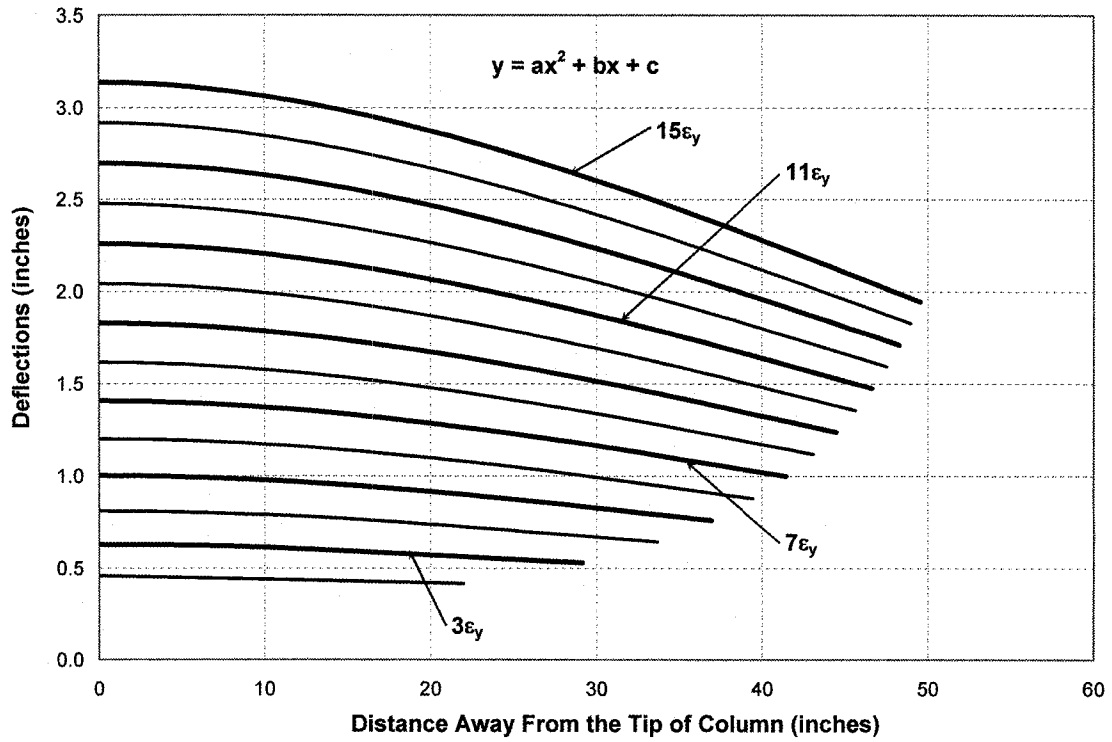


Figure 3-13 Deflections Along Length of Column for all Discrete End Strains.

Strain Level (in/in)	Computed K factor
2ε <sub>y</sub>	1.000
3ε <sub>y</sub>	1.034
4ε <sub>y</sub>	1.069
5ε <sub>y</sub>	1.095
6ε <sub>y</sub>	1.114
7ε <sub>y</sub>	1.130
8ε <sub>y</sub>	1.142
9ε <sub>y</sub>	1.151
10ε <sub>y</sub>	1.158
11ε <sub>y</sub>	1.164
12ε <sub>y</sub>	1.169
13ε <sub>y</sub>	1.173
14ε <sub>y</sub>	1.177
15ε <sub>y</sub>	1.180

Table 3-3 Computed Effective Length Factor K for Discrete Strain Levels.

For the  $1\varepsilon_y$  strain state, the effective length factor has been discussed above and is equal to 1. Figure 3-14 shows the optimal distribution of such factors versus the discrete strain state at the end of the column, i.e., where the maximum end strain state is  $1\varepsilon_y, 2\varepsilon_y, 3\varepsilon_y, \dots, 15\varepsilon_y$ . The distribution of effective length factors versus the discrete strain level has a parabolic characteristic where an equation of the form  $y = ax^3 + bx^2 + cx + d$  best describes the deflected curve. The R-square factor is equal to 1.000.

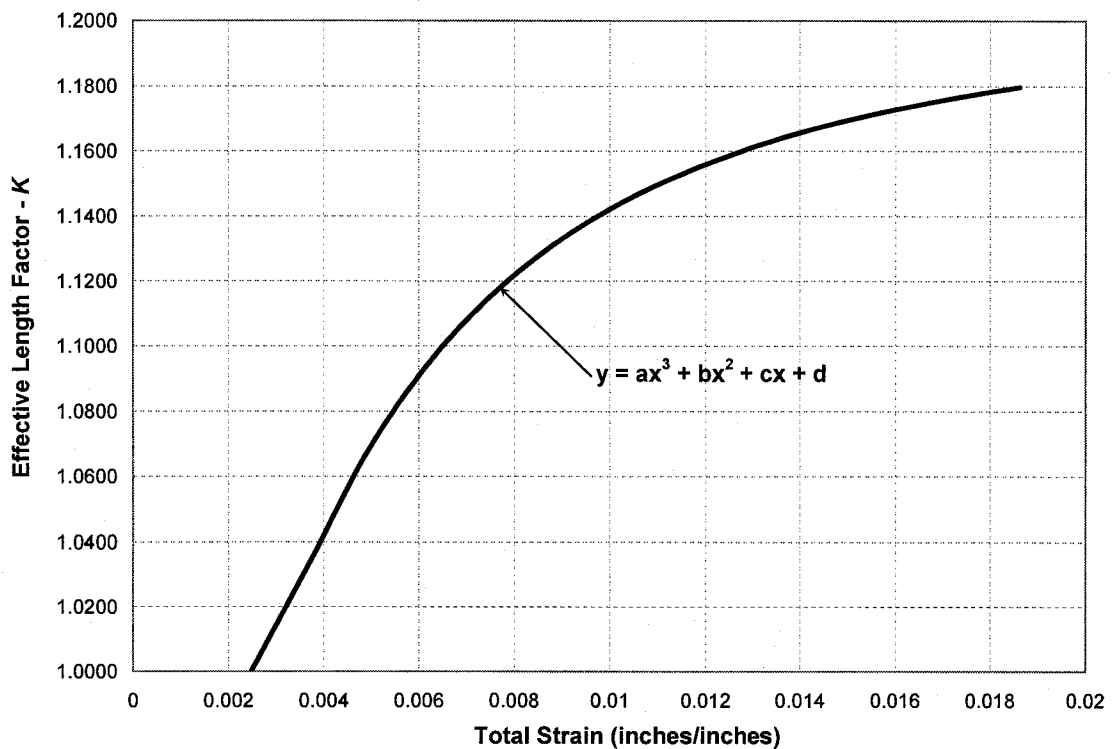


Figure 3-14 Optimal Distribution of Effective Length Factors.

### 3.4 Strength Equations of Columns

The establishment of an acceptable single equation for the critical stress  $F_{cr}$  has been the subject of some controversy since, as has been shown, the shape of the cross section and method of manufacture (i.e., hot-rolling or welding) influence the strength of the column. Furthermore, residual stresses and out-of-straightness are significant factors that while significant are not quantifiable (Salmon and Johnson, 1996). Hall (1981) has compared data from physical tests and has presented statistically-derived expressions for  $F_{cr}$ . In this light, Lui and Chen (1984) have discussed the design of columns with imperfections using beam-column approach.

The critical strength of the column is given by:

$$\text{For } \lambda_c \leq 1.5 \quad F_{cr} = (0.658^{\lambda_c^2}) \sigma_y \quad (3.4.1)$$

$$\text{For } \lambda_c > 1.5 \quad F_{cr} = \left[ \frac{0.877}{\lambda_c^2} \right] \sigma_y \quad (3.4.2)$$

$$\text{Where} \quad \lambda_c = \frac{KL}{r} \sqrt{\frac{\sigma_y}{\pi^2 E}} \quad (3.4.3)$$

These equations are taken from AISC LRFD (2001). Equations (3.4.1) and (3.4.2) are based on a reasonable conversion of research into design equations. These equations are based on an initial out-of-straightness curve of  $\frac{L}{1500}$  (Bjorhovde, 1972 and 1988; Galambos, 1998; Tide, 1985). These sets of equations provide

satisfactory range of reliability, since the limits of out-of-straightness combined with residual stresses have not been clearly established. Furthermore, there has been no history of unacceptable behavior of columns using such equations AISC (LRFD, 2001).

Equations (3.4.1) and (3.4.2) provide a transitional relationship that predicts the stability state for a column as it transitions from elastic behavior as predicted by the Euler equation (3.2.1) (Englekirk, 1994).

Figure 3-15 shows the critical stress  $F_{cr}$  versus slenderness parameter  $\lambda_c$ . Region C defines the inelastic behavior of columns while Region B follows the Euler equation. The critical stress equations (3.4.1) and (3.4.2) are based on the elastic perfectly plastic design philosophy. In view of formulating an axial post-yield stress distribution for analysis and design of beam-column elements of shear frames, the critical stress  $F_{cr}$  is converted in terms of the constitutive model defined in equation (2.2.2.1) by the following equation:

$$\sigma_{axial} = \frac{F_{cr}\sigma_x}{\sigma_y} \quad (3.4.4)$$

Equation 3.4.1 predicts the stability of columns that are included in the inelastic region C of Figure 3-15. The coefficient of 1.5 for  $\lambda_c$ , provides the transition from the inelastic region to the elastic region that is described by equation 3.4.2. Equation 3.4.2 is basically the Euler Buckling equation given by 3.2.1. The slenderness parameter that describes the transition of the boundary of elastic and inelastic behavior, corresponds to a stress limit state of  $\frac{\sigma_y}{2}$ .

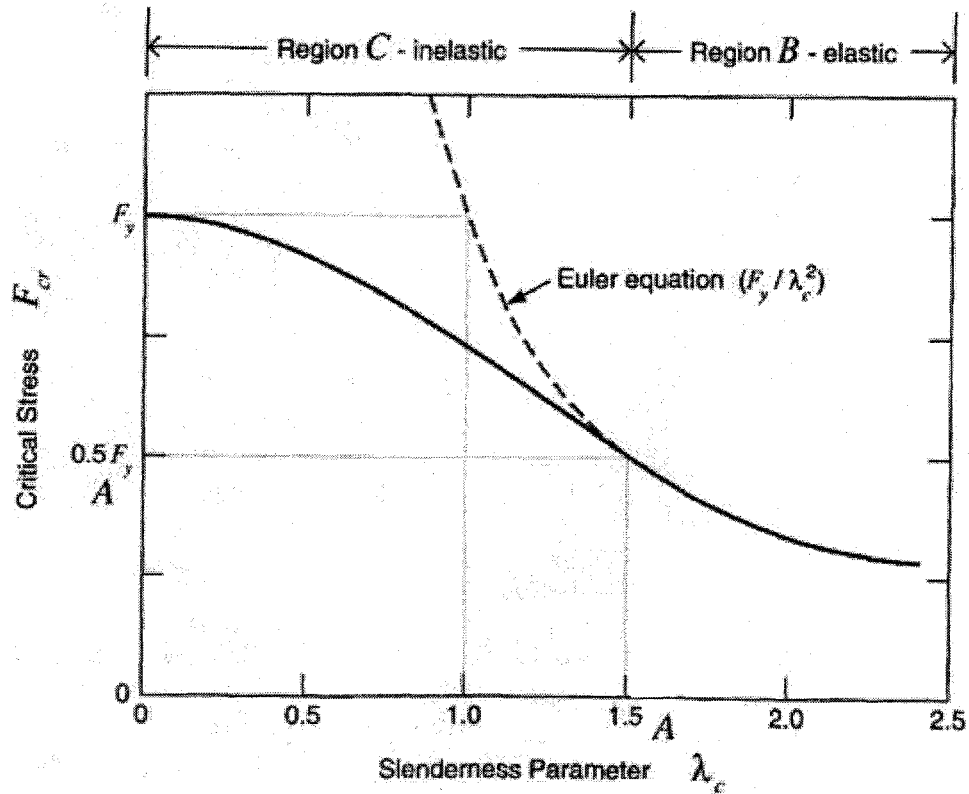


Figure 3-15 Critical Stress as a Function of  $\lambda_c$  (Englekirk, 1994).

As previously discussed in the earlier chapters, equations 3.4.1 and 3.4.2 are projected by equation 3.4.4. For short columns, where  $\lambda_c$  is less than equal to 1.5, the behavior will not comply according to equation 3.4.2, but rather to a post-yield state as shown in Figure 3-1 for observed experimental test results. The proposed method of analysis – given by equation 3.4.4 – determines a new slenderness parameter ( $\lambda_c$ ) which defines an adjusted proportional limit of 0.462. The proportional stress at such limit is somewhat greater than  $4\sigma_y$ . The relationship between the elastic buckling and inelastic transitional curve is shown in Figure 3-16.

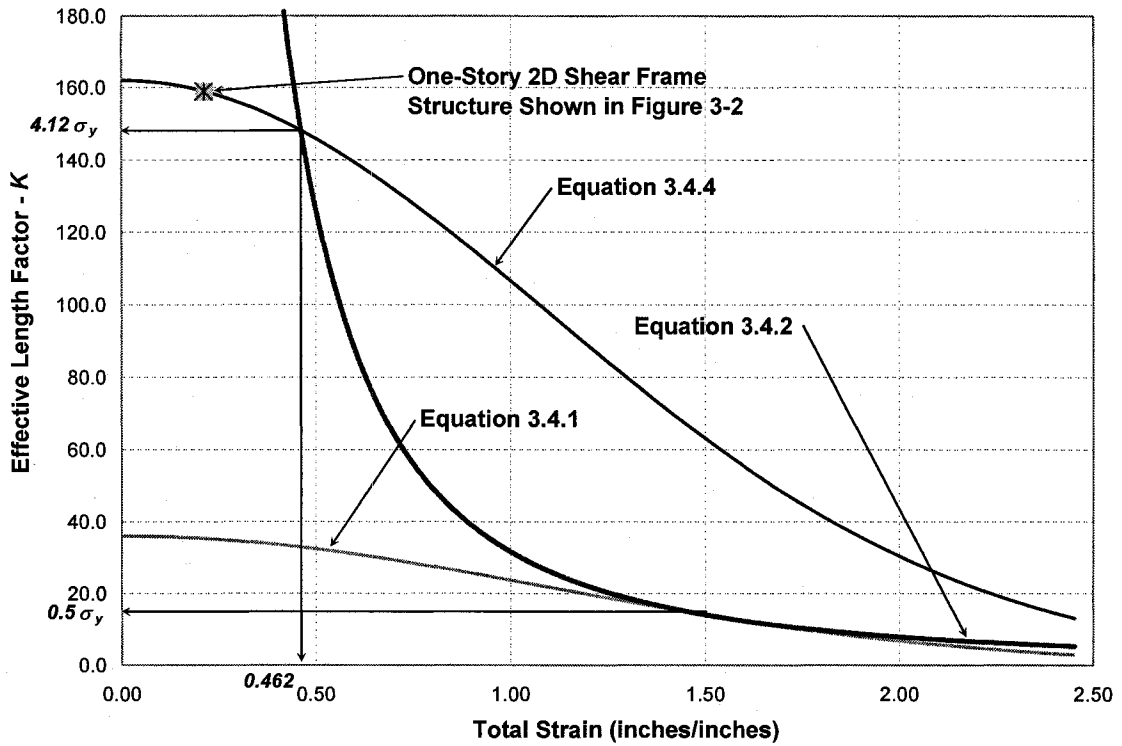


Figure 3-16 Modified Critical Axial Stress as a Function of  $\lambda_c$ .

From Figure 3-16 it is noted that  $\lambda_c = 0.462$  when the parabola given by equation 3.4.4 and Euler hyperbola given by equation 3.4.2 intersect. Such intersection defines the boundary of post-yield behavior of short columns to those of intermediate and long columns that are described by the Euler Buckling equation. The example of the shear frame structure shown in Figure 3-2 is graphed in the modified curve of Figure 3-16. For columns that fall in the values of  $\lambda_c$  greater than 0.462, the Euler equation applies.

## CHAPTER 4

### COMBINED BENDING AND AXIAL LOAD

#### **4.1 Overview**

Beam-columns are defined as members subjected to the combined effects of bending and compression forces. In principle, all members in frame structures are actually beam-columns, with the particular cases of beams (axial forces are equal to zero) and columns (no moments) simply being the two extremes. Depending on 1) the exact manner in which the applied loading is transferred to the member, 2) the form of support provided, and 3) the member's cross sectional shape, the responses will vary significantly. Figure 4-1 shows a beam-column element undergoing lateral deflection as a result of the combination of compression axial load  $V$  and lateral load  $P$ . The moment  $M$  is equal to  $\frac{PL}{2}$  and is caused by the lateral load  $P$ . The moment causes a lateral deflection  $\Delta$  which increases the initial moment by  $V\Delta$ . A significant aspect is the fact that primary moments are then amplified due to the effect of the axial load  $V$  acting through the lateral displacements  $\Delta$ . In other words, the lateral load  $P$  will cause the member to deflect and the axial load  $V$  acting on this deflection will amplify not only this deflection but also the deflection created by the axial load itself. Thus, the combined moment is a function of the lateral load as well as axial load. This effect is called as the secondary moment or *P-delta* effects. Since the *P-delta* effect is a function of the axial load and the tip

displacement of a column, the loss of lateral load resistance due to the *P-delta* effect is unavoidable. The incremental approach undertaken herein is shown to very reasonably model this phenomenon in highly-nonlinear systems.

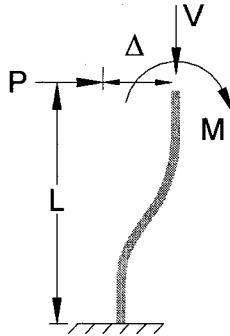


Figure 4-1 Primary and Secondary Moments of Beam-Column Element.

Because of the number of failure modes, no simple design procedure is likely to account for all varied behavior of beam-column elements. Present-day design procedures generally are in one of two categories: (1) limitation on combined stresses; (2) semi-empirical interaction formulas, based on strength. Of the two categories, the interaction equations come closer to describing the true behavior since they account for the stability situations commonly encountered (Salmon and Johnson, 1996). The AISC LRFD (2001) formulas described in chapter 3 can be classified as interaction type.

A new procedure to compute deflections for members subjected to a combination of axial and flexure induced loads is presented for inelastic behavior. Numerical methods described in earlier chapters and the strain increment  $\Delta\epsilon_p$  defined by equation 3.3.1.5 will be used in a similar fashion to predict the lateral displacements of beam-column elements.



## **4.2 Incremental Stresses Analysis Approach**

Structural steel beam-column members do not behave exactly as elastic theory predicts. Inclusion of secondary bending moments becomes necessary as soon as a compression load is applied to the axial members. As a result, this leads to an increase in the lateral deflection due to the further bending of the system and an increase in the amplitude of the lever arm of the external end compression forces. The end result is geometrically nonlinear behavior, which is in addition to the material nonlinearity due to the post-yield straining. It also goes without saying that axial deflections are now also not negligible. As such, not only does the uniaxial strain increase over to the next increment,  $\Delta\varepsilon_p$ , as a result of the axial increment, but the lateral deflection is also amplified. Because geometric linearity is no longer valid (since equilibrium requires a consideration to be given to the deflected shape of the member), the effects of bending and axial loads cannot be simply superimposed in order to describe the actual response since the effects of the material nonlinearity are at work as well. As such, this forces the analysis of the combined effects of bending and axial forces to be made at an incremental level.

The incremental axial deformation at step  $i$ , is derived by the following equation (refer to Figure 4-1):

$$\delta_i = \frac{VL_{initial}}{AE_{initial}} \quad (4.2.1)$$

where,  $L_{initial}$  is defined as the original undeformed length of the column,  $A$  is the cross sectional area as shown in Figure 3-2, and  $E_{initial}$  is the initial modulus at increment step  $i$ . At step  $i+1$ , equation (4.2.1) becomes:

$$\delta_{i+1} = \frac{VL_i}{AE_i} \quad (4.2.2)$$

where  $E_i$  is the plastic modulus at step  $i$ . This equation repeats for the  $N$  number of increment defined in equation (3.3.1.8). The plastic modulus at step  $i$ , is defined as:

$$E_i = \frac{\sigma_{bend\_i} - \sigma_y}{\varepsilon_{p\_i} - \varepsilon_y} \quad (4.2.3)$$

In equation 4.2.3,  $\sigma_{bend\_i}$  is the post-yield bending stress that corresponds to the strain increment given by equation 3.3.1.6 at step  $i$ . At step  $i+1$ , equation (4.2.3) becomes:

$$E_{i+1} = \frac{\sigma_{bend\_i+1} - \sigma_y}{\varepsilon_{p\_i+1} - \varepsilon_{p\_i}} \quad (4.2.4)$$

The tangent plastic modulus values for each state are calculated according to equations (4.2.3) and (4.2.4) and used in the determination of the next post-yield axial strain increment calculation.

The axial post-yield strain at step  $i$ , is defined as:

$$\varepsilon_{axial\_i} = \frac{\delta_i}{L_{initial}} \quad (4.2.5)$$

At step  $i+1$ , equation (4.2.5) becomes (for homogeneous materials):

$$\varepsilon_{axial\_i+1} = \frac{\delta_{i+1} - \delta_i}{L_i} \quad (4.2.6)$$

Similarly (as previously mentioned), this equation repeats for the total  $N$  number of increments. Equation (3.3.1.6) is combined with equation (4.2.5) to determine the incremental total strain at step  $i$ . The process similarly repeats for step  $i+1$ ,  $i+2$ .... up to  $N$  incremental steps. Stresses are combined in an analogous manner and are given below.

The axial post-yield stress at step  $i$ , is defined as:

$$\sigma_{p\_axial\_i} = \frac{F_{cr} \sigma_{bend\_i}}{\sigma_y} \quad (4.2.7)$$

At step  $i+1$ , equation (4.2.7) becomes:

$$\sigma_{p\_axial\_i+1} = \frac{F_{cr} \sigma_{bend\_i+1}}{\sigma_y} \quad (4.2.8)$$

A formulation that is presented allows combining the obtained incremental post-yield stresses and strains. The nonlinear response of the system is generated through the summation of piece-wise linear infinitesimal increments in stress over a pre-established strain increments. Each individual response is used as an initial condition for the forthcoming step, where all the responses are summed together. Individual stress and strain increments are calculated according to the equations presented below. A cumulative summation is maintained to track the total stress-and-strain levels in each post-yield state. The post-yield combined strain at step  $i$ , is defined as:

$$\varepsilon_i = \frac{\sigma_y}{E_{initial}} \quad (4.2.9)$$

At step  $i+1$ , equation (4.2.9) becomes:

$$\varepsilon_{i+1} = \varepsilon_i + (\varepsilon_{p\_axial\_i+1} - \varepsilon_{p\_axial\_i}) \quad (4.2.10)$$

At step i+2, equation (4.2.10) becomes:

$$\varepsilon_{i+2} = \varepsilon_{i+1} + (\varepsilon_{p\_bend\_i+2} - \varepsilon_{p\_bend\_i+1}) \quad (4.2.11)$$

The post-yield combined stress at step i, is defined as:

$$\sigma_i = \sigma_y \quad (4.2.12)$$

At step i+1, equation (4.2.12) becomes:

$$\sigma_{i+1} = \sigma_i + (\sigma_{p\_axial\_i+1} - \sigma_{p\_axial\_i}) \quad (4.2.13)$$

At step i+2, equation (4.2.13) becomes:

$$\sigma_{i+2} = \sigma_{i+1} + (\sigma_{p\_bend\_i+2} - \sigma_{p\_bend\_i+1}) \quad (4.2.14)$$

The process similarly repeats for step i+1, i+2.... up to N incremental steps.

### **4.3 Results**

The incremental form of equations (4.2.9) through (4.2.14) is used to determine the linear increments in post-yield stress-and-strain states. The obtained post-yield stress-strain relationship is shown in Figure 4-2.

The post-yield stresses and strains are updated at the end of each post-yield state (based on all current plastic strain levels) during the incremental loading strategy. The post-yield stress-strain relationship presented in Figure 4-2 provides the graphical representation of the incremental loading strategy for ultimate strain state,  $\varepsilon_{p,max}$ , of  $15\varepsilon_y$  (where  $\Delta\varepsilon = 14$ ) in the outermost fiber.

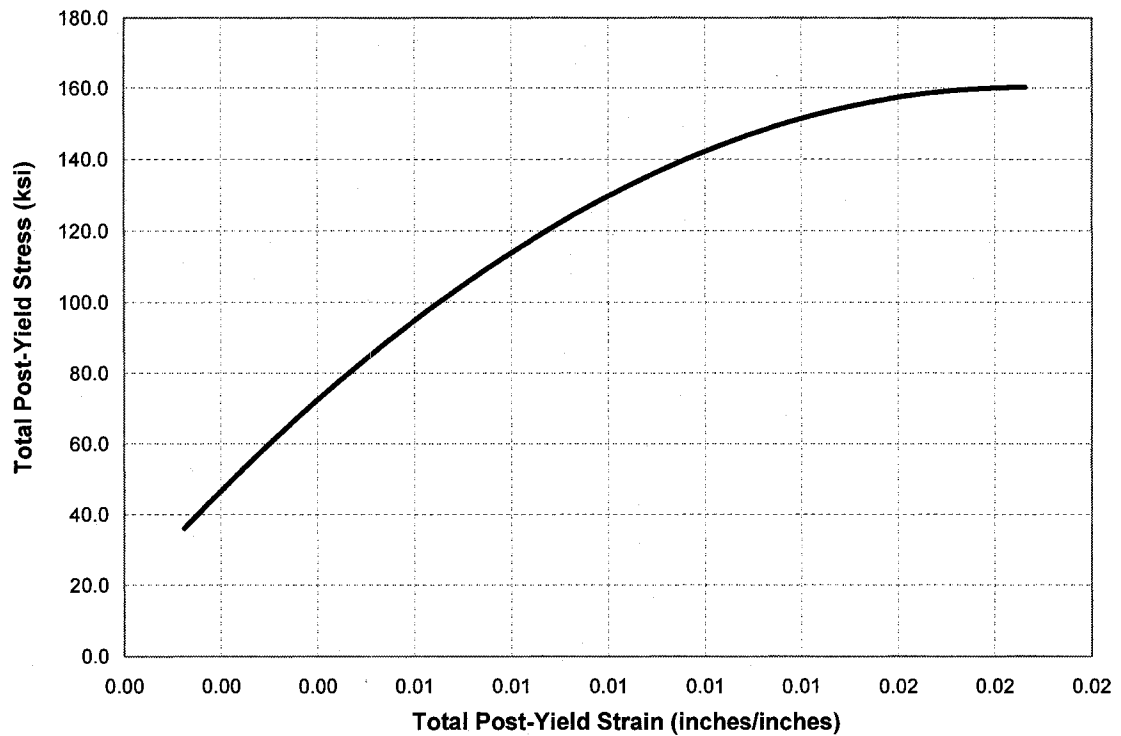


Figure 4-2 Combined Post-Yield Stress-Strain Relationship.

From the perspective of statics the *P-delta* effect can be visualized as an additional lateral loading that causes an increase in member forces and lateral deflections, reduces the lateral load resistance of the structure, and may cause a negative slope in the lateral load-displacement relationship at large displacements resulting in softening (although this is not explicitly discussed herein). For a single-degree-of-freedom (SDOF) system – as shown in Figure 3-2 – of height  $L$  the *P-delta* effect can be represented as illustrated in Figure 4-1. From a dynamic perspective, the *P-delta* phenomena may lead to a significant amplification in the lateral load-displacement relationship leading towards an early failure at a smaller displacement demand during an earthquake event. A given vertical load  $V$  – as shown in Figure 4-1 – is input into the system and stress

and strain increments are calculated according to the equations presented previously. For each state the lateral load is computed by knowing the moment distribution due to lateral effects only. The lateral loads at increment step  $i$ , will produce a lateral deflection that will cause an additional moment due to  $P$ - $\delta$  phenomena discussed previously. Additional secondary moment is added incrementally at each step – up to  $N$  incremental steps – to the primary moment. By knowing the total moment in the system one could calculate the lateral strain at each increment by the use of equation 3.3.1.14. Solving for the cross-sectional linear depth  $e$  at each post-elastic stress state in equation 3.3.1.14 yields the post-yield strain increment that leading to the lateral deflection calculation. During the incremental loading strategy of secondary effects as presented herein, the hardening index parameter  $\alpha$  – that predicts the ultimate failure – is adjusted by an iterative procedure. As previously discussed, the hardening index parameter fits a nonlinear material response curve to a linearized guide that defines an average modulus between any two states – e.g., the yield and ultimate states. For the combined primary and secondary effects, it was determined that the hardening index needed to be adjusted in order for the combined post-yield stress-strain curve to match the relationship shown in Figure 4-2.

As an example, the shear frame shown in Figure 3-2 is used with the following properties: the column height is 120 inches, grade A36 steel is used as the material (for illustrative purposes) the cross section is assumed to be rectangular (10in. x 22in.), and an axial load of 500 kips is applied at each column. The post-yield stress-strain relationship that is shown in Figure 4-2 uses  $\alpha$

of 0.25. The iterative procedure yields  $\alpha$  equal to 0.245 for the combined primary and secondary effects. It is important to note that the value of  $\alpha$  depends on the amount of applied axial load. As the axial load increases,  $\alpha$  will decrease because of the smaller ultimate lateral deflection that will be present when the system finally fails. The relationship between the post-yield primary and secondary moment versus post-yield curvature is shown in Figure 4-3 below.

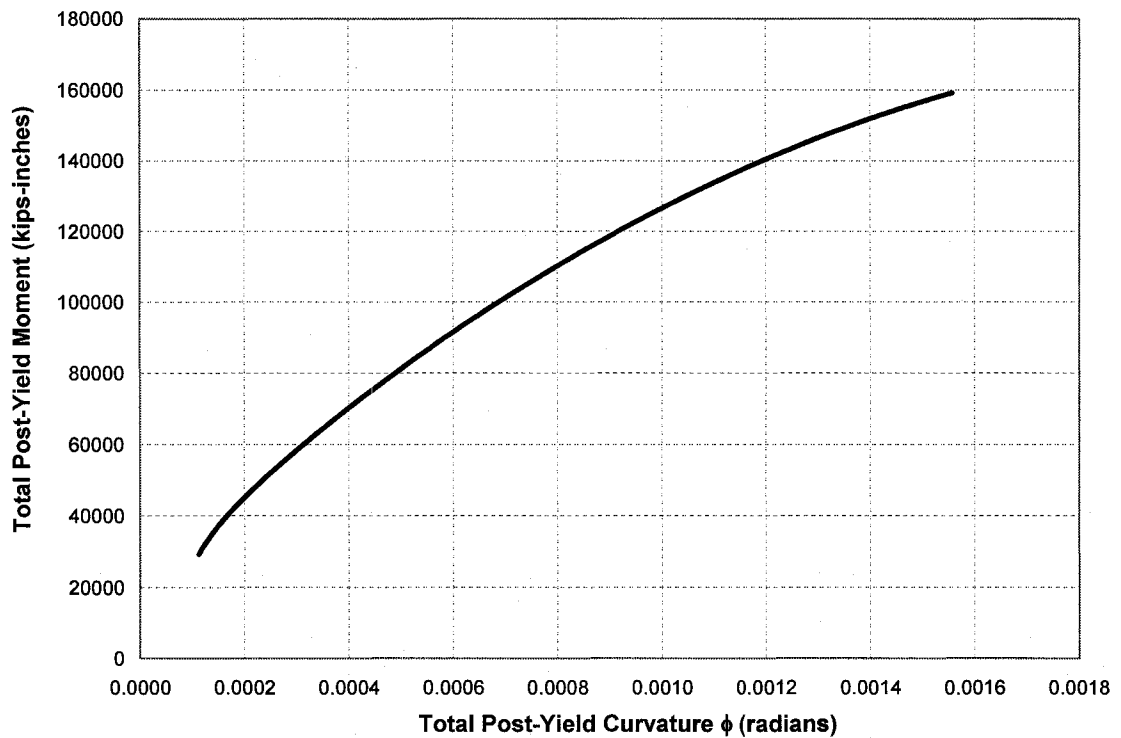


Figure 4-3 Post-Yield Moment Curvature Diagram

The influence of the secondary moments decreases the lateral load resistance. The loss of lateral load resistance due to the degradation of moment capacity and the resulting displacement capacity of a column can be directly attributed to the *P-delta* effect. The moment-curvature relationship, normalized at yield, is shown in Figure 4-4. It is noted that the ultimate moment increases at

an order level of 5.5 times that of yield state while the ultimate curvature increases at an order of 14 times that of yield state.

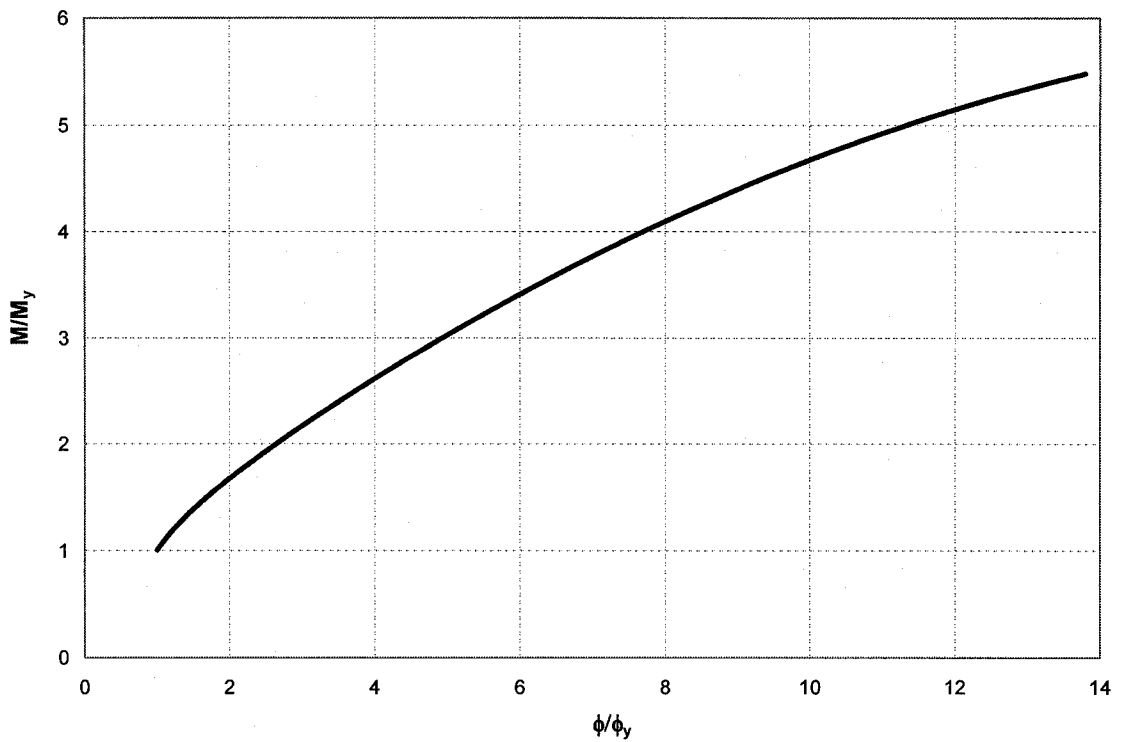


Figure 4-4 Normalized Post-Yield Moment Curvature Relationship

Determining post-yield curvature allows displacements computation through finite elements at discrete strain levels along distance  $q'$  at the very same procedure that was used in chapter 3. Figure 4-5 shows the post-yield curvature for the combined primary and secondary effects. It is important to note that only bending stresses (i.e., primary and secondary) would generate curvature  $\phi$ , that contribute to the lateral deflection calculations.



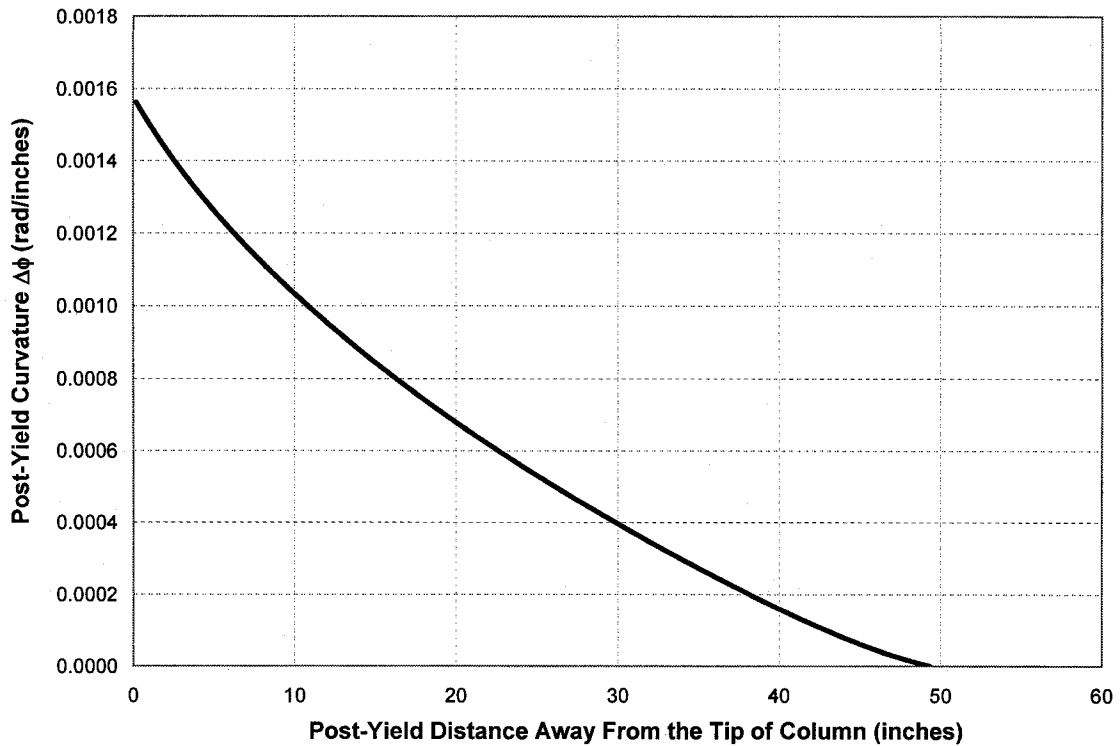


Figure 4-5 Total Post-Yield Curvature Along Length of Column.

The proposed nonlinear analysis method indicates that properties of the structure would be based on explicit modeling of the post-yield behavior of elements. To ensure the safety of civil structures under major earthquakes, it is important to predict the ultimate behavior of steel beam-columns by using the smooth nonlinear curvature distribution. Lateral deflections at each state of stress up to the ultimate state are computed using the analytical rigorous procedure described above. It is noted that post-yield lateral deflections imply that the column has deformed well beyond the elastic limit. Quasi-static loading conditions and a strain rate independent model described by equation 2.2.2.1, lead to a determination of the load-deflection relationship, thereby highlighting

the significant influence of both geometry nonlinearity (i.e., *P-delta* effects) and gradual degradation by the spread of yielding.

It is found that the load-displacement capacity of beam-column elements of Figure 3-2 is dependent on the geometric nonlinearity of the system. Figure 4-6 shows the lateral load-displacement results.

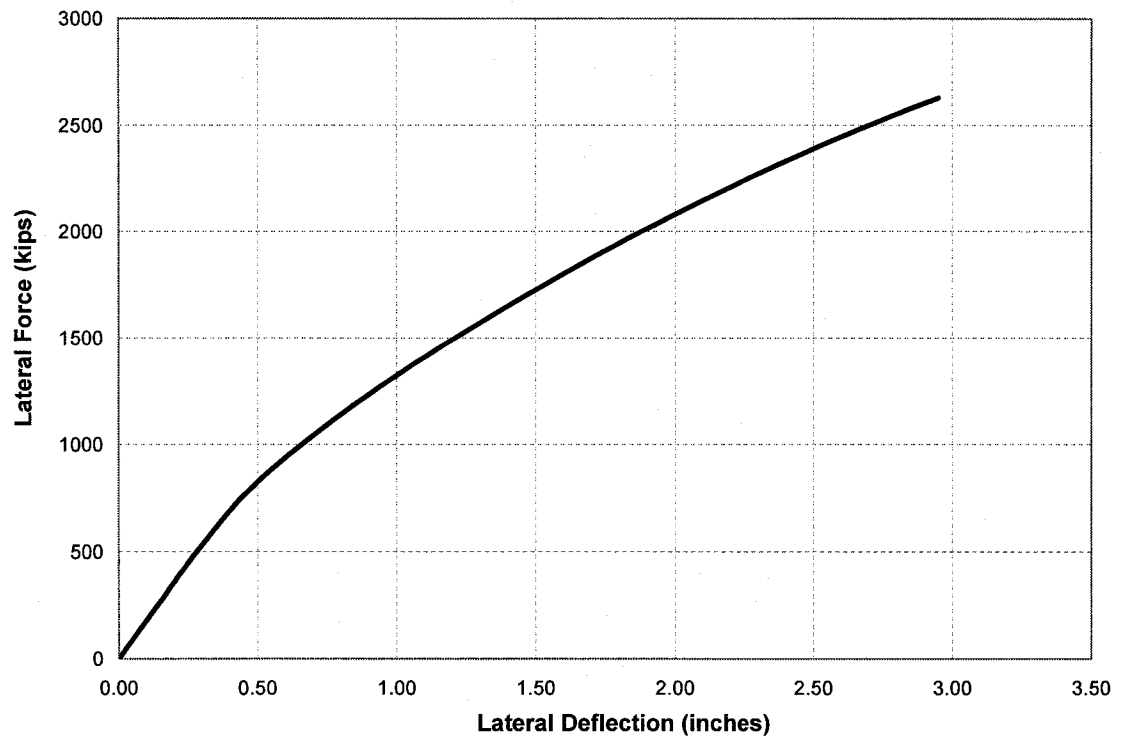


Figure 4-6 Lateral Force-Displacement Curve.

The presented results, which are obtained under the assumptions defined in section 2.2.1, lead one to believe that the *P-delta* phenomena is indeed a potential collapse hazard that needs to be considered explicitly and more realistically than is done in the present design process. The maximum lateral deflection is 2.95 inches for the shear frame model that was referred to above

using the proposed analytical rigorous procedure. If the material stress-strain relationship is assumed to be elastic-perfectly plastic, as done in present design codes, then the plastic hinge length shortens to the height of the cross-section  $h$  (Figure 3-2) as illustrated by literature (Englekirk, 1994). Using such empirical procedures the maximum tip deflection is computed to be 4.06 inches under a quasi-static lateral loading. However, this empirical procedure defines an inaccurate post-yield curvature – that is grossly overconservative – in which the real behavior is not portrayed precisely. Under the quasi-static loading the empirical method is more conservative; however, the small differences carry an important role in predicting the accurate cyclic responses of buildings under dynamic loading since the seismic response becomes very sensitive to modeling assumptions and ground-motion characteristics if the *P-delta* effect is large and the ground motion is sufficiently severe to drive a story in the structure into the range of negative story stiffness, in which the errors become amplified over the course of a hysteresis. The stiffness of the beam-column member of shear frame structure – given in Figure 3-2 – versus lateral deflection is given in Figure 4-7.

The stiffness of the steel beam-column member stays constant prior to yielding. As the material starts to degrade gradually the stiffness reduces nonlinearly as shown in Figure 4-7. Simplified analytical models (e.g., the elastic-perfectly plastic model depicted in Figure 2-1.(a)) may give a misleading picture of the importance of *P-delta* effects, whereas a detailed and accurate finite-element response was obtained using the proposed analytical rigorous model.

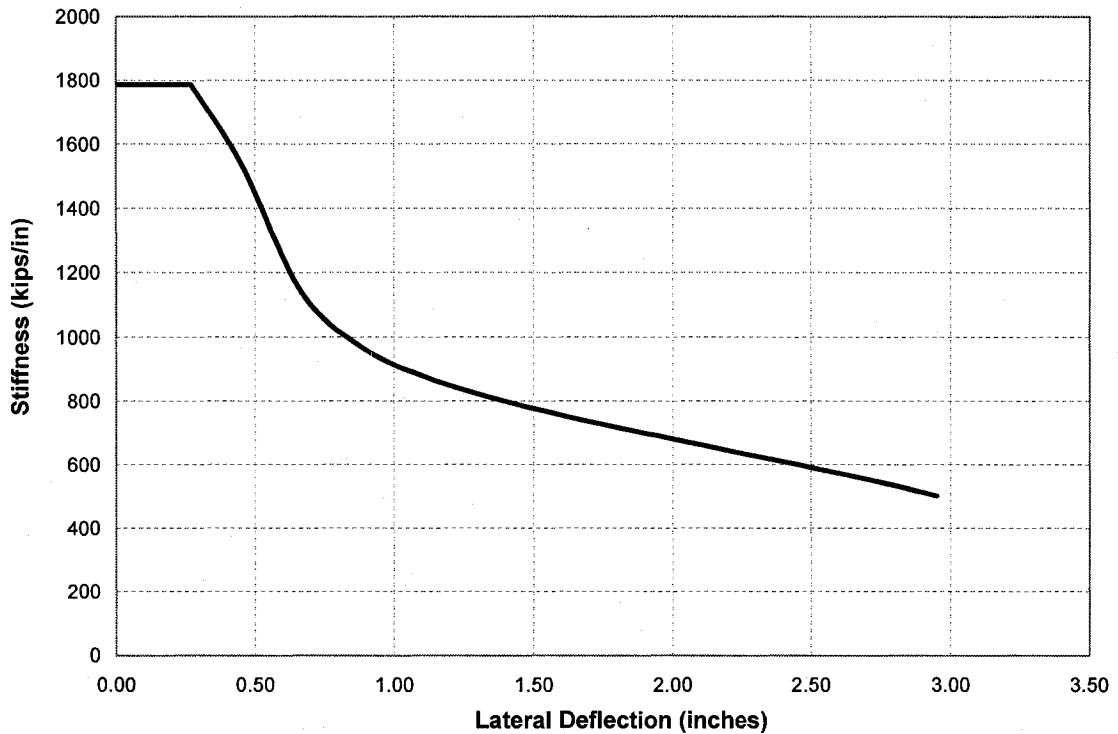


Figure 4-7 Stiffness versus Total Deflection

As previously mentioned, the proposed model is formulated using dislocation theory for conditions where the strain rate is negligible. It is postulated that in addition to the classical deformation by dislocation slip, the interactions between slip dislocations play an additional and critical role in the plastic deformation process in which the dislocation accumulation is only partly reversible due to the post-yield bond annihilation mentioned in the earlier chapters. Dislocation-based plastic deformation processes have a small or negligible dependence on strain rate. It is likely that strain rate contribute to the mild decrease of stiffness during plastic flow, although the exact relative proportion is not known. The effect of increasing the strain rate is generally to

increase the tensile yield (Mendelson, 1999), whereas the Bauschinger effect is left intact.

The validity of the proposed model is examined by comparing it with results of the Finite Element Analysis (FEA) and will be explained in the following chapter.

## CHAPTER 5

### VERIFICATION AND VALIDATION OF THE PROPOSED MODEL

#### **5.1 Overview**

The finite element analysis is now firmly accepted as a powerful technique for numerical solution for a variety of problems that are encountered in engineering (Owen and Hinton, 1980). In this chapter the verification and validation of the aforementioned proposed model is discussed. Different approaches to deciding model validity were considered. It was chosen to utilize MSC.Marc Mentat FEA software to validate the results of the proposed model. MSC.Marc is a general purpose finite element program for advanced FEA simulation. Since 1971, MSC.Marc has been known for its versatility in helping market leaders in various industries to solve simple to complex real-world engineering problems. MSC.Marc Mentat provides expanded support of the nonlinear capabilities.

#### **5.2 Numerical Solution Procedures for Nonlinear Problems**

For nonlinear finite element analysis the solution must proceed on an incremental basis. MSC.Marc Mentat employs iterative procedures for the convergence of the nonlinear solution. The first nonlinear procedure is the Full Newton-Raphson Method or as it has been known as the Variable Parameter of Elasticity. The algorithm for this procedure is given below:

- At load increment  $i$ 
  - Step 0) – Solve for  $\varepsilon_{0,i}$  and  $\sigma_{0,i}$
  - Step 1) – Solve for  $E^{(0,i)}_{\text{effective}}$
  - Step 2) – Solve the problem with new elastic modulus for  $\varepsilon_{1,i}$  and  $\sigma_{1,i}$ . Calculate  $E^{(1,i)}_{\text{effective}}$
- Increment  $i+1$ 
  - Step 3) – Repeat steps 0 through 2 for  $n$ -iterations

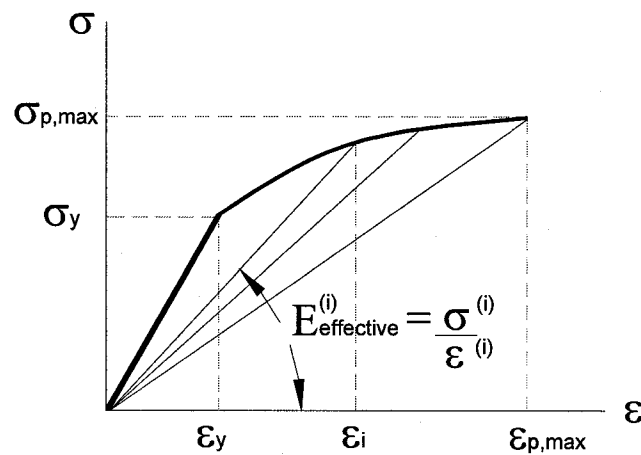


Figure 5-1 Full Newton-Raphson Method.

The iterative procedure is deemed to have converged when some measure of the change in the unknown variable between successive iterations has become tolerably small. In other words, during any step of the iterative process of solution, a tolerance is specified, which will not be satisfied unless convergence has occurred. The procedure is illustrated in Figure 5-1. The aforementioned method requires great computing resources since the stiffness matrix is calculated at step increment  $i$ , although, the Full Newton-Raphson Method

generally gives a more rapid and stable convergence path than the other method that will be described below.

The second nonlinear procedure is the Modified Newton-Raphson Method or as it has been known as the Additional Stresses Method. The algorithm for this procedure is given below:

- Increment  $i$ 
  - Step 0) – Solve for  $\varepsilon_0$  and  $\sigma^{(0)}_{\text{add}}$
  - Step 1) – Solve for  $\varepsilon_1$  and  $\sigma^{(1)}_{\text{add}}$
- Increment  $i+1$ 
  - Step 2) – Repeat steps 0 through 1 for  $n$ -iterations

Similarly as for the Full Newton-Raphson Method, during any step of the iterative process of solution a tolerance is specified, which will only be satisfied when the convergence has occurred. A disadvantage of this method is that convergence of the solution scheme is not guaranteed and cannot be predicted at the initial solution stage, thus requiring more steps and computing effort – although, it requires less computing resources than the Full Newton-Raphson Method since the stiffness matrix does not change with the step increment. Figure 5-2 illustrates the procedure of the Modified Newton-Raphson Method.



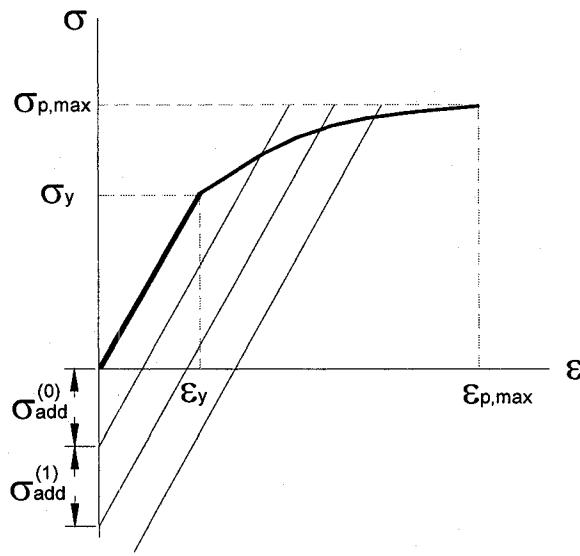


Figure 5-2 Modified Newton-Raphson Method.

### **5.3 FEA Simulations**

The solution of the example shear frame problem formulated in chapter 3, that gives a lateral deflection of 2.95 inches at the ultimate state, would be verified in MSC.Marc Mentat FEA software. Each member of the shear frame structure shown in Figure 3-2 was defined using line finite-elements. Each member was subdivided in 10 elements. The post-yield stress-strain relationship given by Figure 4-2 was manually input into a table. Only 14 data points were used at each discrete strain level (i.e.,  $1\varepsilon_y, 2\varepsilon_y, 3\varepsilon_y \dots 15\varepsilon_y$ ). The software allows a table that defines the stress-strain relationship for an infinite number of data points to be uploaded, but the number of data points that could be used as input appeared to be limited, which seemed to be a shortcoming of the software. Material and geometric properties were defined for the example

problem. The floor was defined as a rigid element in order to represent a shear frame structure. The method of analysis selected was the Full Newton-Raphson Method. A piecewise linear method was used for the data points defining the post-yield stress-strain relationship and a kinematic strain hardening rule was selected.

The maximum lateral deflection at the tip of the column was calculated to be 2.55 inches by the FEA software (see Figures in Appendix). The lateral deflection computed by the proposed rigorous model compares favorably to the results of the FEA. The results indicate that the proposed incremental approach is very reasonable, due to the small discrepancy when compared to the FEA. The marketed FEA approach uses only 14 data points that define the post-yield stress-strain relationship while the proposed model defines the relationship by 1,400 data points. Some accuracy is lost due to this effect. Furthermore, the Full Newton-Raphson Method uses an effective modulus and calculates the solution of the problem based on the post-yield stresses and strains obtained from such a method. The proposed incremental approach uses a tangential stiffness plastic modulus whilst not losing accuracy of the solution.

## CHAPTER 6

### STRUCTURAL RESPONSE TO DYNAMIC LOADING

#### **6.1 Overview**

Natural causes and human activities impose forces of time-dependent variability on simple or complex structures (Paz, 1997). The proposed method of analysis could be used in a design setting office to evaluate seismic requirements of steel beam-column elements under time-dependent inertial forces. It needs to be understood that time-dependency here refers to the imposed dynamic loading and responses; however, the strain-rate itself is negligible in keeping consistent with the proposed plasticity model. New structures should be designed for ground motions of sufficient magnitude that have caused damage in the past. Generally, design codes make such requirements. For existing structures, this means implementing seismic retrofitting strategies as one method of mitigating the risk that currently exists, whilst preventing structural failure that could lead to loss of property and life. The options of not doing seismic retrofitting and thus accepting the risk of failure, and abandoning or replacing the existing structures may be considered for both the importance and degree of vulnerability.

## **6.2 P-delta Effects on a Shear Building**

Horizontal forces in buildings, such as those produced by earthquakes are often resisted by the columns. The floor of a multistory or single story shear building is assumed to be rigid and the weight or masses at each floor are treated as concentrated loads that are lumped at each floor level. The response of a particular structure is then a function of these masses and the stiffnesses of columns at each floor level. In the analysis of the single-degree-of-freedom (SDOF) system – as shown in Figure 3-2 – the restoring force is not proportional to the displacement. Furthermore, the energy dissipated by the viscous damping force is assumed to be proportional to the relative velocity of the building member (assuming Rayleigh Damping). As such, the equation of motion for the above mentioned shear frame structure, is a second order ordinary nonlinear differential equation. The nonlinear force-displacement curve is analyzed at an incremental level. That is, the incremental force is proportional to the incremental displacement. The mass of the aforementioned single story one-bay shear frame structure is taken as  $2.5901 \frac{(kips)(sec)^2}{inches}$ . The hysteretic behavior of the steel beam-column elements is obtained when the structure is subjected to an artificially-generated stationary ground motion. The artificial earthquake record that is shown in Figure 6-1, is generated as Gaussian White Noise and then passed through a Kanai-Tajimi filter function to represent specific ground conditions ( $\omega = \frac{15.6rad}{sec}$  and  $\xi_g = 0.6$ ). The peak ground acceleration is

2316.5  $\frac{\text{inches}}{\text{sec}^2}$ . The dynamic equation of motion of the structure is given as

$m\ddot{x} + c\dot{x} + F_R = -m\ddot{x}_g$ , where  $m$  refers to the mass of the system,  $c$  is the viscous damping,  $F_R$  is the nonlinear restoring force function developed insofar incrementally, and  $\ddot{x}_g$  is the ground acceleration applied to the structure.

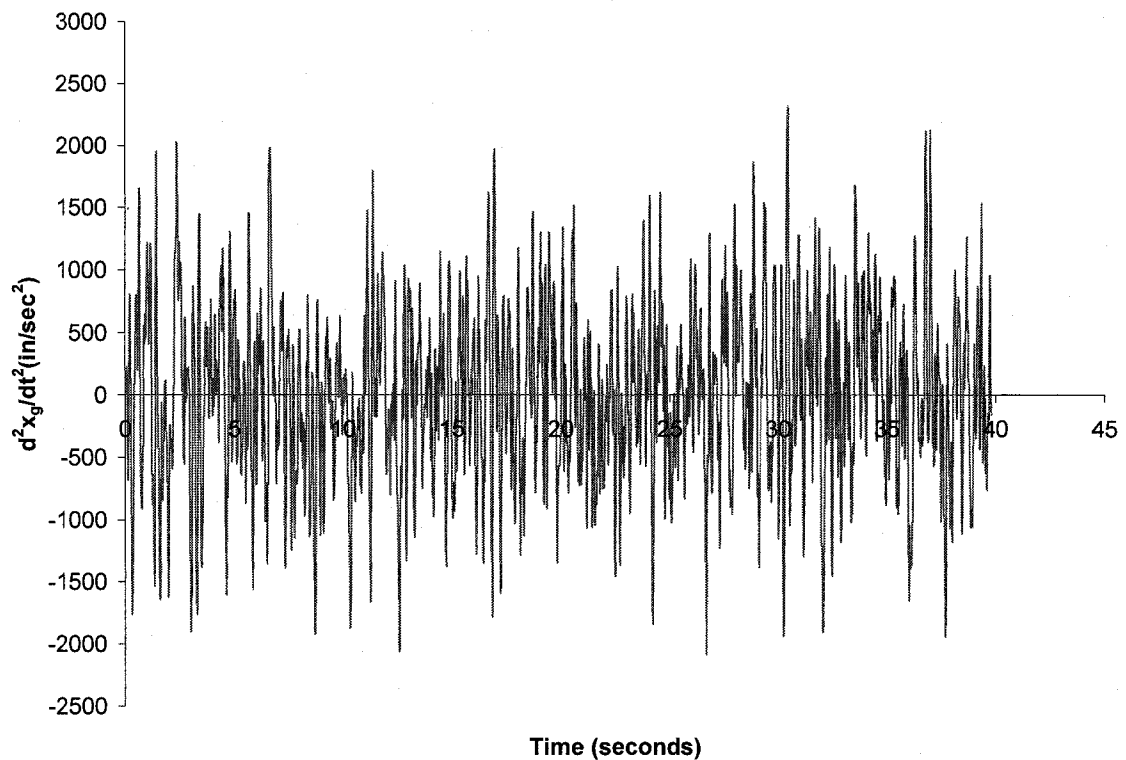


Figure 6-1 Artificial Earthquake Record (6.0g) for SDOF Shear Frame Structure.

The second-order moments that result from the vertical forces acting over the incremental moment arms caused by the lateral deflections are included on the force-displacement curve. Since the lateral second-order effects are manifested after the lateral deflections have occurred, the iterative procedure explained in chapter 4 has been used.

One of the most effective means of providing a substantial level of damping is through hysteretic energy dissipation. The term hysteretic refers to the offset between the loading and unloading curves under cyclic loading. Energy that is not recovered during unloading is lost from the system and dissipated as heat in most cases. Figure 6-2 shows the hysteretic behavior of the steel beam-column element where the energy absorbed by the hysteretic loop increases with the increase of the displacement amplitude.

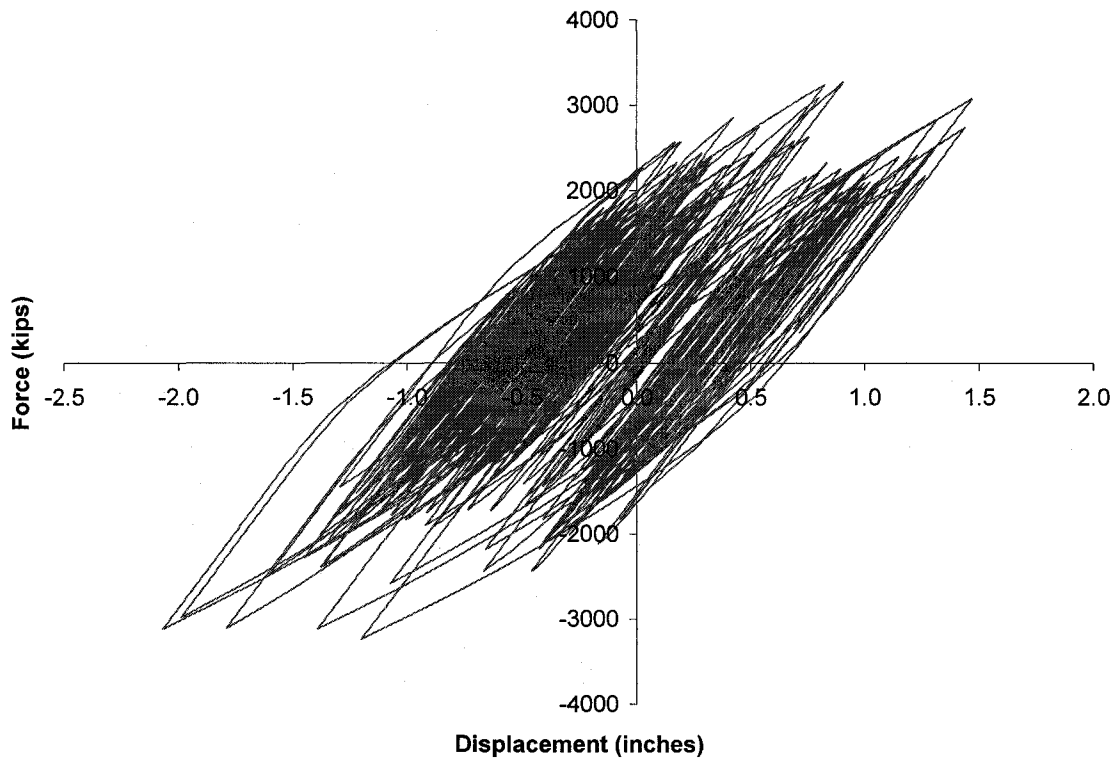


Figure 6-2 Hysteresis of a SDOF Shear Frame Structure (Artificial Excitation of 6.0g).

The hysteresis response is obtained as a result of the structure excited by the artificial earthquake ground motion record shown in Figure 6-1. The stiffness and

restoring force of the column is defined in Figure 4-7. The maximum tip deflection is 2.07 inches. The time history response of the shear frame structure is shown in Figure 6-3.

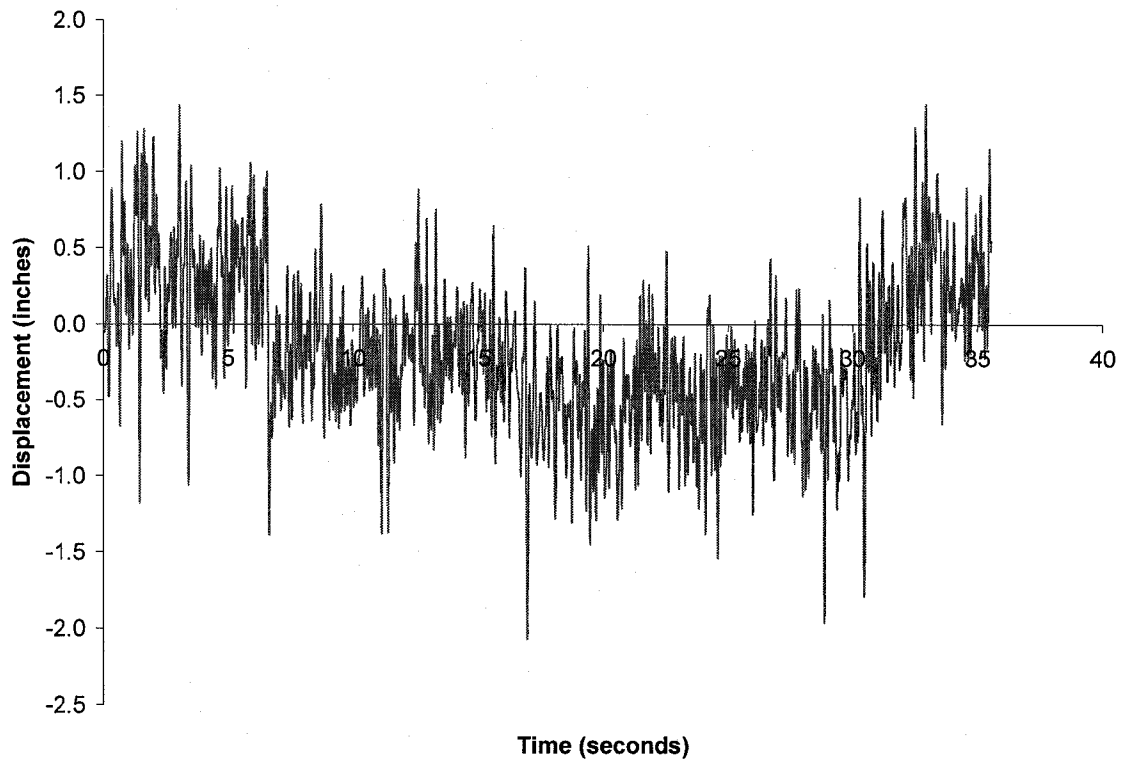


Figure 6-3 Time History Response of a SDOF Shear Frame Structure (Artificial Excitation of 6.0g).

To amplify the effects of P-delta effects the mass of the single story one-bay shear frame structure shown in Figure 3-2 was increased to 5.1802

$\frac{(kips)(sec)^2}{inches}$ . An artificial earthquake record is generated and shown in Figure 6-

4. The peak ground acceleration is 1g, or  $386.4 \frac{inches}{sec^2}$ . It is noted that the

stationary artificial earthquake record produce steady-state and stationary

displacement – time-history and hysteresis responses (i.e., where the hysteretic loop is generally centered for the most part about the origin).

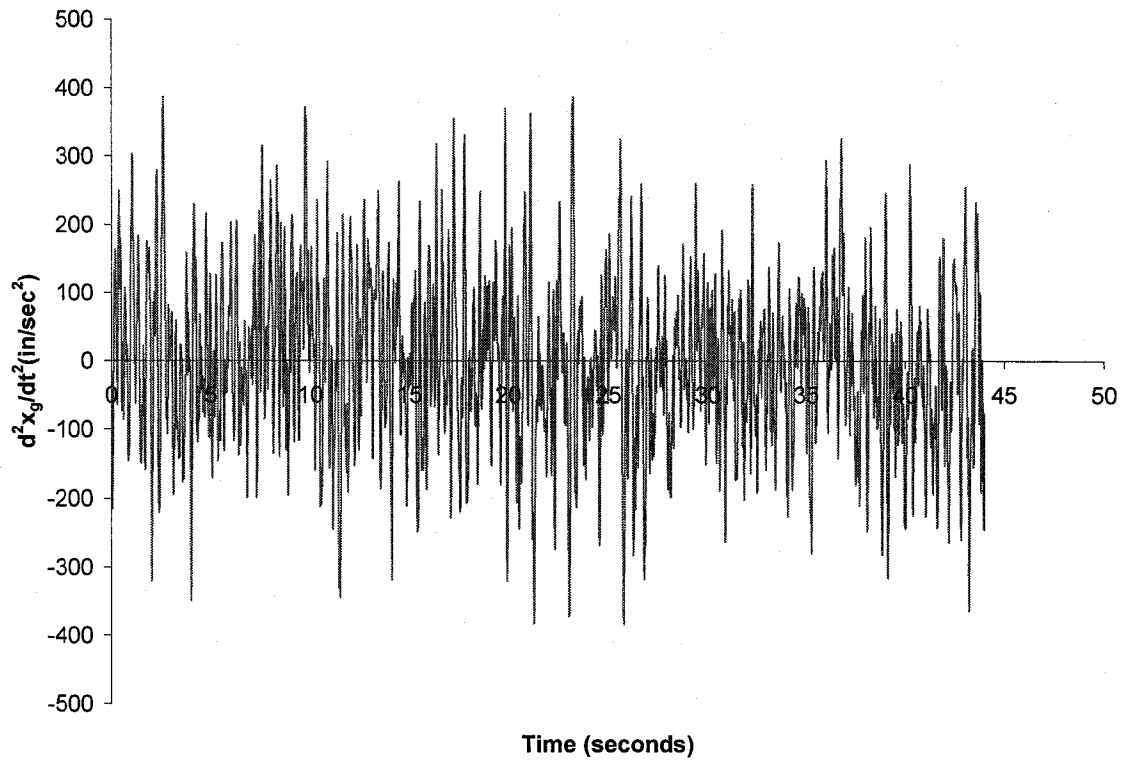


Figure 6-4 Artificial Earthquake Record (1.0g) for SDOF Shear Frame Structure.

Figure 6-5 shows the hysteretic behavior of the steel beam-column element when the floor mass is double of that shown in Figure 6-2. It is noted that the *P-delta* effect leads to significant amplification of the displacement response. There is a higher potential for collapse even though the artificial earthquake record is in the order level of 6 times less that of Figure 6-2. Larger tip deflections are seen, and this observation suggests that *P-delta* effect can have a significant effect on the predicted response of the system. Structures are



sensitive to *P-delta* effects, which might cause dynamic instability that they may lead to a failure state.

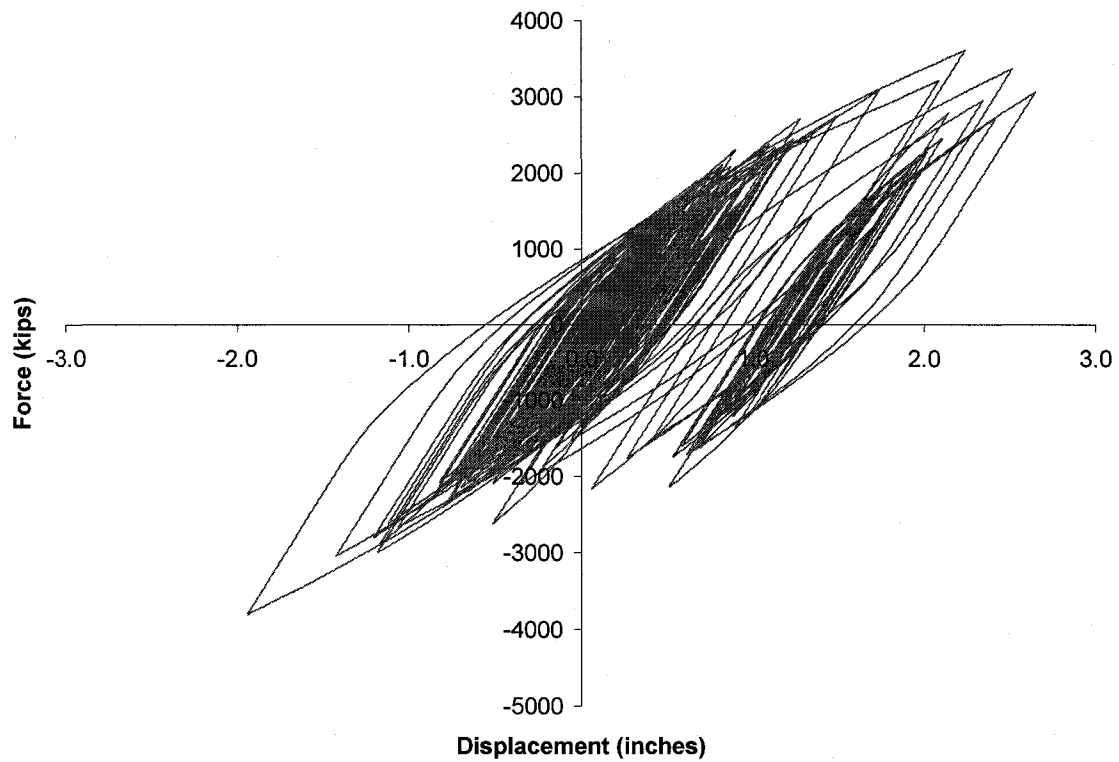


Figure 6-5 Hysteresis of a SDOF Shear Frame Structure (Artificial Excitation of 1.0g).

The time history response of the SDOF shear frame structure subjected to 1.0g intensity artificial earthquake is shown in Figure 6-6.

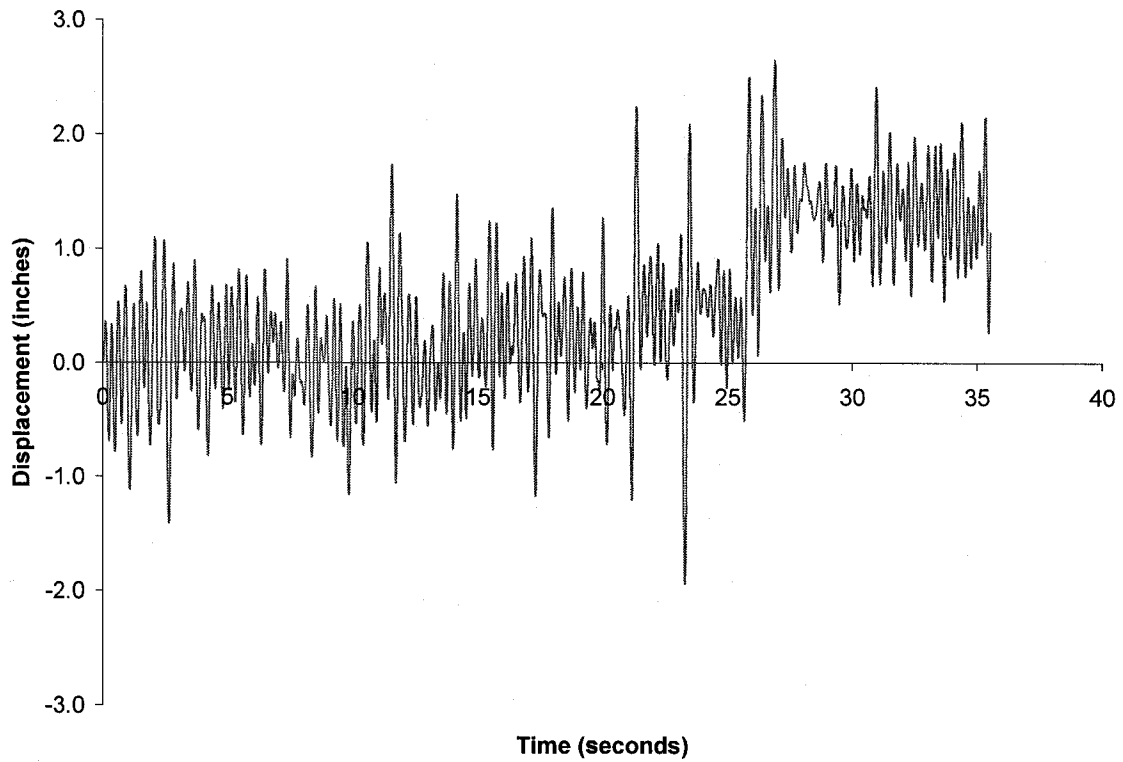


Figure 6-6 Time History Response of a SDOF Shear Frame Structure (Artificial Excitation of 1.0g).

In addition to the SDOF shear frame structure illustrated in Figure 3-2, a multi-degree-of-freedom (MDOF) four-story shear frame structure was considered to compute the interstory displacement drifts during an earthquake excitation. Story drift is defined as the relative displacement between consecutive floor levels that are produced by the earthquake-induced ground motions. The four-story shear frame is depicted in Figure 6-7.

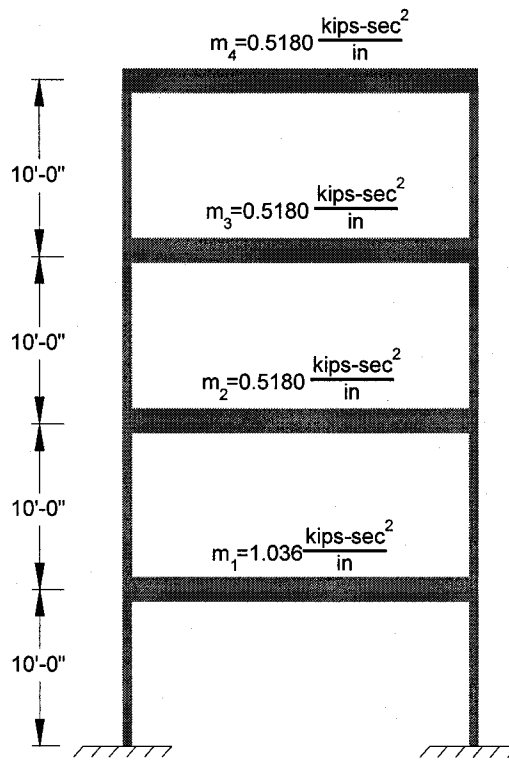


Figure 6-7 Four-story MDOF Shear Frame Structure.

The four-story shear frame structure has been subjected to an artificial earthquake. The artificial earthquake record that is generated is shown in Figure

6-8. The peak ground acceleration is  $965.2 \frac{\text{inches}}{\text{sec}^2}$ , or 2.5g.

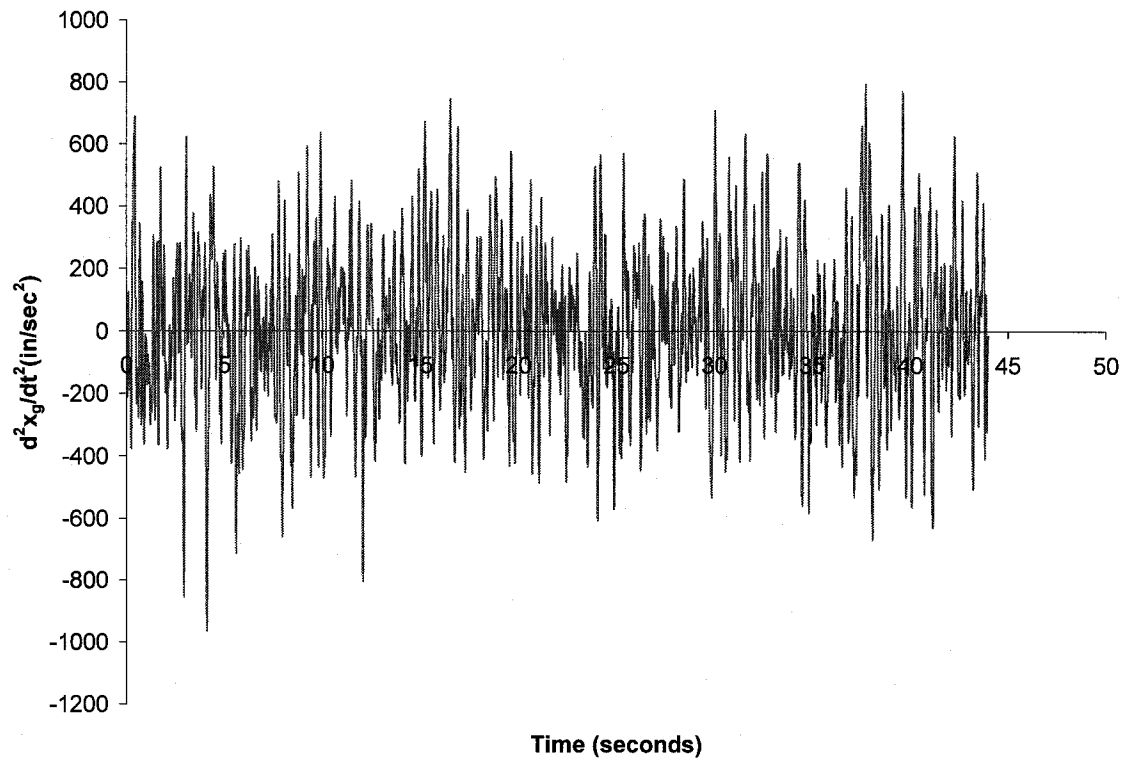


Figure 6-8 Artificial Earthquake Record (2.5g) for MDOF Shear Frame Structure.

Each floor of the four-story shear frame structure shown in Figure 6-7 has a height of 120 inches and the cross section of each column is assumed to be rectangular (10in. x 22in.). The first floor is defined at the ground level. Figures 6-9 through 6-12 illustrate the hysteretic behavior of each floor level.

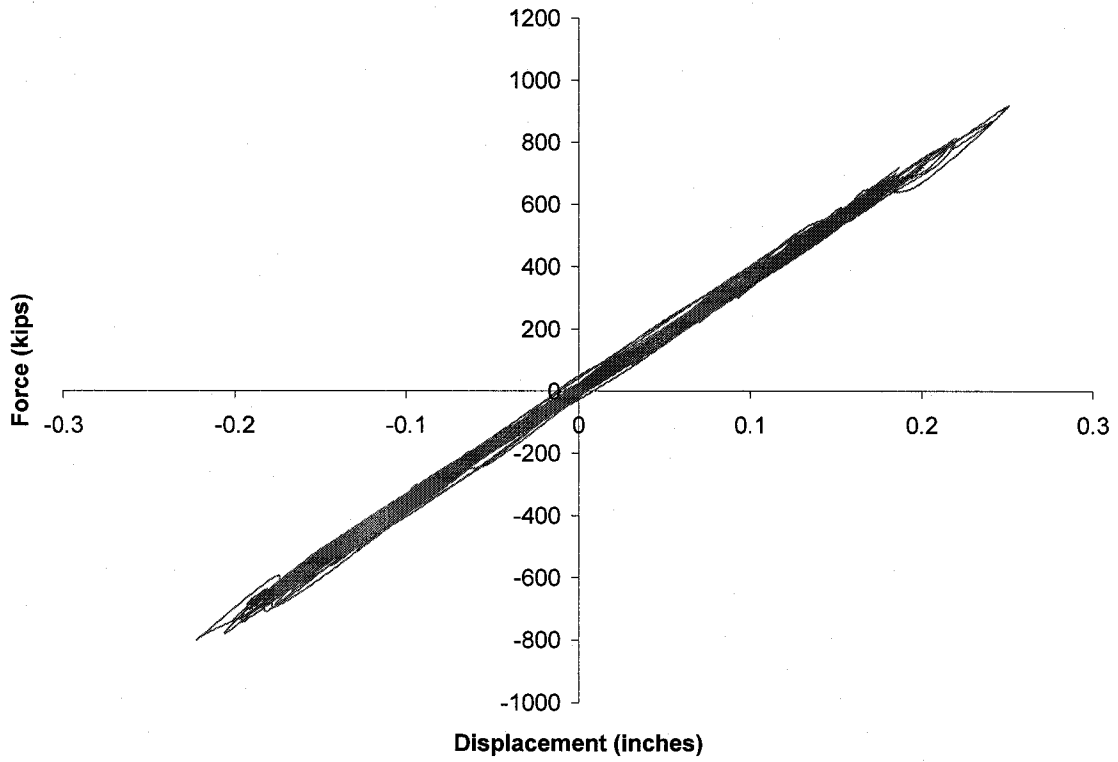


Figure 6-9 Hysteresis of 4<sup>th</sup> Floor of a MDOF Shear Frame Structure (Artificial Excitation of 2.5g).

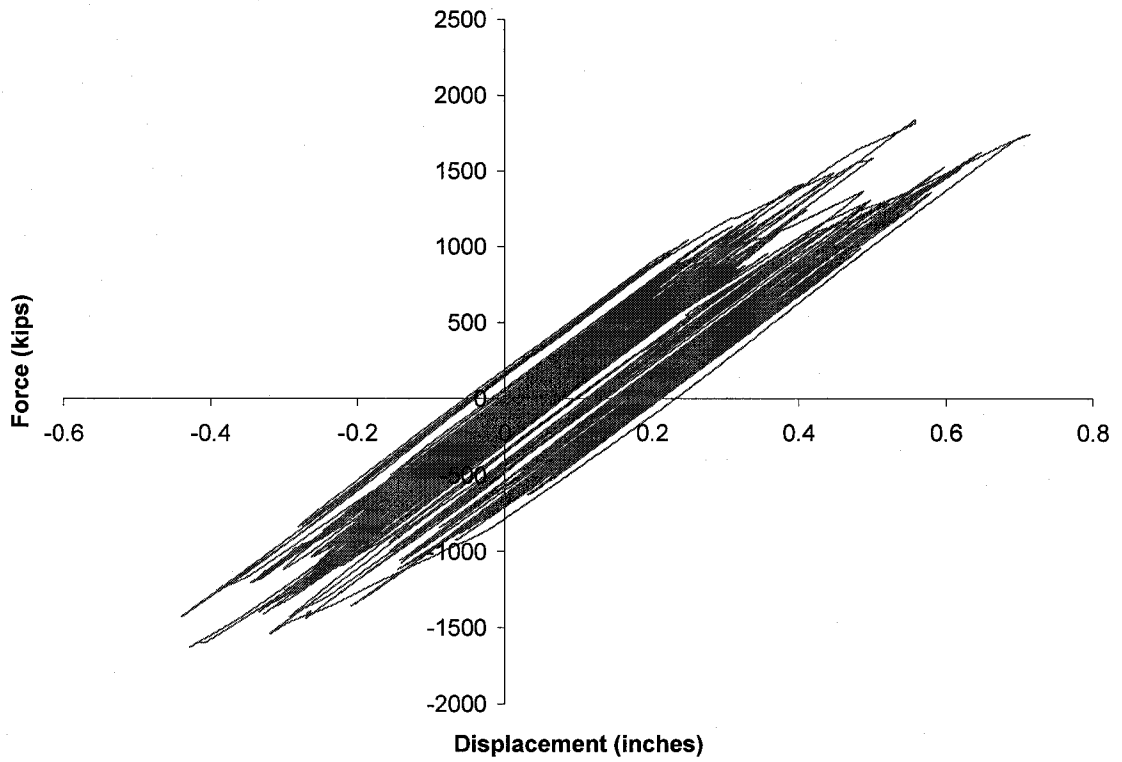


Figure 6-10 Hysteresis of 3<sup>rd</sup> Floor of a MDOF Shear Frame Structure (Artificial Excitation of 2.5g).

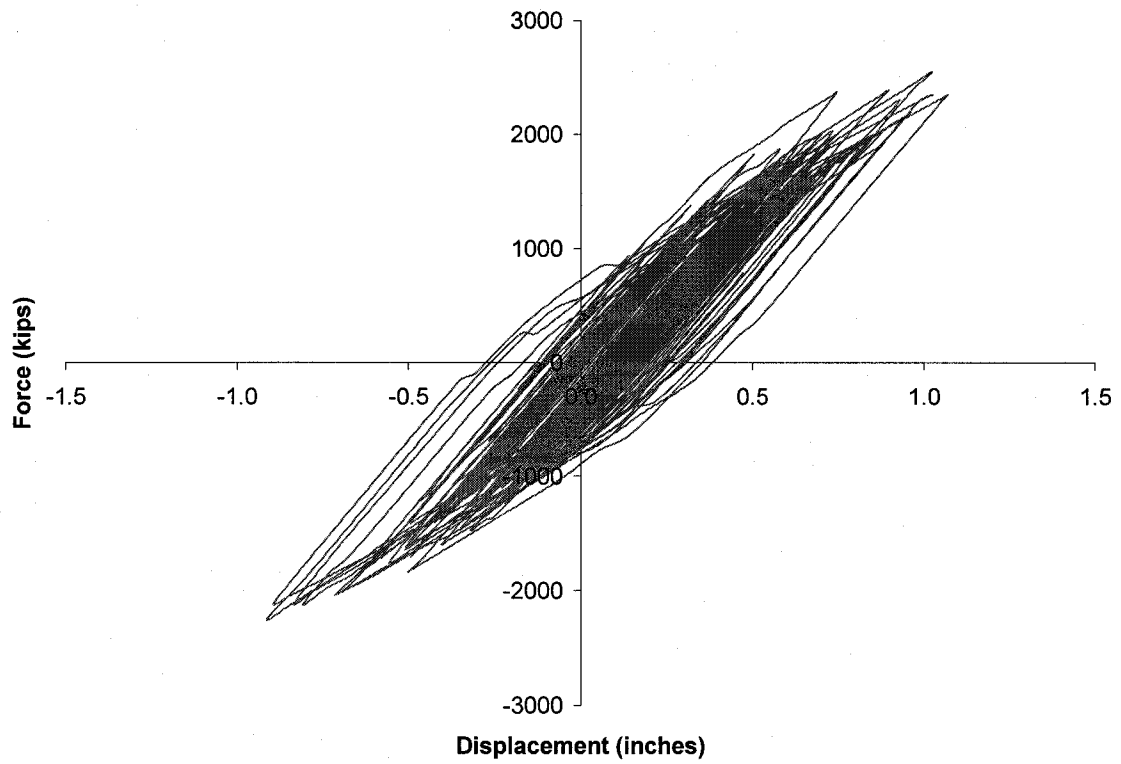


Figure 6-11 Hysteresis of 2<sup>nd</sup> Floor of a MDOF Shear Frame Structure (Artificial Excitation of 2.5g).

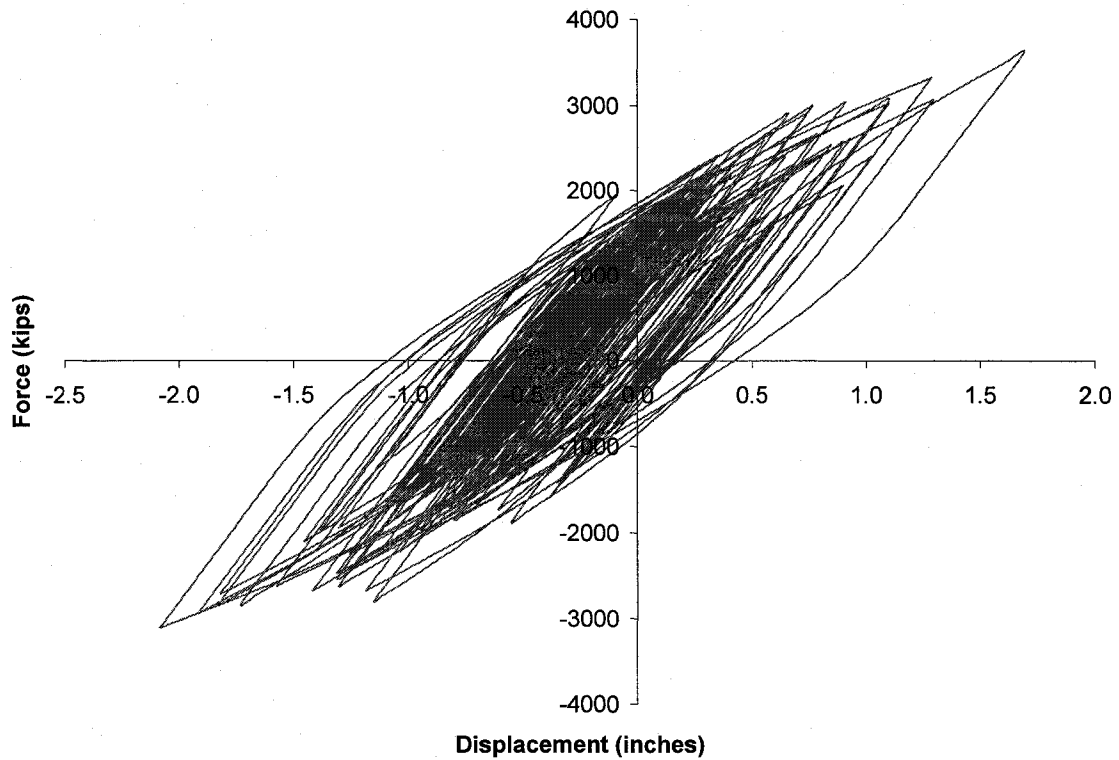


Figure 6-12 Hysteresis of 1<sup>st</sup> Floor of a MDOF Shear Frame Structure (Artificial Excitation of 2.5g).

As expected, the bottom two stories experience the largest amount of degradation. Figures 6-13 through 6-16 show the displacement time-histories of each story of the MDOF shear frame structure subjected to the 2.5g artificial earthquake shown in Figure 6-8.



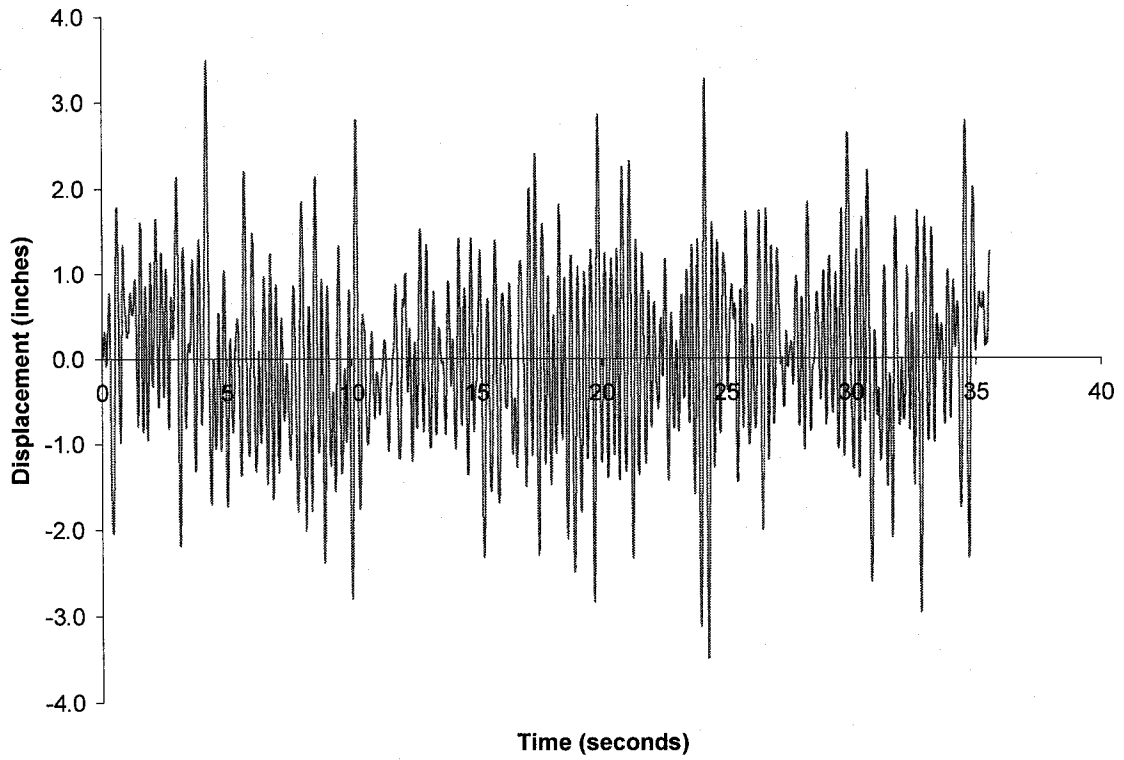


Figure 6-13 Time History Response of 4<sup>th</sup> Floor of a MDOF Shear Frame Structure (Artificial Excitation of 2.5g).

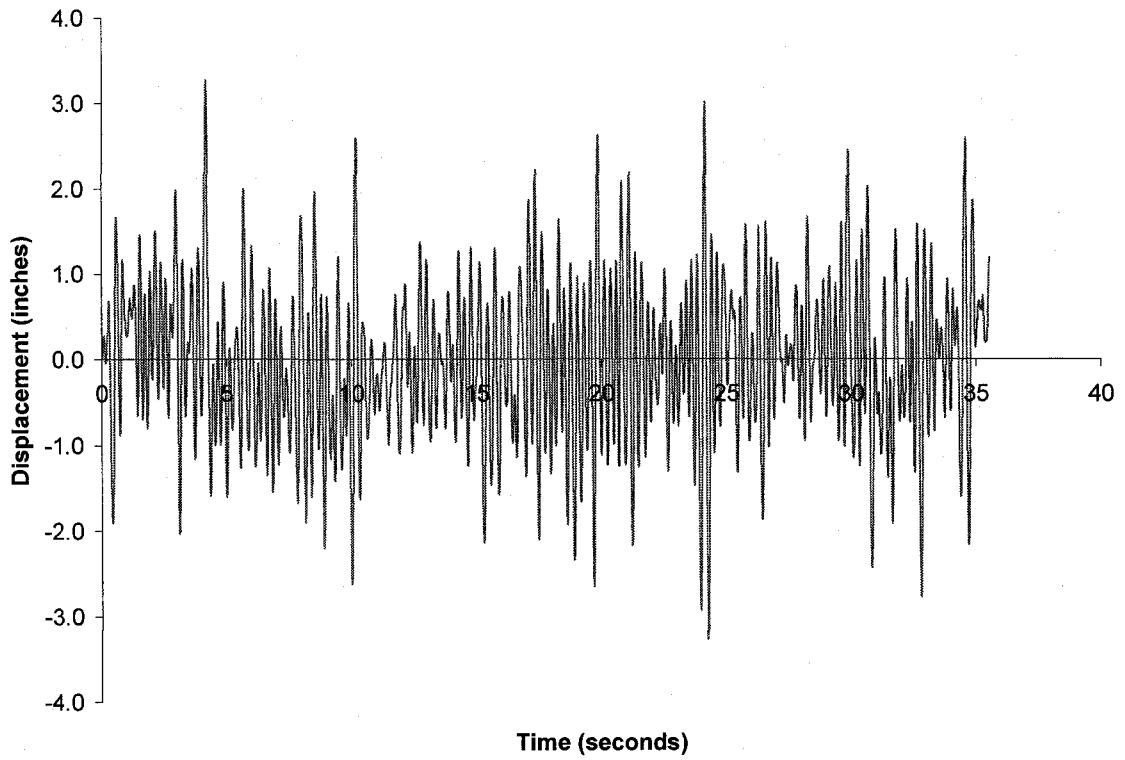


Figure 6-14 Time History Response of 3<sup>rd</sup> Floor of a MDOF Shear Frame Structure (Artificial Excitation of 2.5g).

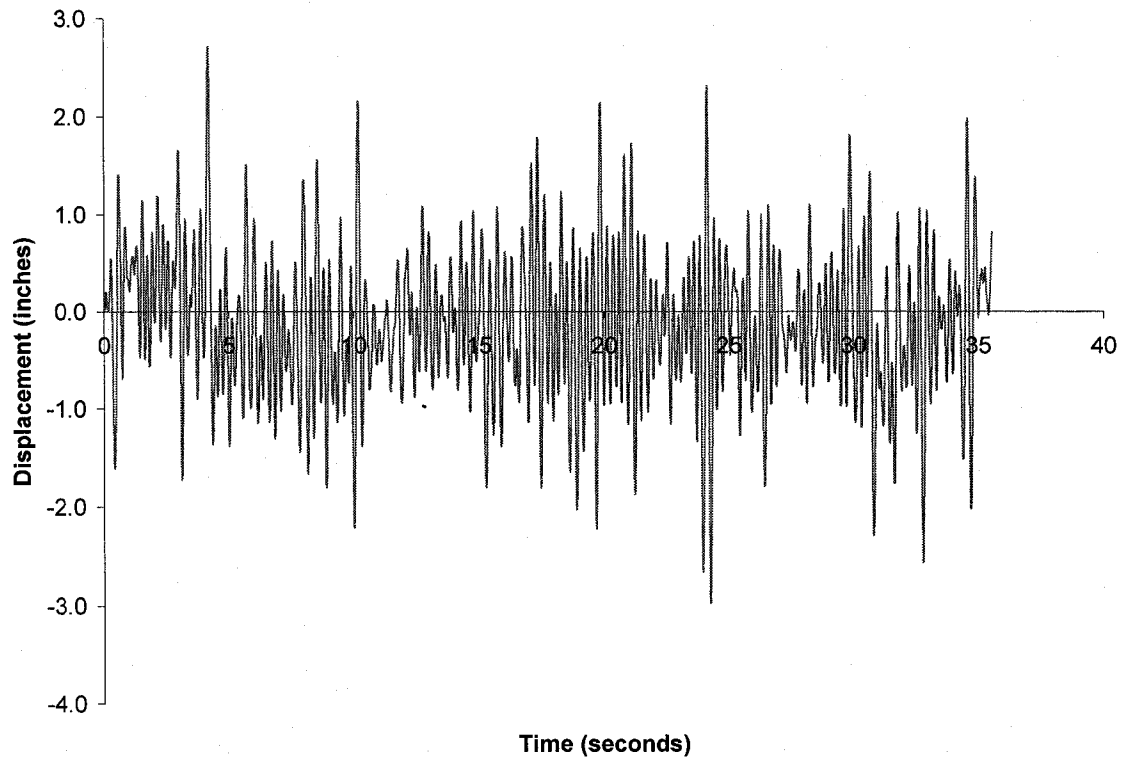


Figure 6-15 Time History Response of 2<sup>nd</sup> Floor of a MDOF Shear Frame Structure (Artificial Excitation of 2.5g).

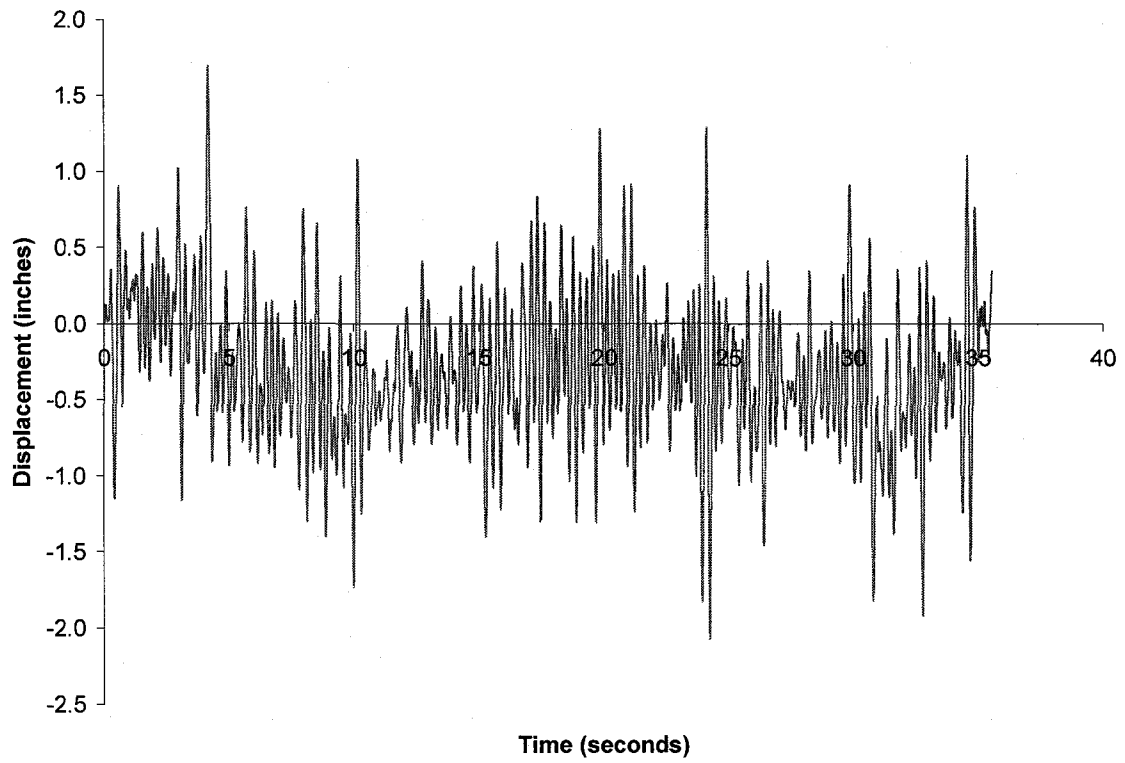


Figure 6-16 Time History Response of 1<sup>st</sup> Floor of a MDOF Shear Frame Structure (Artificial Excitation of 2.5g).

As a final illustration, the four-story shear frame structure has been subjected to the 1971 San Fernando earthquake (modified, 5x). Figure 6-17 shows the San Fernando earthquake record that was recorded during the 1971 San Fernando earthquake.

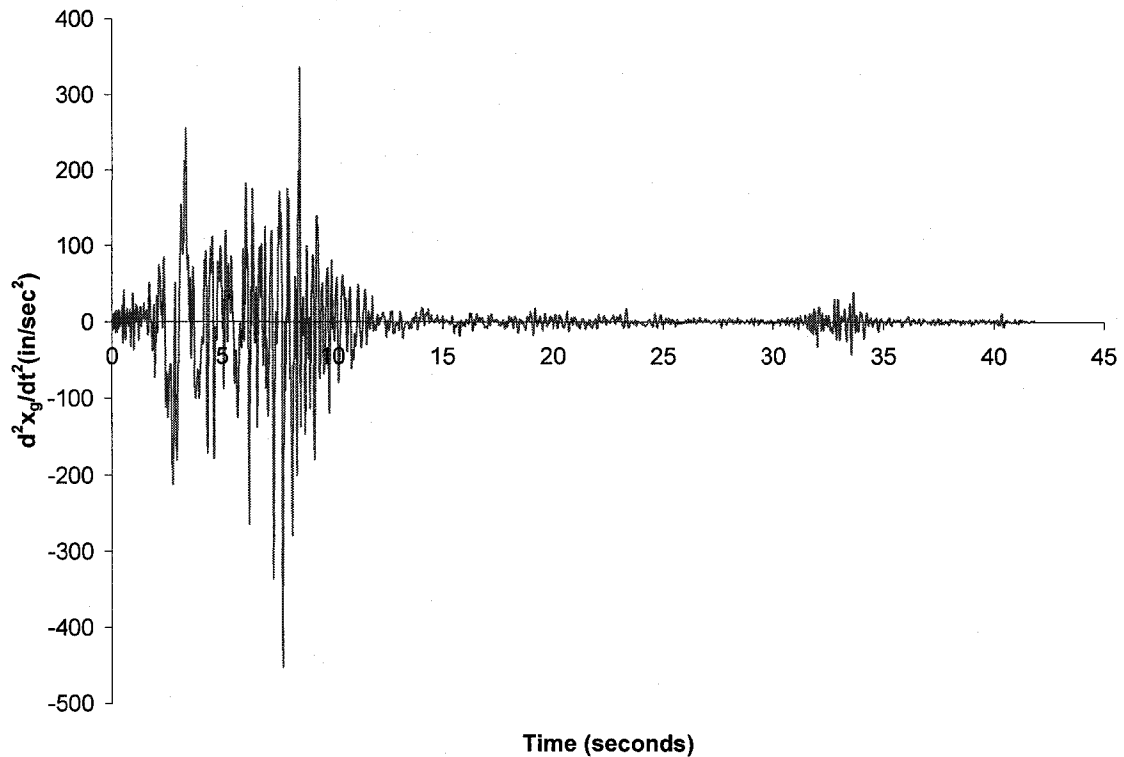


Figure 6-17 San Fernando Earthquake Record for MDOF Shear Frame Structure.

Figures 6-18 through 6-21 show the hysteretic behavior of each floor level of the MDOF shear frame structure subjected to the modified San Fernando earthquake.

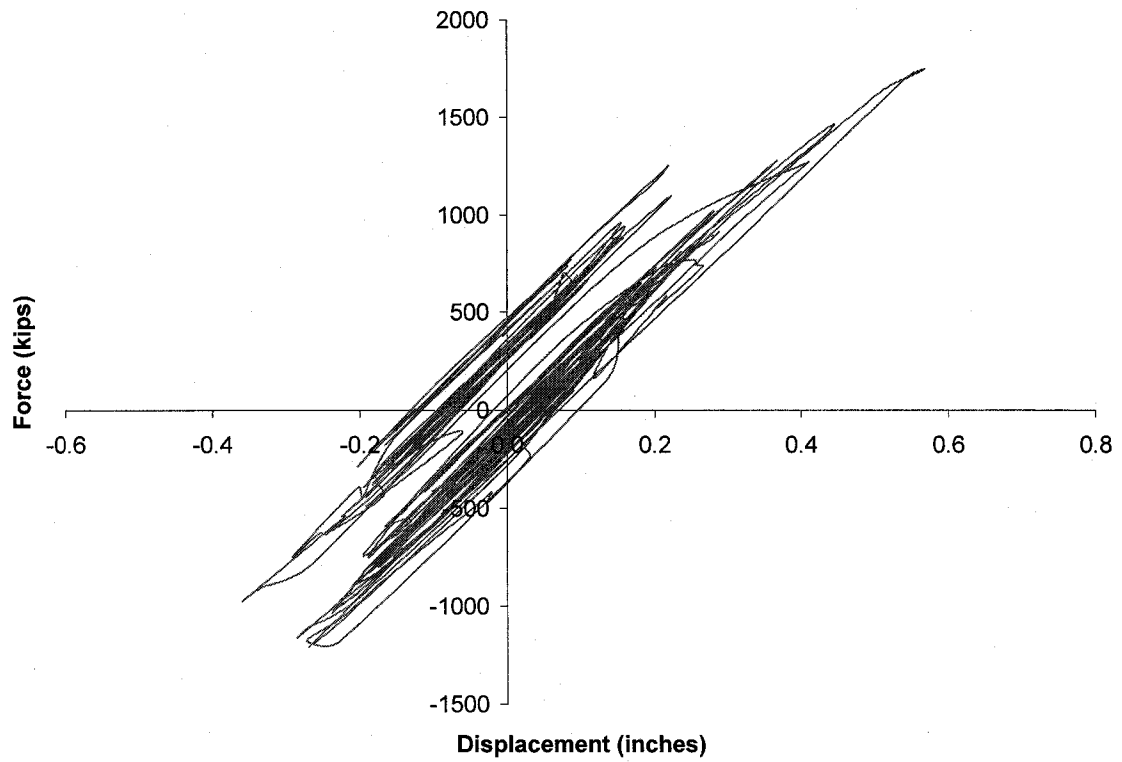


Figure 6-18 Hysteresis of 4<sup>th</sup> Floor of a MDOF Shear Frame Structure (San Fernando 5x).

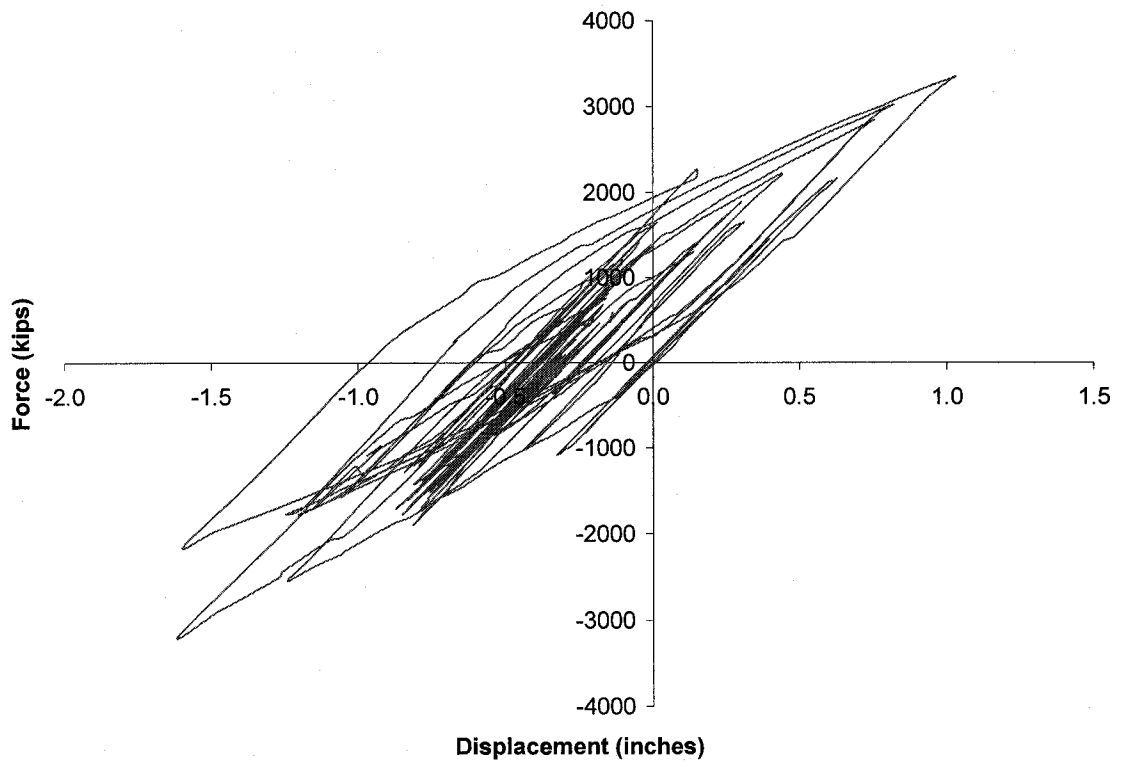


Figure 6-19 Hysteresis of 3<sup>rd</sup> Floor of a MDOF Shear Frame Structure (San Fernando 5x).

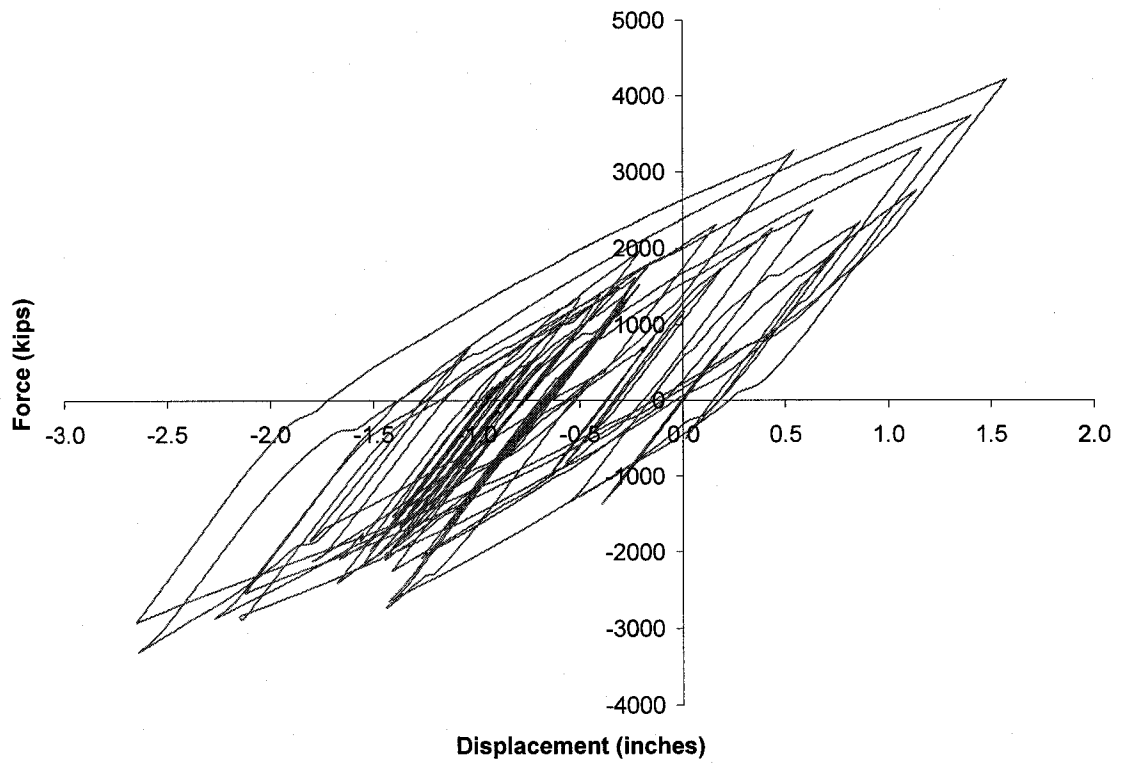


Figure 6-20 Hysteresis of 2<sup>nd</sup> Floor of a MDOF Shear Frame Structure (San Fernando 5x).



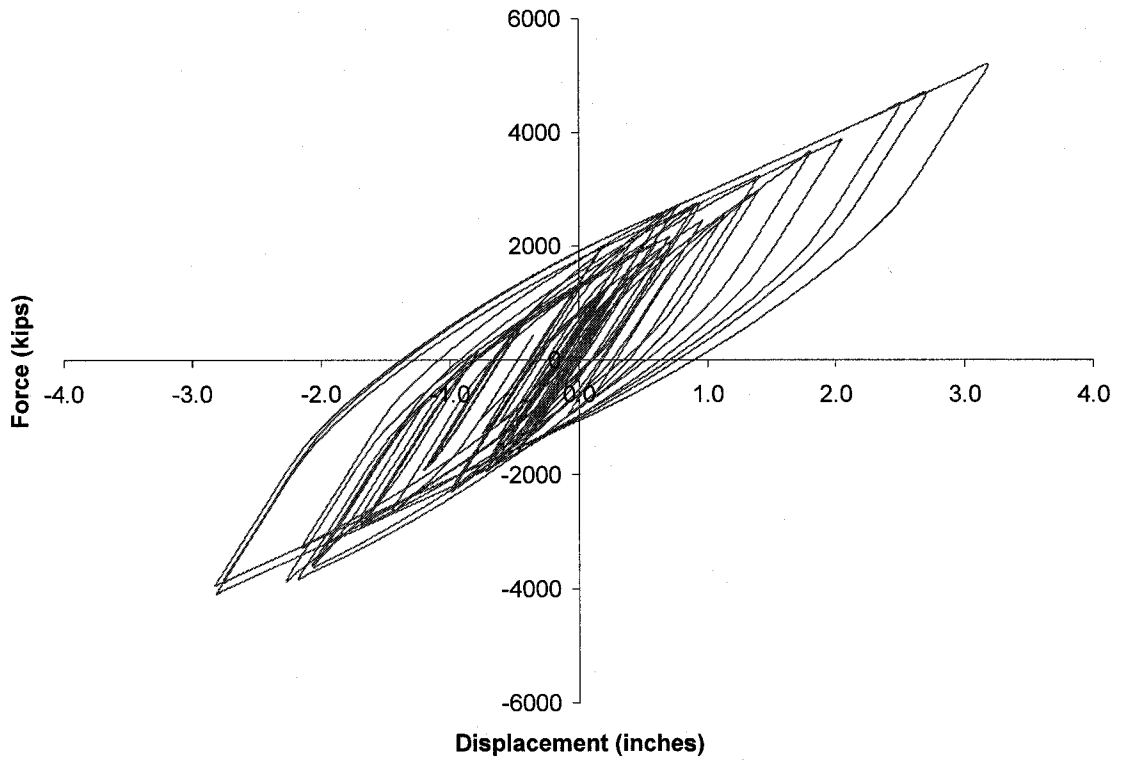


Figure 6-21 Hysteresis of 1<sup>st</sup> Floor of a MDOF Shear Frame Structure (San Fernando 5x).

Figures 6-21 through 6-24 show the displacement time-histories of each floor level of the MDOF shear frame structure subjected to the modified San Fernando earthquake.

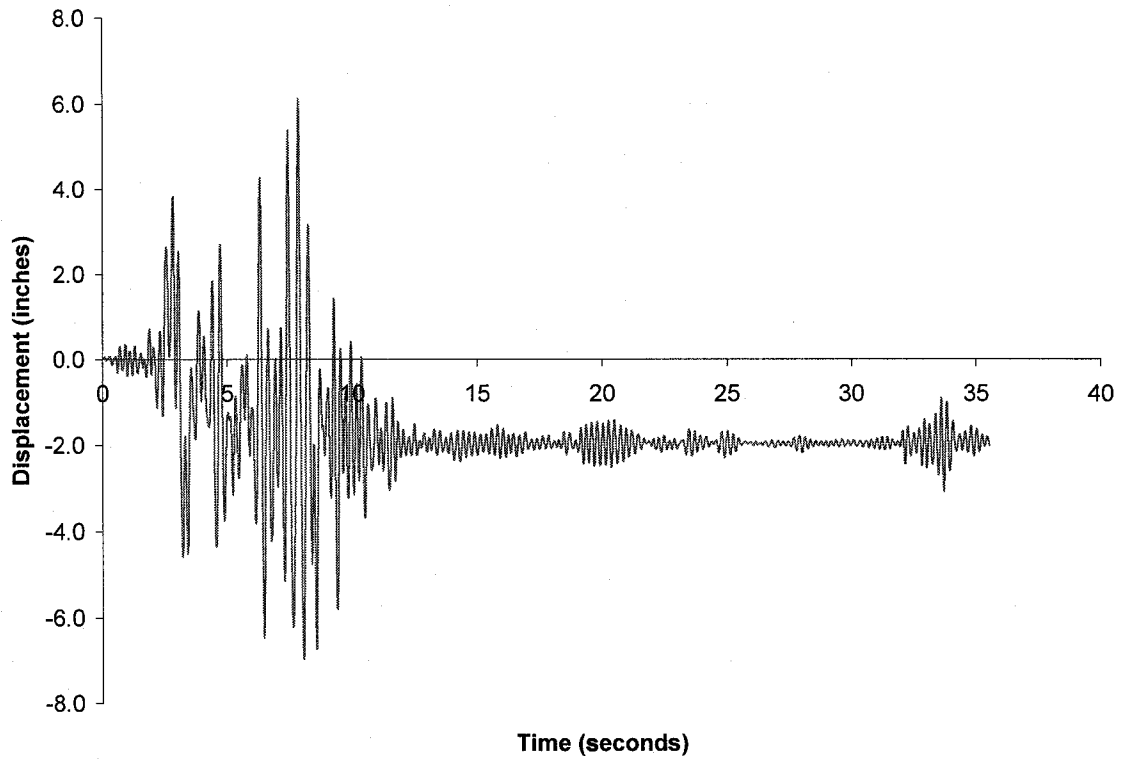


Figure 6-22 Time History Response of 4<sup>th</sup> Floor of a MDOF Shear Frame Structure (San Fernando 5x).

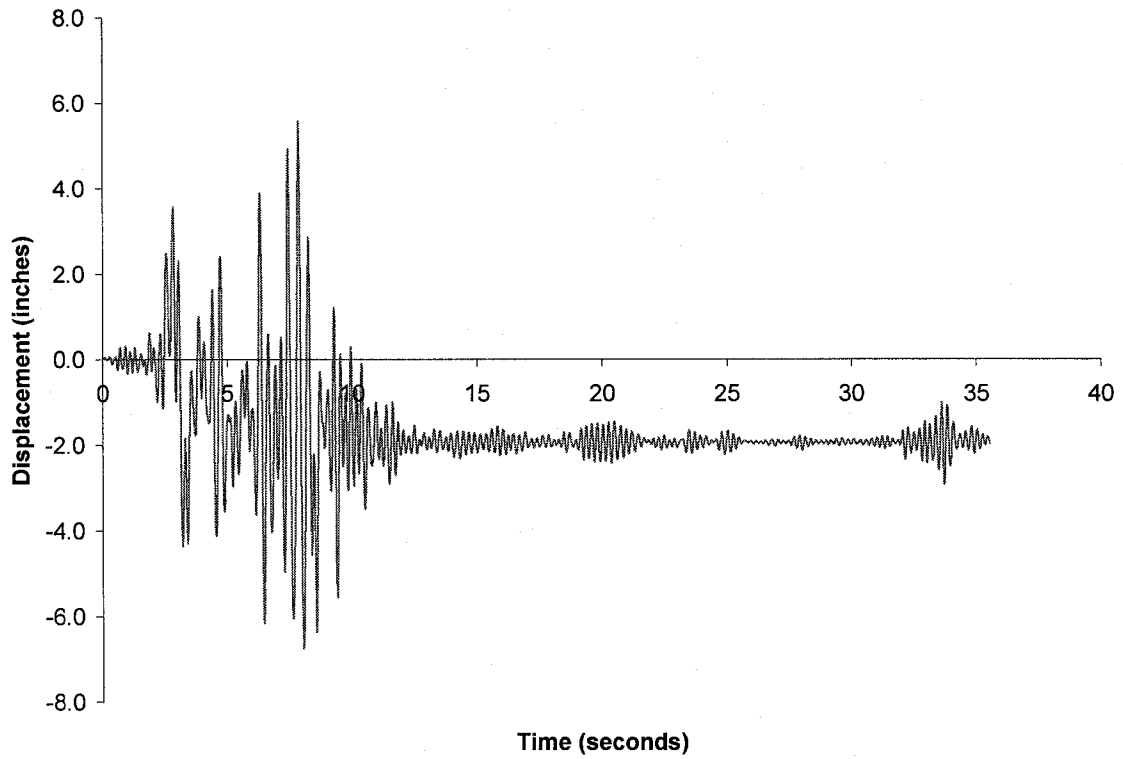


Figure 6-23 Time History Response of 3<sup>rd</sup> Floor of a MDOF Shear Frame Structure (San Fernando 5x).

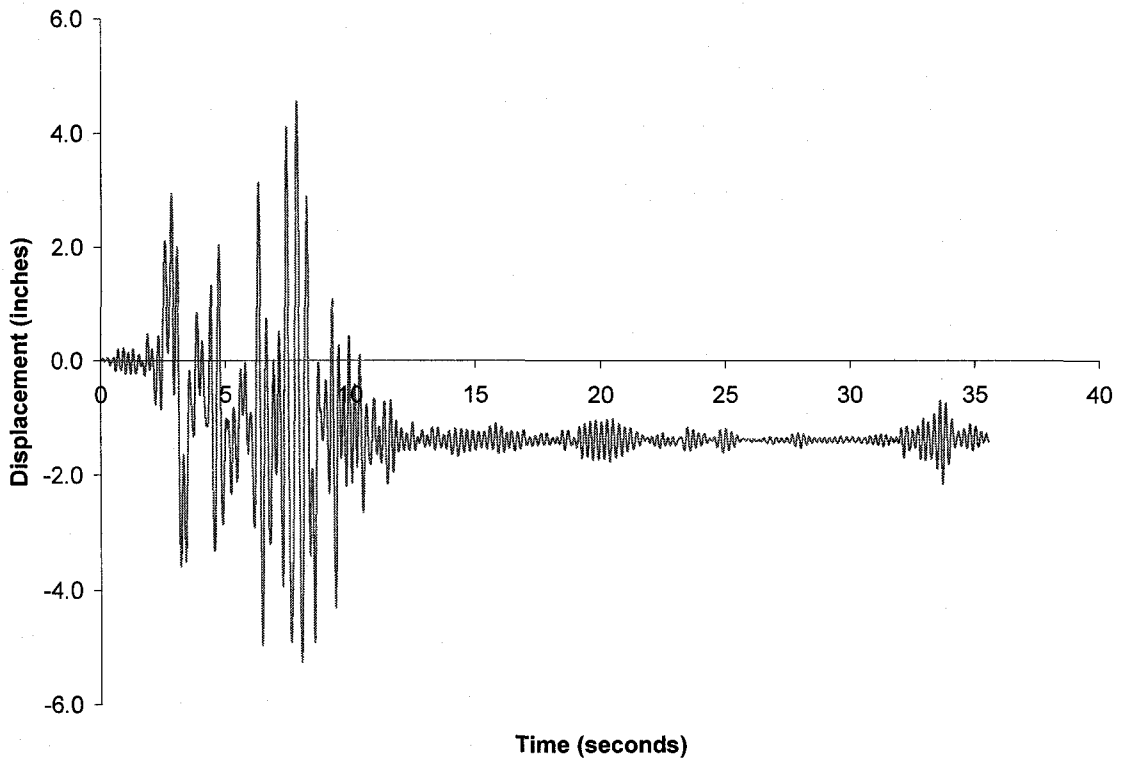


Figure 6-24 Time History Response of 2<sup>nd</sup> Floor of a MDOF Shear Frame Structure (San Fernando 5x).

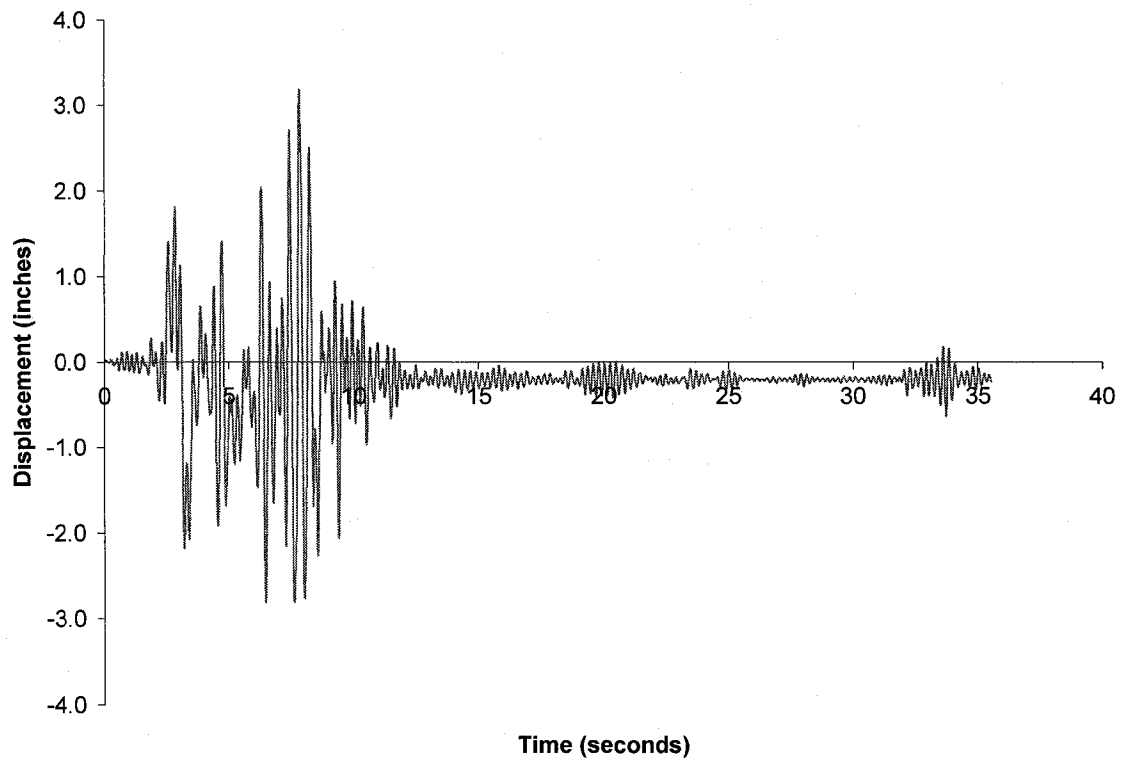


Figure 6-25 Time History Response of 1<sup>st</sup> Floor of a MDOF Shear Frame Structure (San Fernando 5x).

From the above figures it is noted that P-delta effects are not negligible, and such effects are manifested after the building has experienced lateral displacements. The proposed approach gives a prediction of the expected displacements and makes an assessment of structural response and models the

structural behavior due to earthquake motions through the post-yield behavior of the ductile steel components of the shear frame. Various material nonlinearities such as secondary moment and spread of plasticity of steel beam-column elements are modeled. The *P-delta* effects influence the response of the structure by increasing displacements above those calculated by simple first-order analyses. *P-delta* effects reduce the lateral strength of a particular structure.

## CHAPTER 7

### SUMMARY AND CONCLUSIONS

The primary focus of this research was to compute the inelastic deformations of steel beam-column elements by considering bending stresses, axial stresses, and the resulting *P-delta* effects. A detailed nonlinear strain hardening model assesses the material degradation through the spread of plasticity for shear frame structures under quasi-static and dynamic loading and predicts the response of such structure types. Inclusion of geometrically nonlinear behavior (i.e., secondary bending moments) was an important aspect of this research as it created an additional lateral loading resulting in an increase in member forces and lateral deflections, thus reducing the lateral load resistance of the structure. Analysis of the combined effects of bending and axial forces is made at an incremental level over the range of all post-yield strains leading towards the failure state.

From a dynamic and cyclic perspective the *P-delta* phenomena may lead to a significant amplification in displacement response of lateral load-displacement relationship. It is postulated that *P-delta* effects are negligible up to a certain level but potentially disastrous thereafter, because of the dynamic instability that they may lead to. The results of obtained effective length factors closely conform to those of recommended for design by current design procedures, which validates the incremental method of analysis to begin with. The computed effective length factor increases gradually as the ultimate state is

approached. Unlike the current design code procedures, wherein a constant effective length factor has been used, this research predicts the behavior of steel beam-column elements by gradually updating the  $K$  factor as the material starts to degrade. In other words, there is a certain  $K$  factor for each state of discretized post-yield stress leading to the ultimate failure state using the proposed incremental approach.

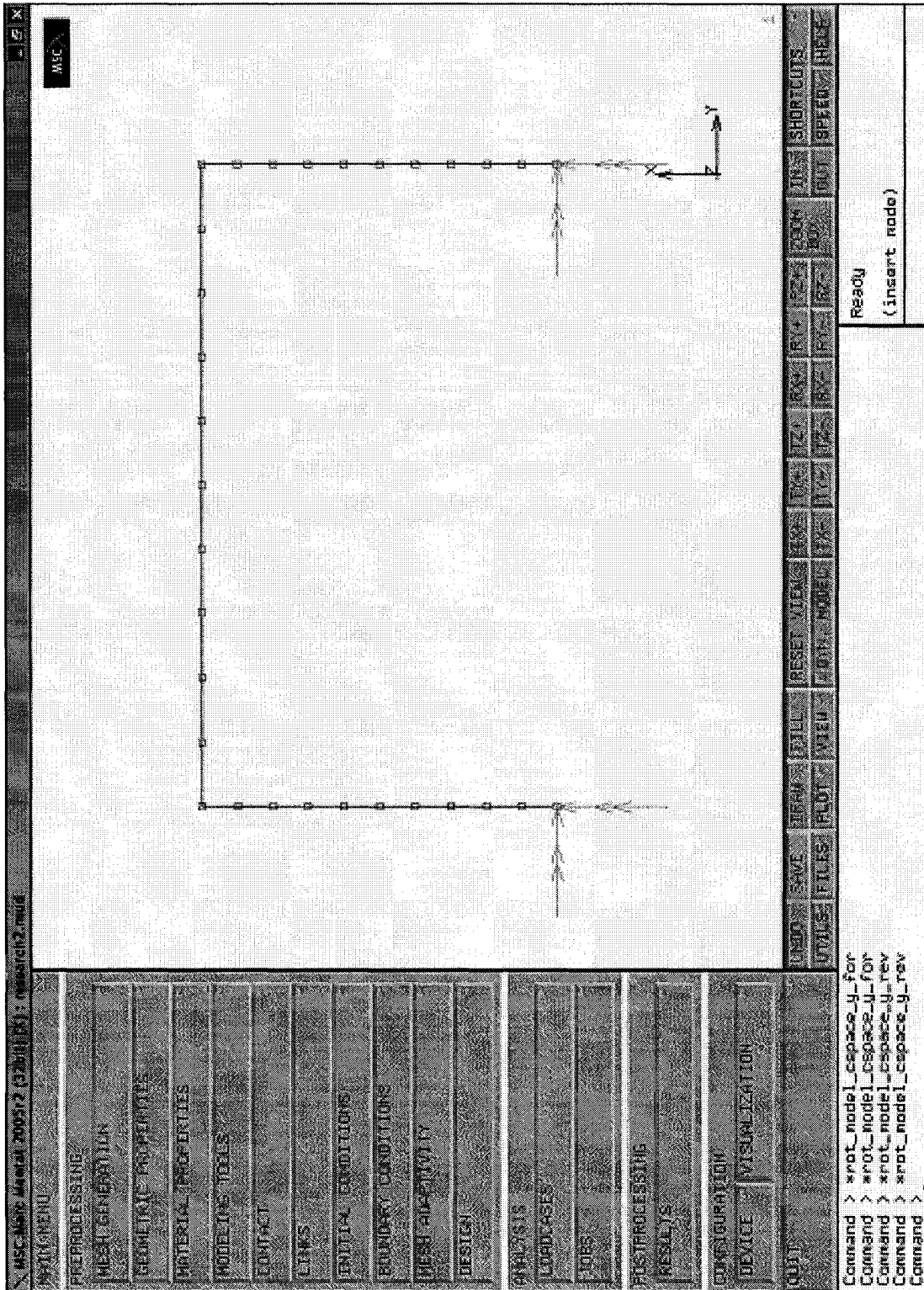
The use of the proposed method of analysis was demonstrated using a single-degree-of-freedom (SDOF) system and a 4-story structure under cyclic conditions. Furthermore, the post-yield results obtained using the constitutive nonlinear strain hardening model for the SDOF system closely agree with the results of FEA analysis. The difference of the lateral deflections between the FEA and the proposed incremental approach was approximately 14 percent. This error is due to the large step sizes used to define the post-yield stress-strain curve in the FEA procedure, which is believed was a limitation of the software. In the proposed incremental approach, 1,400 points were used to define the post-yield stress-strain relationship, while the FEA procedure used only 14 points. It is anticipated that the difference between these two procedures would decrease substantially if the strain increment step is reduced in the FEA procedure. The accuracy for small plastic strains increments to achieve accurate results is greatly increased as the strain step is kept reasonably small compared to the initial yield strain of the material. Furthermore, the FEA iterative procedure use an effective modulus that calculates the solution of the problem based on the post-yield stresses and strains. The proposed incremental approach uses a tangential stiffness plastic modulus whilst not losing accuracy of the solution. This is another



reason for the discrepancy and further validates the accuracy of the proposed incremental approach. Also, in using the FEA procedure, the *P-delta* effects are not computed, which therefore indicates the added accuracy that the proposed method provides and also illustrates its robustness.

The results presented are a valid indicator of the accuracy of the incremental approach. The small differences in the monotonic responses are a result of the added accuracy and detail given to the *P-delta* analysis using the proposed approach applied to the nonlinear constitutive strain-hardening model. The fundamental results of this research improve the quality of design by providing structural engineers with more reliable prediction tools. This enables the performance of steel beam-column elements when subjected to a cyclic dynamic loading environment to be accurately predicted (negligible strain-rate effects). The proposed incremental method can be used to evaluate the seismic performance of both new and existing structural systems. It is concluded that the model be additionally verified with experimental work to find a proper and optimum hardening index parameter,  $\alpha$  and the plastic strain coefficient  $\Delta_{\epsilon}$ , for other types of materials, in order to quantitatively describe the real material behavior.

## APPENDIX: FEA SIMULATIONS



MSC Marc 2005/2 (32,000) (X) : hsearch2.mud
MSC

**MATERIAL PROPERTIES**

NAME: material1 | READ | EDIT

**MECHANICAL MATERIAL TYPES**

ISOTROPIC

**ISOTROPIC PROPERTIES**

YOUNG'S MODULUS: 23000 | TABLES

POISSON'S RATIO: 0.3 | TABLES

DENS DENSITY: 1

COST VOLUME: 0

COST MASS: 0

**FORMING**

PLASTICITY:  PLASTIC-PLASTIC

RIGID-PLASTIC

DAMAGE EFFECTS:  DYNAMIC LIMIT

CRACKING

DAMAGE

FAILURE

RESET

**OTHER EFFECTS**

THERMAL EXP

THERMO-ELASTIC

THERMO-PLASTIC

THERMO-VISCOELASTIC

CREEP

VISCOELASTIC

RESET

UNDO | REDO | FILE | VIEW | PLOT | MODEL | SIZE | T1 | T2 | R1 | R2 | R3 | R4 | R5 | R6 | R7 | R8 | R9 | R10 | R11 | R12 | R13 | R14 | R15 | R16 | R17 | R18 | R19 | R20 | R21 | R22 | R23 | R24 | R25 | R26 | R27 | R28 | R29 | R30 | R31 | R32 | R33 | R34 | R35 | R36 | R37 | R38 | R39 | R40 | R41 | R42 | R43 | R44 | R45 | R46 | R47 | R48 | R49 | R50 | R51 | R52 | R53 | R54 | R55 | R56 | R57 | R58 | R59 | R60 | R61 | R62 | R63 | R64 | R65 | R66 | R67 | R68 | R69 | R70 | R71 | R72 | R73 | R74 | R75 | R76 | R77 | R78 | R79 | R80 | R81 | R82 | R83 | R84 | R85 | R86 | R87 | R88 | R89 | R90 | R91 | R92 | R93 | R94 | R95 | R96 | R97 | R98 | R99 | R100

Ready  
(insert mode)

Command > \*rot\_model\_cspace\_4\_rev

Command > \*rot\_model\_cspace\_4\_rev

Command > \*geometry\_type\_mech\_thru\_base\_ela

Command > \*material\_type\_mechanical:isotropic

Command >

MSC Marc Mental 2005r2 (32bit) (X) : research4.mud

table1

F (x100)

V1 (x.01)

0.124 1.89

0.36 1.7

1 15

2 3 4 5 6 7 8 9 10 11 12 13 14

TABLES

NEW | REN | READ | WRITE

NAME table1

COPY | PASTE | EDIT

VARIABLES | FIT | MORE

INDEPENDENT VARIABLE V1

TYPE none

MIN 0.00124

MAX 0.0189

STEPS 10

FUNCTION VALUE F

MIN 36

MAX 179

STEPS 10

DATA POINTS | FORMULA

ADD | REMOVE | EDIT | CLEAR

SHIFT | SCALE | SWAP AXES

INTEGRATE | DIFFERENTIATE

SHOW TABLE

FILLED | CURVES SHOW ID 1

GENERALIZED XY PLOT | COPY TO

RETURN MAIN

UNDO | SAVE | BRAH | FILL | RESET VIEW | TX+ | TX- | TZ+ | TZ- | RX+ | RX- | RY+ | RY- | RZ+ | RZ- | BOX | ZOOM IN | SHORTCUTS

UTILS | FILES | PLOT | VIEW | JOYN. MODEL | TX- | TX+ | TZ- | TZ+ | RX- | RX+ | RY- | RY+ | OUT | SPEED | HELP

Ready

Command > \*set\_md\_table\_max\_v 1 0.018

Command > \*set\_md\_table\_max\_v 1 0.018

Command > \*set\_md\_table\_max\_v 1 0.018

Command > \*set\_md\_table\_max\_v 1 0.0189

Command >











## REFERENCES

- 1 Anderson, J. P., and Woodward, J. H. (1972). "Calculation of effective lengths and effective slenderness ratios of stepped columns." *Engineering Journal, AISC*, 9, 157-166.
- 2 AISC, (2001). "Load and Resistance Factor Design Specifications." AISC, Chicago, IL.
- 3 Attalla, M., Deierlein, G., and McGuire, W. (1994). "Spread of plasticity: Quasi-plastic-hinge approach." *Journal of Structural Engineering*, 120(8), 2451-2473.
- 4 Attard, T. (2003). "Modeling of higher-mode effects in various frame structures using a pushover analysis." Ph.D. Dissertation, Arizona State University, Tempe, AZ.
- 5 Attard, T. (2005). "Post-Yield material nonlinearity: Optimal homogeneous shear-frame sections and hysteretic behavior," *International Journal of Solids and Structures*, 42(21-22), 5656-5668.
- 6 Bayrak, O., and Sheikh, S. (2001). "Plastic Hinge analysis." *Journal of Structural Engineering*, 127(9), 1092-1100.
- 7 Barsan, G., and Chiorean, C. (1999). "Computer program for large deflection elastoplastic analysis of semi-rigid steel frameworks." *Computers and Structures*, 72(6), 699-711.
- 8 Bjorhovde, R. (1972), "Deterministic and probabilistic approaches to the strength of steel columns, Ph.D. Dissertation, Lehigh University, Bethlehem, PA.
- 9 Bjorhovde, R. (1978). "The Safety of steel columns." *Journal of the Structural Division, ASCE*, 104(ST3), 463-477.
- 10 Bjorhovde, R. (1988). "Columns: From theory to practice." *Engineering Journal, AISC*, 26(1), 21-34.
- 11 Chen, P., and Powell, G. (1982). "Generalized plastic hinge concepts for 3D beam-column elements." EERC Report No. 80/20, University of California, Berkeley.
- 12 Dafalias, Y., and Popov, E. (1975). "A model of nonlinearly hardening materials for complex loading." *Acta Mechanica*, 21(3), 173-192.

- 13 Doltsinis, I. (2000). "Elements of Plasticity: Theory and computation." WIT Press, Southampton, UK.
- 14 Englekirk, R. (1994). "Steel Structures: Controlling behavior through design", John Wiley & Sons, New York, NY.
- 15 Fraser, D. J. (1989). "Uniform Pin-based crane columns, effective lengths." *Engineering Journal, AISC*, 26(2), 61-65.
- 16 Galambos, T. V. (1998). "Guide to stability design criteria for metal structures." Structural Stability Research Council, John Wiley & Sons, New York, NY.
- 17 Gao, L., and Haldar, A. (1995). "Nonlinear seismic analysis of space structures with partially restrained connections." *International Journal of Rock Mechanics*, 32(5), 240A-240A.
- 18 Hall, D. H. (1981). "Proposed steel column strength criteria." *Journal of the Structural Division, ASCE*, 107(ST4), 649-670.
- 19 Johnson, W., and Mellor, P. B. (1962). "Plasticity for Mechanical Engineers." Van Nostrand, Princeton, NJ.
- 20 Handelman, G. H., and Prager W. (1948). "Plastic buckling of a rectangular plate." NACA Technical Note 1530.
- 21 Harichandran, R. S. (1991). "Stiffness reduction factor for LRFD of columns." *Engineering Journal, AISC*, 28(3), 129-130.
- 22 Hassan, K. (1968). "On the determination of buckling length of frame columns." *International Association for Bridge and Structural Engineering*, 28(II), 91-101.
- 23 Karabinis, A., and Kiouisis, P. (2001). "Plasticity model for reinforced concrete elements subjected to overloads." *Journal of Structural Engineering*, 127(11), 1251-1256.
- 24 Kassawara, R. (1989). "The October 17, 1989 Loma Prieta Earthquake." EQE Engineering, San Francisco, CA.
- 25 Kavanagh, T. C. (1962). "Effective length of framed columns." *Transactions, ASCE*, 127(II), 81-101.
- 26 King, W. S., White, D. W., and Chen, W. F. (1992). "Second-order inelastic methods for steel-frame design." *Journal of Structural Engineering*, 118(2), 408-428.

- 27 Liew, J., Chen, H., Shanmugam, N., and Chen, W. (2000). "Improved nonlinear plastic hinge analysis of space frame structures." *Engineering Structures*, 22(10), 1324-1338.
- 28 Liew, J., Yu, C., Ng, Y., and Shanmugam, N. (1997). "Testing of semi-rigid, unbraced frames for calibration of 2<sup>nd</sup> order inelastic analysis." *Journal of Constructional Steel Research*, 41(2/3), 159-195.
- 29 Lu, L. W. (1965). "Effective length of columns in gabel frames." *Engineering Journal, AISC*, 2(1), 6-7.
- 30 Lui, E. M., and Chen, W. F. (1984). "Simplified approach to the analysis and design of columns with imperfections." *Engineering Journal, AISC*, 22(2), 99-117.
- 31 Marcon, A., Bittencourt, E., Creus, G. (1999). "On the integration of stresses in large deformations plasticity." *Engineering Computations*, 16(1), 49-69.
- 32 Mendleson, A. (1999). "Plasticity: Theory and Application." Macmillan, New York, NY.
- 33 McGuire, W., Gallagher, R. H., and Ziemian, R. D. (2000). "Matrix Structural Analysis." John Wiley & Sons, New York, NY.
- 34 Needleman, A. (1985). "On finite element formulations for large elastic-plastic deformations." *Computers & Structures*, 20(1-3), 247-257.
- 35 Orbison, J. G. (1982). "Nonlinear static analysis of three-dimensional steel frames." Ph.D. Dissertation, Cornell University, Ithaca, NY.
- 36 Owen, D. R. J., and Hinton, E. (1980). "Finite Elements in Plasticity: Theory and practice." Pineridge Press Limited, Swansea, UK.
- 37 Paz, M. (1997). "Structural Dynamics: Theory and computation." Kluwer Academic Publishers Group, Dordrecht, Netherlands.
- 38 Petersson, H., and Popov, E. (1977). "Constitutive relation for generalized loading." *Journal of Engineering Mechanics, ASCE*, 104(4), 611-627.
- 39 Plastic Design of Multi-Story Frames Vols. 1 and 2. (1965). Department of Civil Engineering, Lehigh University, Bethlehem, PA.
- 40 Porter, F. L. and Powell, G. H. (1971). "Static and dynamic analysis of inelastic framed structures." Rep. No. EERC 71-3, Earthquake Engineering Research Center, University of California, Berkeley, CA.

- 41 Popov, E. (1987). "Panel zone flexibility in seismic moment joints." *Journal of Constructional Steel Research*, 8, 91-118.
- 42 Prager, W. (1945). "Strain hardening under combined stress." *Journal of Applied Physics*, 16, 837-840.
- 43 Prager, W. (1955). "The Theory of Plasticity-A survey for recent Achievements." *Proc. Inst. Mech. Engrs., London, UK*, 169, 41.
- 44 Prager, W. (1995). "The Theory of Plasticity: A Survey of Recent Achievements," *Proc. Inst. Mech. Eng.*, 169, 41-57.
- 45 Rutenber, A., and Scarlat, A. (1990). "Roof bracing and effective length of columns in one-story industrial buildings." *Journal of Structural Engineering*, 116(10), 2551-2566.
- 46 Ramberg, W., and Osgood, W. R. (1943). "Description of stress-strain curves by three parameters." *NACA Technical Note No. 902*.
- 47 Salmon, C. G., and Johnson, J. E. (1996). "Steel Structures: Design and Behavior", Prentice Hall, Upper Saddle River, NJ.
- 48 Sandhu, B. S. (1972). "Effective length of columns with intermediate axial load." *Engineering Journal, AISC*, 9(3), 154-156.
- 49 Shames, I. H., and Cozzarelli, F. A. (1997). "Elastic and inelastic stress analysis." Taylor and Francis, Philadelphia, PA.
- 50 Shanley, F. R. (1946). "The column paradox." *Journal of the Aeronautical Sciences*, 13(12), 678.
- 51 Shanley, F. R. (1947). "Inelastic column theory." *Journal of Structural Engineering*, 14(5), 261-264.
- 52 Smyrell, A. G. (2001). "Approximate Formulas for Effective Length factors of Steel Columns." *Journal of Structural Engineering*, 120(9), 2793-2801.
- 53 Stoman, S. H. (1989). "Effective length spectra for cross-bracing." *Journal of Structural Engineering*, 115(12), 3112-3122.
- 54 Sutton, M. A., Deng, X., Liu, J., and Yang, L. (1996.) "Determination of elastic-plastic stresses and strains from measured surface strain data." *Experimental Mechanics*, 99-112.
- 55 Tide, R. H. R. (1985). "Reasonable column design equations." *Proceedings 1985 Annual Technical Session, Structural Stability*

Research Council, April, Cleveland, OH, Lehigh University, Bethlehem, PA.

- 56 Uniform Building Code. (1997). International Conference of Building Officials, Pasadena, Calif.
- 57 Vogel, U. (1985). "Calibration Frames." *Stahlbau*, 10, 1-7.
- 58 White, D. W. (1985). "Material and geometric nonlinear analysis of local planar behavior in steel frames using interactive computer graphics." MS Thesis, Cornell University, Ithaca, NY.
- 59 White, D. W., and Chen, W. F. (1993). "Plastic hinge based methods for advanced analysis and design of steel frames-An assessment of the state-of-the-art." Structural Stability Research Council, Bethlehem, PA.
- 60 Ziemian, R. D. and McGuire, W., and Deierlein, G. G. (1992a). "Inelastic limit states design: Part I-planar frame studies." *Journal of Structural Engineering*, 118(9), 2532-2549.
- 61 Ziemian, R. D. and McGuire, W., and Deierlein, G. G. (1992b). "Inelastic limit states design: Part II-three-dimensional frame studies." *Journal of Structural Engineering*, 118(9), 2550-2568.